2018

Single-molecule FRET investigation of SNARE-mediated exocytosis regulation

Linxiang Yin
Iowa State University

Single-molecule FRET investigation of SNARE-mediated exocytosis regulation

by

Linxiang Yin

A dissertation submitted to graduate faculty

in partial fulfillment of the requirements for the degree of

DOCTOR OF PHILOSOPHY

Major: Biochemistry

Program of Study Committee:
Yeon-Kyun Shin, Major Professor
Aragula Gururaj Rao
Scott W. Nelson
Mark S. Hargrove
Dipali G. Sashital
Nigel Forest Reuel

The student author, whose presentation of the scholarship herein was approved by the program of study committee, is solely responsible for the content of this dissertation. The Graduate College will ensure this dissertation is globally accessible and will not permit alterations after a degree is conferred.

Iowa State University

Ames, Iowa

2018

TABLE OF CONTENTS

Page

ABSTRACT

In the neuron, neurotransmitter release is mediated by SNARE (soluble NSF (N-ethylmaleimide-sensitive factor) attachment protein receptor) proteins. SNARE-dependent synaptic vesicle membrane and plasma membrane fusion is a multiple-step event and a tightly regulated process. Vesicle-anchored (v-) SNARE from synaptic vesicles associates with target plasma membrane-anchored (t-) SNARE to form a *trans*-SNAREpin complex. When the triggering signal arrives, v-SNARE and t-SNARE mediate the membrane full fusion and extend on one side of the membrane, forming a *cis*-conformation. During the whole process, SNARE complex with the help of regulators overcomes the energy barriers to fuse two apposed membranes and ensures that fusion proceeds at the correct time and place.

Currently, there are some key questions that remain regarding SNARE-mediated exocytosis regulation. First, among the SNARE regulators, complexin is a small SNARE-binding protein that is thought to inhibit membrane fusion before Ca^{2+} triggering signal arrives. Although such an inhibitory role of complexin has been reported, its structural basis is very controversially discussed. Second, as the central machinery of neurotransmitters release, all three SNARE proteins are targets of different botulinum neurotoxins (BoNTs). Even though BoNT A and E cleave SNAP-25 at the C-terminus to inhibit SNARE-dependent membrane fusion, the detailed effects of BoNT A and E cleavage on SNARE complex folding pathway, conformation and function remain largely elusive. Third, the *cis*-SNARE complex contains 16 layers. BoNT E and A cleave SNAP-25 at residue 180 within layer '+2' and residue 197 within layer '+7', separately. The effect of SNAP-25 layers on SNARE complex formation has not been systematically studied. Also, another knowledge gap is why naturally selected BoNT E and A choose to cleave SNAP-25 at residue 180 and 197.

Previous studies using soluble SNARE proteins without transmembrane domains and two apposed lipid environments may actually represent *cis*-conformation of the SNARE complex as opposed to *trans*-conformation. To solve this problem, we used SNARE-incorporated nanodiscs to solubilize full-length SNARE membrane proteins syntaxin 1A and VAMP2. The t-SNARE-incorporated nanodisc and v-SNARE-incorporated nanodisc can form a trapped *trans*-SNAREpin structure without full fusion, providing us a perfect platform to study the *trans*-SNAREpin conformation regulation.

In this thesis, to solve the aforementioned questions, we primarily used single-molecule fluorescence resonance energy transfer (smFRET) to investigate the *trans*-SNAREpin and *cis*-SNARE complex formation and structure in the presence of SNARE regulators. Our results demonstrate that complexin splits the SNARE core in the C-terminal region to inhibit further SNARE zippering. We also conclude that the two membranes are necessary for the proper complexin function and are an integral part of the synaptic vesicle fusion regulatory machinery. SNAP-25E, the cleavage product by BoNT E, significantly decreases t- and v-SNARE pairing. The cleavage product by BoNT A SNAP-25A, however, does not affect the t- and v-SNARE pairing but mildly decreases SNARE zippering. In addition, our results unveil a delicate alpha-helix nucleation process at the SNAP-25 C-terminal motif (SC) downstream layers. The results also shed light on why BoNT E but not BoNT A can induce neuron degeneration.

CHAPTER 1: GENERAL INTRODUCTION

SNAREs and Membrane Fusion

Soluble N-ethylmaleimide-sensitive factor attachment protein receptor (SNARE) protein is the main fusion machinery of almost all intracellular membrane fusion events like neurotransmitter release and hormone release (Y. A. Chen & Scheller, 2001; Karatekin et al., 2010; Weimbs et al., 1997). Neurotransmitter release, a critical step in chemical synaptic transmission during which presynaptic vesicles fuse with the presynaptic membrane to release the neurotransmitters into the synaptic cleft, is mediated by the neuronal SNARE complex (Brunger, Weninger, Bowen, & Chu, 2010; Zhou et al., 2015). The neuronal SNARE complex consists of an acceptor complex containing two plasma membrane proteins syntaxin and synaptosomal-associated protein 25 (SNAP-25) and a vesicular protein vesicle-associated membrane protein (VAMP) (Bennett, Calakos, & Scheller, 1992; Oyler et al., 1989; Trimble, Cowan, & Scheller, 1988).

SNARE proteins contain SNARE motifs, which are 60-70 conserved amino acids including eight heptad repeats with a high propensity to form coiled-coil structure (Jahn, Lang, & Sudhof, 2003). Syntaxin and VAMP2 each contribute one SNARE motif while SNAP-25 contributes two SNARE motifs (Sutton, Fasshauer, Jahn, & Brunger, 1998). Syntaxin also has an independently-folded helical N-terminal regulatory domain (Habc domain), a C-terminal transmembrane domain, and a short linker domain between the SNARE motif and the transmembrane domain (Fernandez et al., 1998; Margittai, Fasshauer, Jahn, & Langen, 2003). In VAMP2, a short linker domain also connects the SNARE motif and a C-terminal transmembrane domain. In SNAP-25, the two

SNARE motifs are connected by a long loop between them and anchored to the membrane by palmitoylation of cysteine residues in this loop region. SNARE complex formation is mediated through the interaction of the SNARE motifs (Figure 1) (Ramakrishnan, Drescher, & Drescher, 2013; Rizo, 2009).

During SNARE complex formation, Syntaxin and SNAP-25 first form a 1:1 target membrane or t-SNARE binary complex (Fasshauer & Margittai, 2004; Pobbati, Stein, & Fasshauer, 2006; Weninger, Bowen, Choi, Chu, & Brunger, 2008). For the t-SNARE complex, besides the 1:1 t-SNARE complex, *in vitro* studies also show syntaxin may interact with SNAP-25 at a 2:1 molar ratio to form a misfolded off-pathway non-functional 2:1 t-SNARE complex (Fasshauer & Margittai, 2004; Margittai, Fasshauer, Pabst, Jahn, & Langen, 2001; Xiao, Poirier, Bennett, & Shin, 2001). In our study, we focused on the on-pathway 1:1 t-SNARE complex. The 1:1 t-SNARE is the target for SNARE regulators like Munc13, Munc18, synaptotagmins, and complexin (Weninger et al., 2008; Zhang et al., 2016). The preformed largely ordered 1:1 t-SNARE is also important for SNARE zippering to proceed in at a fast rate and controlled manner (Gao et al., 2012; Zhang et al., 2016).

The 1:1 t-SNARE complex then binds to vesicle or v-SNAREs to form the ternary SNARE complex (Sudhof & Rothman, 2009). Formation of the ternary complex begins from distal to the membrane surfaces and proceeds toward them, bringing membranes into close proximity, which is referred to as the SNARE zippering model (Fasshauer & Margittai, 2004; Gao et al., 2012; Lou, Shin, Yang, Kim, & Shin, 2014; Lou & Shin, 2016; Sørensen, Wiederhold, Milosevic, & Groot, 2006). SNARE proteins first associate spontaneously *in trans*, which is called *trans*-SNARE, where t-SNARE and v-SNARE are anchored to apposed membranes. This *trans*-SNARE provides the energy to overcome energy barrier to draw the lipid bilayer membranes into close apposition

and also provides a platform for SNARE regulators such as complexin and synaptotagmins to regulate membrane fusion. When fully zippered, each SNARE is anchored to the same membrane; it is then called *cis*-SNARE (Figure 2) (Stein, Weber, Wahl, & Jahn, 2009; Sutton et al., 1998).

Structure of the SNARE Complex

Currently, the *cis*-SNARE structure has been extensively studied *in vitro*. Electron paramagnetic resonance (EPR) first showed that SNARE motifs are a parallel four-stranded coiled-coil (Figure 3) (Poirier, Wenzhong, et al., 1998), which was then confirmed by X-ray crystallography (Sutton et al., 1998). The *cis*-SNARE contains heptad repeat domains (SNARE motifs). The SNARE motifs interaction is the basis for SNARE complex formation (Fasshauer, Otto, Eliason, Jahn, & Bru, 1997; Lou & Shin, 2016; Poirier, Hao, et al., 1998). The SNARE motifs are stabilized by 16 (numbered -7 to +8) stacked layers of highly conserved interacting amino acid side chains. The most highly conservative layer 0 is maintained by ionic interactions in nature so it is also called the ionic layer. The upstream (layers -7 to -1) and downstream (layer +1 to +8) layers are maintained by hydrophobic side chains (Sutton et al., 1998). However, the effects of these layers on SNARE complex folding pathway, formation and structure have not been systematically studied.

Compared with the *cis*-SNARE, the detailed structure of *trans*-SNARE has been less well studied. Previous efforts to investigate *trans*-SNARE structures were mostly elucidated in the absence of membranes, likely representing the *cis*-complex, but not the *trans*-complex structures. Emerging studies have shown the importance of the membrane in the SNARE-mediated membrane fusion research system (Weninger et al., 2008; Zhang et al., 2016).

Currently, the folding and structure of the t-SNARE have also been well understood. The t-SNARE forms from the N-terminal domain (NTD) (from -7 layer to -1 layer) and then to the C-terminal domain (CTD) (from 0 layer to +4 layer). The 1:1 t-SNARE complex has a parallel three-helix bundle structure with a small frayed C-terminal end (from +5 to +8 layers) (Zhang et al., 2016). The 1:1 t-SNARE structure can be stabilized with the help of SNARE regulators like Munc18-1, synaptotagmins, and complexin (Weninger et al., 2008).

Complexin

Among the major SNARE regulators that regulate synaptic vesicle exocytosis, complexin (Cpx) is a small soluble SNARE-binding protein mainly found in the presynaptic terminal (Ishizuka, Saisu, Odani, & Abe, 1995; McMahon, Missler, Li, & Sudhof, 1995). Previous studies have shown the two opposite effects of Cpx during two modes of synaptic vesicle fusion: regulating random spontaneous synaptic vesicle fusion (Hobson, Liu, Watanabe, & Jorgensen, 2011; Huntwork & Littleton, 2007; Maximov, Tang, Yang, Pang, & Südhof, 2009; McMahon et al., 1995) and activating evoked synaptic vesicle fusion (Chapman, 2008; Fernández-Chacón et al., 2001).

Cpx has four domains involved in different functions (Figure 4): the N-terminal domain, the C-terminal domain, the accessory helix (AH) domain, and the central helix (CH) domain. The central helix (CH) domain is indispensable for the SNARE complex binding thus is necessary for all functions of Cpx. Cpx N-terminal domain has a strong positive function on Ca2+-triggered evoked synaptic vesicle release in mouse neurons (Maximov et al., 2009; Xue et al., 2007, 2010). Cpx N-terminal domain mutants M5E/K6E and N-terminal truncation Cpx27-134 both suppress

spontaneous synaptic vesicle fusion significantly, suggesting that Cpx N-terminal domain has a fusion-facilitating ability (Xue et al., 2007, 2010). The C-terminal domain of worm and mammalian Cpx contains a membrane-binding motif, which enables its direct interaction with membranes in a curvature-dependent manner (Gong et al., 2016; Snead, Wragg, Dittman, & Eliezer, 2014).

Cpx may alter spontaneous synaptic vesicle fusion by inhibiting complete SNARE zippering. Currently, the structural basis for the inhibitory role of complexin on SNARE zippering is a very controversially discussed question (Krishnakumar et al., 2015; Trimbuch et al., 2014; Trimbuch & Rosenmund, 2016; Xue et al., 2008; Yang, Cao, & Südhof, 2013). There are two classical models on this issue: the binding model (X. Chen et al., 2002) (Figure 4) and the zigzag array model (Kümmel et al., 2011) (Figure 5). In the first model study, a combination of X-ray crystallography, NMR spectroscopy and hydrogen-deuterium exchange studies on the interaction of complexin 1 with the SNARE core complex showed that Cpx binds to and stabilizes the surface groove between the syntaxin 1A and VAMP2 SNARE motifs in an antiparallel manner (X. Chen et al., 2002). However, Daniel Kümmel *et al.* concerned that the complexin-SNARE complex structure in the binding model contains a fully-zippered SNARE core. They proposed such complexin-SNARE complex structure represents the post-fusion complexin-SNARE complex. However, Cpx mainly regulates synaptic vesicle fusion before SNARE full fusion. In their research, they prepared the pre-fusion SNAREpin without the VAMP2 C-terminal portion that zippers last to trigger fusion and solved the complexin-bound truncated SNARE core complex X-ray crystallography structure. They showed that the AH and CH from just one Cpx could crosslink two adjacent partially zippered SNAREs. In their structure, the Cpx CH is anchored to one partially zippered SNARE core complex, the AH domain of the same Cpx extends away from its CH

domain to bridge a second partially zippered SNARE by occupying the open pocket of its t-SNARE. In their model, Cpx cross-links and organizes the pre-fusion SNAREs into a fusion-incompatible zigzag array topology (Kümmel et al., 2011).

In both models, just SNARE motifs were used rather than full-length SNARE membrane proteins syntaxin 1A and VAMP2 in both X-ray crystallography studies. In the latter research trying to mimic the pre-fusion SNAREpin, the X-ray crystallography study was carried out in the absence of two opposite membranes (X. Chen et al., 2002; Kümmel et al., 2011). However, the two apposed membranes are indispensable components to form the pre-fusion *trans*-SNARE structure. In addition, the truncated C-terminal portion of VAMP2 in the latter study is supposed to compete with Cpx during Cpx regulation (Lu, Song, & Shin, 2010).

So here we tested whether the membrane would be the essential player in this Cpx regulatory machinery by pursuing the approach of phospholipid bilayer containing nanodiscs. We also tested whether the effects of truncated version of SNARE proteins could fully represent the function of full-length SNAREs in their researches.

BoNT A and E

Compared with SNARE regulators that ensure synaptic vesicle fusion temporally and spatially proceeding both correctly and efficiently, botulinum neurotoxins (BoNTs) are toxic proteins acting on nerve endings to block SNARE-mediated neurotransmitter release. BoNTs are produced by the gram-positive anaerobic bacterium *Clostridium Botulinum* and related species. They inhibit synaptic vesicle exocytosis by selective and specific proteolysis of different SNARE

proteins at different sites (Lacy, Tepp, Cohen, Dasgupta, & Stevens, 1998; Montal, 2010; G Schiavo, Matteoli, & Montecucco, 2000).

There are seven major serotypes of botulinum toxins, which are denoted BoNT A through BoNT G. BoNT A and BoNT E cleave SNAP25; BoNT B, BoNT D, BoNT F and BoNT G only cleave VAMP; and BoNT C cleaves both SNAP25 and syntaxin (Blasi, Juan et al., 1993; Blasi et al., 1993; Pantano & Montecucco, 2014; Giampietro; Schiavo et al., 1992) (Figure 6). BoNTs targeting syntaxin 1A or VAMP2 inhibit SNARE-dependent membrane fusion because BoNTs truncated syntaxin 1A or VAMP2 cannot form the membrane-bridging *trans*-SNARE complex. However, SNAP-25 targeting BoNTs can still sufficiently reduce or abolish neurotransmitter release even in the presence of intact both syntaxin 1A and VAMP2 (Pantano & Montecucco, 2014).

Specifically, BoNT A has the highest level of toxicity for humans, and BoNT A as well as E are the predominant causes for contaminated food-borne intoxication and wound infection botulism poisoning in humans (Cherington, 1998; Gill, 1982; Li et al., 2011). Even though BoNT A and E both cleave SNARE proteins by removing the C-terminal end cytosolic segments of SNAP-25, the effects of BoNT A and E on membrane fusion are different (Blasi, Juan et al., 1993; Rossetto, Pirazzini, & Montecucco, 2014; Schiavo et al., 1993). Previous studies have shown BoNT A only removes the last nine residues from SNAP 25 C-terminus (Schiavo et al., 1993) and this truncated version of SNAP 25 can still form SNARE complex (Fasshauer & Margittai, 2004). The neurotransmitter release inhibition induced by BoNT A can still be rescued with high concentration of Ca^{2+} (Lundh, Stefan, & Stephen, 1977), suggesting a delicate mechanism of the reaction of BoNT A on SNARE. BoNT E removes 26 residues of SNAP 25 C-terminus (Schiavo

et al., 1993) and totally abolishes SNARE-dependent membrane fusion (Pantano & Montecucco, 2014). The detailed mechanism of BoNT A and E cleavage on SNARE structure and function remains largely elusive.

Nanodisc

In this dissertation, nanodiscs are employed to solubilize single SNARE membrane protein VAMP-2 or syntaxin-1A. The nanodisc is a nanometer-sized planar phospholipid bilayer encircled by two amphipathic membrane scaffolding proteins (MSPs) (Bayburt, Carlson, & Sligar, 1998; Bayburt & Sligar, 2010) (Figure 7). Traditional MSPs are modified versions of apolipoprotein A1(apoA1), the major constituent of high-density lipoprotein (Bayburt et al., 1998; Bayburt & Sligar, 2010). The nanodisc provides a detergent-free model for the solubilization and stabilization of membrane proteins. Nanodiscs therefore enable a physiologically more relevant environment than liposomes, detergent micelles and bicelles (Borch & Hamann, 2009). In addition, the ratio between lipids, MSPs and membrane proteins can be adjusted such that each nanodisc contains at most one membrane protein. The aforementioned qualities make nanodiscs a good nanodevice to study membrane proteins at the single-molecule level (Bayburt & Sligar, 2010).

Single-Molecular Fluorescence (Förster) Resonance Energy Transfer (smFRET)

This study at single molecule level is achieved by smFRET. FRET is a physical phenomenon describing distance-dependent energy transfer between two light-sensitive molecules (chromophores or dyes). In these two-chromophores system, there are one energy donor and one energy acceptor. If there is overlap of the emission spectrum of the donor and the absorption

spectrum of the acceptor, the excited donor chromophore may transfer energy to the acceptor chromophore in proximity (typically within 1-10 nm) (Joo & Ha, 2012; P R Selvin, 1995; Stryer & Haugland, 1967). For a given FRET pair, their Förster radius (R_0, the distance between the donor dye and the acceptor dye at which 50% FRET occurs) is a constant value (Clapp et al., 2004). The FRET efficiency (E) varies with the sixth power of distance between the donor and the acceptor (R), as defined by the equation:

$$E = \frac{R_0^6}{R_0^6 + R^6}$$

FRET efficiency can also be measured by calculating the intensity of the emission light of the two chromophores. The E is defined as:

$$E = \frac{I_A}{I_A + I_D}$$

Using both equations, the distances between the two molecules (R) can be calculated with known FRET efficiencies I_A and I_D recorded during the experiment (Paul R Selvin, 2000).

The traditional FRET is usually carried out in bulk FRET assay. The total donor and acceptor fluorescent signals collected from the bulk FRET assay may miss the individual or transient observable single-molecular events like conformational fluctuations, multistep catalysis, and transient interactions by assemble averaging. SmFRET enables us accessible to conformational distributions, real-time or transient asynchronous dynamics information of individual molecules (Ha et al., 1996; Hamadani et al., 2017; Weiss, 1999) (Figure 8). The smFRET experiment is achieved by fluorescence microscope recording using highly-diluted surface-immobilized or freely-diffusing molecules (Funatsu, Harada, Tokunaga, Saito, &

Yanagida, 1995). The real-time single-molecule intensities can be derived from videos collected by recording well-separated labeled molecules within a small imaging area using charge coupled device (CCD) cameras.

To reduce the background noise during imaging, in our system, we used total internal reflection fluorescence microscope (TIRFM) (Figure 9). TIRFM is a kind of microscope that induces and utilizes the unique properties of an evanescent wave (Funatsu et al., 1995; Tokunaga, Kitamura, Saito, Iwane, & Yanagida, 1997). The penetration depth of TIRFM evanescent wave is typically less than 200 nm, so TIRFM can selectively illuminate labeled protein samples within a restricted thin region close to the slide-water interface. Thus, TIRFM is especially useful for selectively visualizing of signals constrained in a thin surface region and enables signals with dramatically reduced background noise (Fish, 2009; Matsuoka, Miyanaga, Yanagida, & Ueda, 2012).

The combination of smFRET and nanodiscs is a powerful research tool to investigate the conformational changes, movements and dynamics of large membrane protein complexes at the single molecule level.

References

Bayburt, T. H., Carlson, J. W., & Sligar, S. (1998). Reconstitution and imaging of a membrane protein in a nanometer-size phospholipid bilayer. *Journal of Structural Biology*, *123*(1), 37–44. http://doi.org/10.1006/jsbi.1998.4007

Bayburt, T. H., & Sligar, S. G. (2010). Membrane Protein Assembly into Nanodiscs. *FEBS Letters*, *584*(9), 1721–1727. http://doi.org/10.1016/j.febslet.2009.10.024.

Bennett, M. K., Calakos, N., & Scheller, R. H. (1992). Syntaxin： A synaptic protein implicated in docking of synaptic vesicles at presynaptic active zones. *Science*, *257*(5067), 255–259.

Blasi, Juan, Chapman, E. R., Egenhard, Link, Thomas, Binz, Shinji, Y., Pietro, D. C., … Reinhard, J. (1993). Botulinum neurotoxin A selectively cleaves the synaptic protein SNAP-25. *Nature*, *365*(9), 160–163.

Blasi, J., Chapman, E. R., Yamasaki, S., Binz, T., Niemann, H., & Jahn, R. (1993). Botulinum neurotoxin C1 blocks neurotransmitter release by means of cleaving HPC-1/syntaxin. *EMBO Journal*, *12*(12), 4821–4828.

Borch, J., & Hamann, T. (2009). The nanodisc: a novel tool for membrane protein studies. *Biological Chemistry*, *390*(8), 805–814. http://doi.org/10.1515/BC.2009.091

Brunger, A. T., Weninger, K., Bowen, M., & Chu, S. (2010). Single molecule studies of the neuronal SNARE fusion machinery. *Annual Review of Biochemistry*, (7), 903–928. http://doi.org/10.1146/annurev.biochem.77.070306.103621.

Chapman, E. R. (2008). How does synaptotagmin trigger neurotransmitter release? *Annual Review of Biochemistry*. http://doi.org/10.1146/annurev.biochem.77.062005.101135

Chen, X., Tomchick, D. R., Kovrigin, E., Arac, D., Machius, M., & Su, T. C. (2002). Three-dimensional structure of the complexin/SNARE complex. *Neuron*, *33*(3), 397–409.

Chen, Y. A., & Scheller, R. H. (2001). SNARE-mediated membrane fusion. *Nature Reviews Molecular Cell Biology*, *2*(2), 98–106.

Cherington, M. (1998). Clinical spectrum of botulism. *Muscle & Nerve*, *21*(6), 701–710.

Clapp, A. R., Medintz, I. L., Mauro, J. M., Fisher, B. R., Bawendi, M. G., & Mattoussi, H. (2004). Fluorescence resonance energy transfer between quantum dot donors and dye-labeled protein acceptors. *Journal of the American Chemical Society*, *126*(1), 301–310. http://doi.org/10.1021/ja037088b

Fasshauer, D., & Margittai, M. (2004). A transient N-terminal interaction of SNAP-25 and syntaxin nucleates SNARE assembly. *Journal of Biological Chemistry*, *279*(9), 7613–7621. http://doi.org/10.1074/jbc.M312064200

Fasshauer, D., Otto, H., Eliason, W. K., Jahn, R., & Bru, A. T. (1997). Structural changes are associated with soluble N -ethylmaleimide-sensitive fusion protein attachment protein receptor complex formation. *Journal of Biological Chemistry*, *272*(44), 28036–28041.

Fernández-Chacón, R., Königstorfer, A., Gerber, S. H., García, J., Matos, M. F., Stevens, C. F., … Südhof, T. C. (2001). Synaptotagmin I functions as a calcium regulator of release probability. *Nature*, *410*(6824), 41–49. http://doi.org/10.1038/35065004

Fernandez, I., Ubach, J., Dulubova, I., Zhang, X., Sudhof, T. C., & Rizo, J. (1998). Three-dimensional structure of an evolutionarily conserved N-terminal domain of syntaxin 1A. *Cell*, *94*(6), 841–849.

Fish, K. N. (2009). Total internal reflection fluorescence (TIRF) microscopy. *Current Protocols in Cytometry*, 12–18. http://doi.org/10.1002/0471142956.cy1218s50

Funatsu, T., Harada, Y., Tokunaga, M., Saito, K., & Yanagida, T. (1995). Imaging of single fluorescent molecules and individual ATP turnovers by single myosin molecules in aqueous solution. *Nature*, *374*(6522), 555–559.

Gao, Y., Zorman, S., Gundersen, G., Xi, Z., Ma, L., Sirinakis, G., … Zhang, Y. (2012). Single reconstituted neuronal SNARE complexes zipper in three distinct stages. *Science*, *337*(6100), 1340–1344.

Gill, D. M. (1982). Bacterial toxins: a table of lethal amounts. *Microbiological Reviews*, *46*(1), 86–94.

Gong, J., Lai, Y., Li, X., Wang, M., Leitz, J., & Hu, Y. (2016). C-terminal domain of mammalian complexin-1 localizes to highly curved membranes. *Proceedings of the National Academy of Sciences*, *201609917*, E7590–E7599. http://doi.org/10.1073/pnas.1609917113

Ha, T., Enderle, T., Ogletree, D. F., Chemla, D. S., Selvin, P. R., & Weiss, S. (1996). Probing the interaction between two single molecules: Fluorescence resonance energy transfer between a single donor and a single acceptor. *Proceedings of the National Academy of Sciences*, *93*(13), 6264–6268. http://doi.org/10.1073/pnas.93.13.6264

Hamadani, K. M., Howe, J., Jensen, M. K., Wu, P., Cate, J. H. D., & Marqusee, S. (2017). An in vitro tag-and-modify protein sample generation method for single-molecule fluorescence resonance. *Journal of Biological Chemistry*, *292*(38), 15636–15648. http://doi.org/10.1074/jbc.M117.791723

Hobson, R. J., Liu, Q., Watanabe, S., & Jorgensen, E. M. (2011). Complexin maintains vesicles in the primed state in C. elegans. *Current Biology*, *21*(2), 106–113. http://doi.org/10.1016/j.cub.2010.12.015

Huntwork, S., & Littleton, J. T. (2007). A complexin fusion clamp regulates spontaneous and synaptic growth. *Nature Neuroscience*, *10*(10), 1235–1237. http://doi.org/10.1038/nn1980

Ishizuka, T., Saisu, H., Odani, S., & Abe, T. (1995). Synaphin: A protein associated with the docking/fusion complex in presynaptic terminals. *Biochemical and Biophysical Research Communications*, *213*(3), 1107–1114. http://doi.org/10.1006/bbrc.1995.2241

Jahn, R., Lang, T., & Sudhof, T. C. (2003). Membrane Fusion. *Cell*, *112*(3), 519–533.

Joo, C., & Ha, T. (2012). Objective-type total internal reflection microscopy (emission) for single-molecule FRET. *Cold Spring Harbor Protocols*, *2012*(11), 1192–4. http://doi.org/10.1101/pdb.prot072033

Karatekin, E., Di, J., Iborra, C., Coleman, J., Shaughnessy, B. O., & Seagar, M. (2010). A fast , single-vesicle fusion assay mimics physiological SNARE requirements. *Proceedings of the National Academy of Sciences*, *107*(8), 3517–3521. http://doi.org/10.1073/pnas.0914723107

Krishnakumar, S. S., Li, F., Coleman, J., Schauder, C. M., Pincet, F., Rothman, J. E., & Reinisch, K. M. (2015). Re-visiting the trans insertion model for complexin clamping. *eLife*, *4*, e04463. http://doi.org/10.7554/eLife.04463

Kümmel, D., Krishnakumar, S. S., Radoff, D. T., Li, F., Giraudo, C. G., Pincet, F., … Reinisch, K. M. (2011). Complexin cross-links prefusion SNAREs into a zigzag array. *Nature Structural & Molecular Biology*, *18*(8), 927–933. http://doi.org/10.1038/nsmb.2101

Lacy, D. B., Tepp, W., Cohen, A. C., Dasgupta, B. R., & Stevens, R. C. (1998). Crystal structure of botulinum neurotoxin type A and implications for toxicity. *Nature Structural Biology*, *5*(10), 898–902.

Li, B., Peet, N. P., Butler, M. M., Burnett, J. C., Moir, D. T., & Bowlin, T. L. (2011). Small molecule inhibitors as countermeasures for botulinum neurotoxin intoxication. *Molecules*, *16*(1), 202–220. http://doi.org/10.3390/molecules16010202

Lou, X., Shin, J., Yang, Y., Kim, J., & Shin, Y.-K. (2014). Synaptotagmin 1 is an antagonist for Munc18-1 in SNARE zippering. http://doi.org/10.1074/jbc.M114.631341

Lou, X., & Shin, Y.-K. (2016). SNARE zippering. *Bioscience Reports*, *36*(3), e00327–e00327. http://doi.org/10.1042/BSR20160004

Lu, B., Song, S., & Shin, Y. (2010). Accessory alpha-helix of complexin I can displace VAMP2 locally in the complexin-SNARE quaternary complex. *Journal of Molecular Biology*, *396*(3), 602–609. http://doi.org/10.1016/j.jmb.2009.12.020

Lundh, H., Stefan, L., & Stephen, T. (1977). Antagonism of the paralysis produced by botulinum toxin in the rat. The effects of tetraethylammonium, guanidine and 4-aminopyridine. *Journal of the Neurological Sciences*, *32*(1), 29–43.

Margittai, M., Fasshauer, D., Jahn, R., & Langen, R. (2003). The Habc domain and the SNARE core complex are connected by a highly flexible linker. *Biochemistry*, *42*(14), 4009–4014. http://doi.org/10.1021/bi027437z

Margittai, M., Fasshauer, D., Pabst, S., Jahn, R., & Langen, R. (2001). Homo- and heterooligomeric SNARE complexes studied by site-directed spin labeling. *Journal of Biological Chemistry*, *276*(16), 13169–13177. http://doi.org/10.1074/jbc.M010653200

Matsuoka, S., Miyanaga, Y., Yanagida, T., & Ueda, M. (2012). Single-molecule imaging of stochastic signaling events in living cells. *Cold Spring Harbor Protocols*, *7*(3), 267–278. http://doi.org/10.1101/pdb.top068189

Maximov, A., Tang, J., Yang, X., Pang, Z. P., & Südhof, T. C. (2009). Complexin controls the force transfer from SNARE complexes to membranes in fusion. *Science*, *323*(5913), 516–521. http://doi.org/10.1126/science.1166505

McMahon, H. T., Missler, M., Li, C., & Sudhof, T. C. (1995). Complexins: Cytosolic proteins that regulate SNAP receptor function. *Cell*, *83*(1), 111–119. http://doi.org/10.1016/0092-8674(95)90239-2

Montal, M. (2010). Botulinum neurotoxin: A marvel of protein design. *Annual Review of Biochemistry*. http://doi.org/10.1146/annurev.biochem.051908.125345

Oyler, G. A., Higgins, G. A., Hart, R. A., Battenberg, E., Billingsley, M., Bloom, F. E., & Wilson, M. C. (1989). The identification of a novel synaptosomal-associated protein, SNAP-25, differentially expressed by neuronal subpopulations. *The Journal of Cell Biology*, *109*(6), 3039–3052.

Pantano, S., & Montecucco, C. (2014). The blockade of the neurotransmitter release apparatus by botulinum neurotoxins. *Cellular and Molecular Life Sciences*, *71*(5), 793–811. http://doi.org/10.1007/s00018-013-1380-7

Pobbati, A. V, Stein, A., & Fasshauer, D. (2006). N- to C-terminal SNARE complex assembly promotes rapid membrane fusion. *Science*, *313*(5787), 673–676. http://doi.org/10.1126/science.1129486

Poirier, M. A., Hao, J. C., Malkus, P. N., Chan, C., Moore, M. F., King, D. S., & Bennett, M. K. (1998). Protease resistance of syntaxin SNAP-25 VAMP complexes. *Journal of Biological Chemistry*, *273*(18), 11370–11377.

Poirier, M. A., Wenzhong, X., Macosko, J. C., Chan, C., Yeon-Kyun, S., & Bennett, M. K. (1998). The synaptic SNARE complex is a parallel four- stranded helical bundle. *Nature Structural Biology*, *5*(9), 765–769.

Ramakrishnan, N. A., Drescher, M. J., & Drescher, D. G. (2013). The SNARE complex in neuronal and sensory cells. *Molecular and Cellular Neuroscience*, *50*(1), 58–69. http://doi.org/10.1016/j.mcn.2012.03.009.

Rizo, J. (2009). SNAREs. *Encyclopedia of Neuroscience*, *2*, 11–19.

Rossetto, O., Pirazzini, M., & Montecucco, C. (2014). Botulinum neurotoxins: genetic, structural and mechanistic insights. *Nature Reviews Microbiology*, *12*(8), 535–549. http://doi.org/10.1038/nrmicro3295

Schiavo, G., Benfenati, F., Poulain, B., Rossetto, O., Polverino de Laureto, P., DasGupta, B. R., & Montecucco, C. (1992). Tetanus and botulinum-B neurotoxins block neurotransmitter release by proteolytic cleavage of synaptobrevin. *Nature*, *359*(6398), 832–835.

Schiavo, G., Matteoli, M., & Montecucco, C. (2000). Neurotoxins affecting neuroexocytosis. *Physiological Reviews*, *80*(2), 717–766.

Schiavo, G., Santuccib, A., Dasguptac, B. R., Mehtad, P. P., Jontesd, J., Benfenati, F., … Montecucco, C. (1993). Botulinurn neurotoxins serotypes A and E cleave SNAP-25 at distinct COOH-terminal peptide bonds. *FEBS Letters*, *335*(1), 99–103.

Selvin, P. R. (1995). Fluorescence resonance energy transfer. *Methods in Enzymology*. http://doi.org/10.1016/0076-6879(95)46015-2

Selvin, P. R. (2000). The renaissance of fluorescence resonance energy transfer. *Nature Structural Biology*, *7*(9), 730–734.

Snead, D., Wragg, R. T., Dittman, J. S., & Eliezer, D. (2014). Membrane curvature sensing by the C-terminal domain of complexin. *Nature Communications*, *5*, 4955. http://doi.org/10.1038/ncomms5955

Sørensen, J. B., Wiederhold, K., Milosevic, I., & Groot, B. L. De. (2006). Sequential N- to C-terminal SNARE complex assembly drives priming and fusion of secretory vesicles. *The EMBO Journal*, *25*(5), 955–966. http://doi.org/10.1038/sj.emboj.7601003

Stein, A., Weber, G., Wahl, M. C., & Jahn, R. (2009). Helical extension of the neuronal SNARE complex into the membrane. *Nature*, *460*(7254), 525–528. http://doi.org/10.1038/nature08156

Stryer, L., & Haugland, R. P. (1967). Energy transfer: a spectroscopic ruler. *Proceedings of the National Academy of Sciences*, *58*(2), 719–726.

Sudhof, T. C., & Rothman, R. E. (2009). Membrane fusion: grappling with SNARE and SM proteins. *Science*, *323*(5913), 474–477. http://doi.org/10.1126/science.1161748

Sutton, R. B., Fasshauer, D., Jahn, R., & Brunger, A. T. (1998). Crystal structure of a SNARE complex involved in synaptic exocytosis at 2.4 Å resolution. *Nature*, *395*(6700), 347–353. http://doi.org/10.1038/26412

Tokunaga, M., Kitamura, K., Saito, K., Iwane, A. H., & Yanagida, T. (1997). Single molecule imaging of fluorophores and enzymatic reactions achieved by objective-type total internal reflection fluorescence microscopy. *Biochemical and Biophysical Research Communications*, *235*(1), 47–53. http://doi.org/10.1006/bbrc.1997.6732

Trimble, W. S., Cowan, D. M., & Scheller, R. H. (1988). VAMP-1 : A synaptic vesicle-associated integral membrane protein. *Proceedings of the National Academy of Sciences*, *85*(12), 4538–4542.

Trimbuch, T., & Rosenmund, C. (2016). Should I stop or should I go? The role of complexin in neurotransmitter release. *Nature Reviews Neuroscience*, *17*(2), 118–125. http://doi.org/10.1038/nrn.2015.16

Trimbuch, T., Xu, J., Flaherty, D., Tomchick, D. R., Rizo, J., & Rosenmund, C. (2014). Re-examining how complexin inhibits neurotransmitter release: SNARE complex insertion or electrostatic hindrance? *eLife*, (3), e02391. http://doi.org/10.7554/eLife.02391

Weimbs, T., Low, S. H., Chapin, S. J., Mostov, K. E., Bucher, P., & Hofmann, K. (1997). A conserved domain is present in different families of vesicular fusion proteins : A new superfamily. *Proceedings of the National Academy of Sciences*, *94*(7), 3046–3051.

Weiss, S. (1999). Fluorescence spectroscopy of single biomolecules. *Science*, *283*(5408), 1676–1683. http://doi.org/10.1126/science.283.5408.1676

Weninger, K., Bowen, M. E., Choi, U. B., Chu, S., & Brunger, A. T. (2008). Accessory proteins stabilize the acceptor complex for synaptobrevin , the 1 : 1 syntaxin / SNAP-25 complex. *Structure*, *16*(2), 308–320. http://doi.org/10.1016/j.str.2007.12.010

Xiao, W., Poirier, M. A., Bennett, M. K., & Shin, Y. (2001). The neuronal t-SNARE complex is a parallel four-helix bundle. *Nature Structural Biology*, *8*(4), 308–311.

Xue, M., Craig, T. K., Xu, J., Chao, H.-T., Rizo, J., & Rosenmund, C. (2010). Binding of the complexin N terminus to the SNARE complex potentiates synaptic-vesicle fusogenicity. *Nature Structural & Molecular Biology*, *17*(5), 568–575. http://doi.org/10.1038/nsmb.1791

Xue, M., Reim, K., Chen, X., Chao, H.-T., Deng, H., Rizo, J., … Rosenmund, C. (2007). Distinct domains of complexin I differentially regulate neurotransmitter release. *Nature Structural & Molecular Biology*, *14*(10), 949–958. http://doi.org/10.1038/nsmb1292

Xue, M., Stradomska, A., Chen, H., Brose, N., Zhang, W., Rosenmund, C., & Reim, K. (2008). Complexins facilitate neurotransmitter release at excitatory and inhibitory synapses in mammalian central nervous system. *Proceedings of the National Academy of Sciences of the United States of America*, *105*(22), 7875–7880. http://doi.org/10.1073/pnas.0803012105

Yang, X., Cao, P., & Südhof, T. C. (2013). Deconstructing complexin function in activating and clamping Ca2+-triggered exocytosis by comparing knockout and knockdown phenotypes. *Proceedings of the National Academy of Sciences of the United States of America*, *110*(51), 20777–20782. http://doi.org/10.1073/pnas.1321367110

Zhang, X., Rebane, A. A., Ma, L., Li, F., Jiao, J., Qu, H., … Zhang, Y. (2016). Stability, folding dynamics, and long-range conformational transition of the synaptic t-SNARE complex. *Proceedings of the National Academy of Sciences*, *113*(50), E8031–E8040. http://doi.org/10.1073/pnas.1605748113

Zhou, Q., Lai, Y., Bacaj, T., Zhao, M., Lyubimov, A. Y., Uervirojnangkoorn, M., … Su, T. C. (2015). Architecture of the synaptotagmin- SNARE machinery for neuronal exocytosis. *Nature*, *525*(7567), 62–67. http://doi.org/10.1038/nature14975

Figures with Titles and Legends

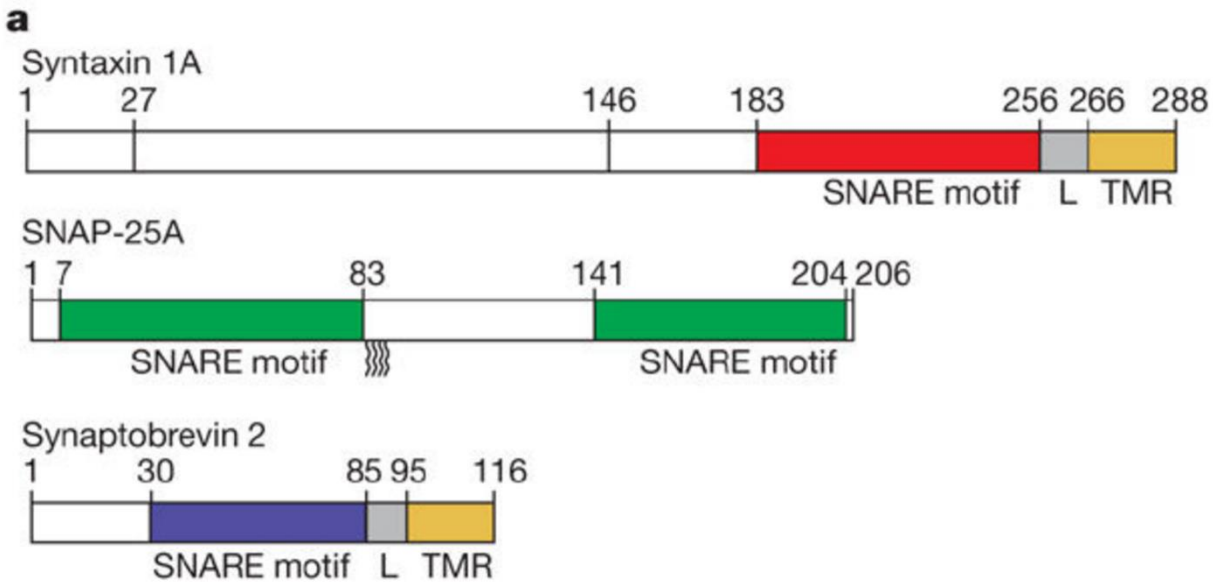

Figure 1 The domains of SNARE motifs of SNARE proteins. Nature. 2009 Jul 23;460(7254):525-8.

Syntaxin 1A contains a Habc domain (amino acids 27-146), a SNARE motif (red), a short linker region (grey), and a C-terminal transmembrane region (yellow). SNAP-25 contains two SNARE motifs (green), a long loop region between them (amino acids 83-141). VAMP2 (synaptobrevin 2) contains a SNARE motif (blue), a transmembrane region (yellow), and a short linker between them (grey).

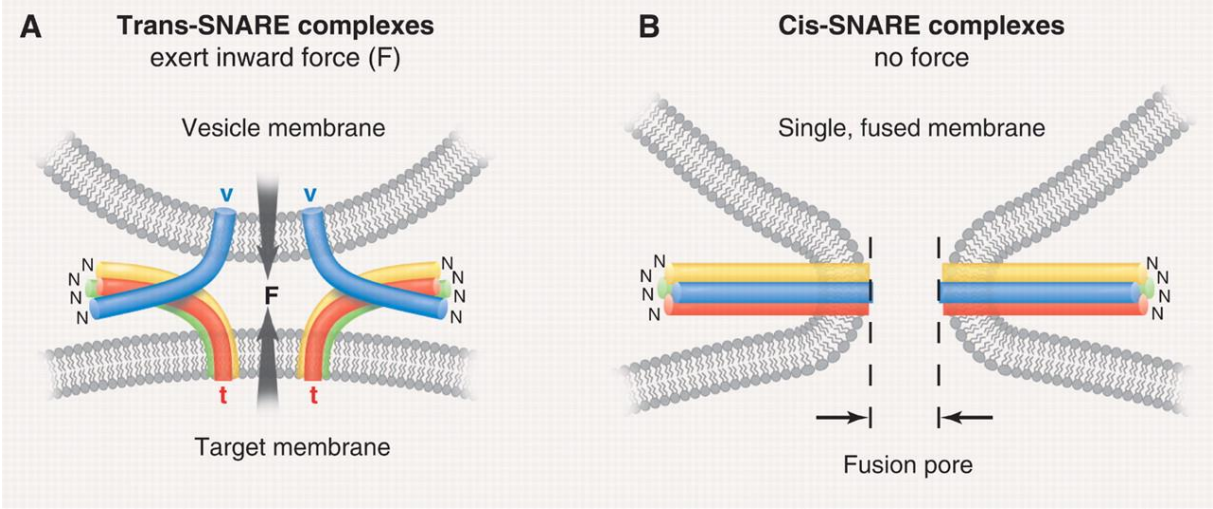

Figure 2 Trans- and cis-SNARE complexes. Science. 2009 Jan 23;323(5913):474-7.

(A) In the *trans*-SNARE complex, t-SNARE and v-SNARE reside in two opposite membranes.

(B) In the *cis*-SNARE complex, t-SNARE and v-SNARE reside in one same membrane.

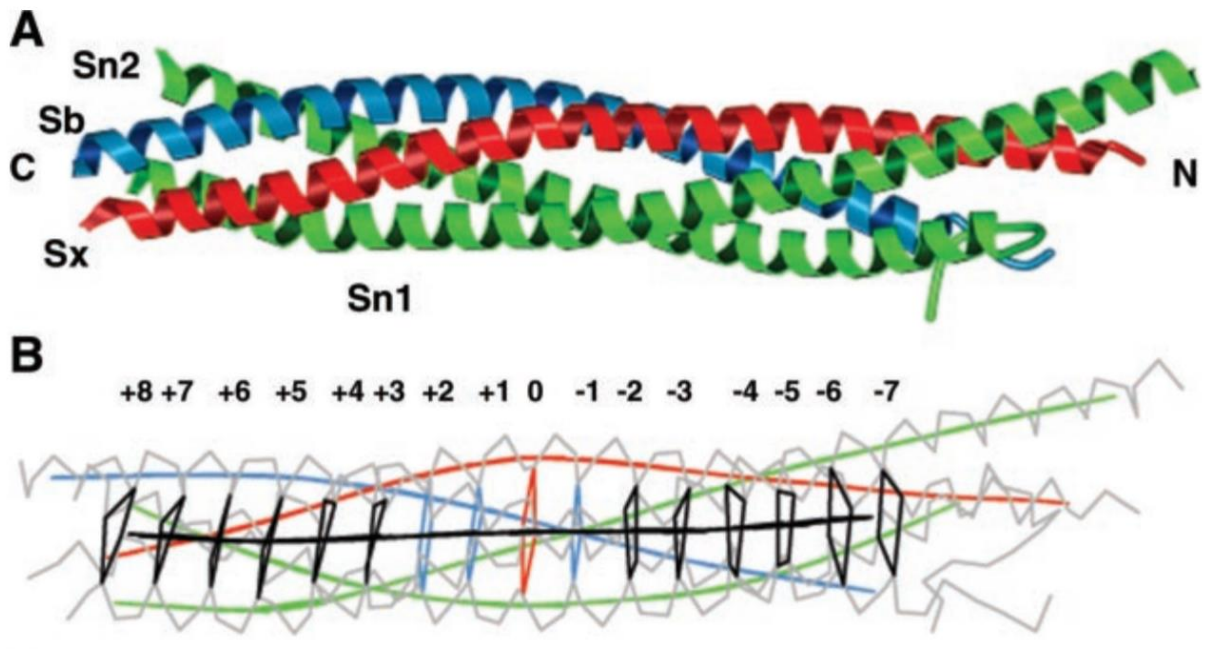

Figure 3 Crystal structure of the neuronal cis-SNARE complex. Am J Physiol Cell Physiol. 2003 Aug;285(2):C237-49.

(A)The neuronal *cis*-SNARE complex structure is a four-helix bundle. Syntaxin (red) contributes one helix (Sx). VAMP2 (blue) contributes one helix (Sb). SNAP-25 (green) contributes two helixes (Sn1 and Sn2). (B) The 16 layers of the SNARE complex, layer numbers (-7 to +8) are labeled on the top.

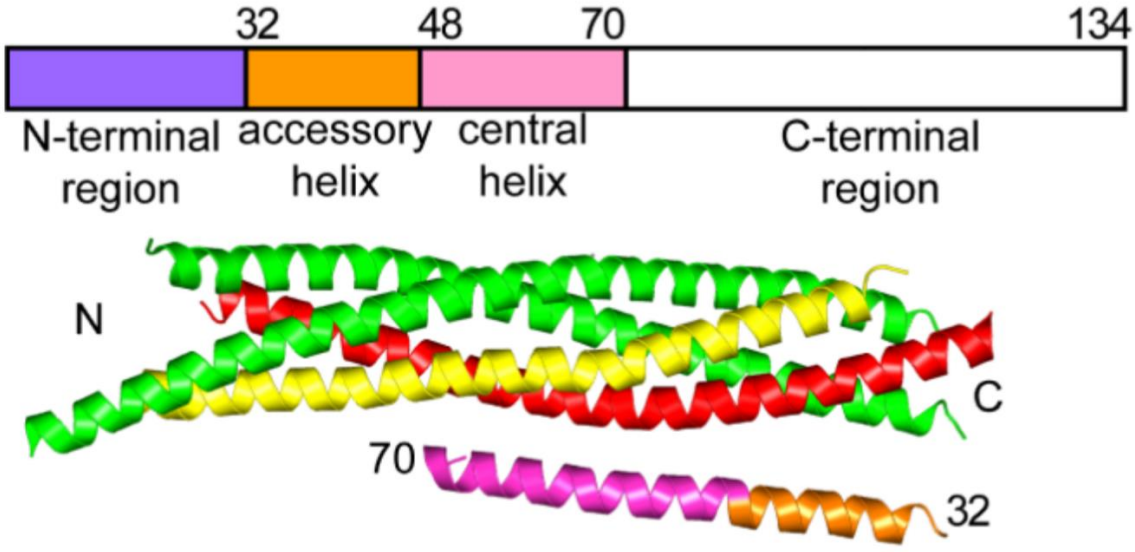

Figure 4 Cpx domains and the binding model. J Mol Biol. 2013 Sep 23; 425(18): 3461–3475.

Top: Cpx has four domains: the N-terminal domain, the C-terminal domain, the accessory helix domain and the central helix domain. Bottom: The Cpx-ternary SNARE complex binding model. Cpx binds and stabilizes the surfaces of syntaxin 1A (yellow) and VAMP2 (red). Cpx accessory helix is in orange and central helix is in pink. SNAP-25 is in green.

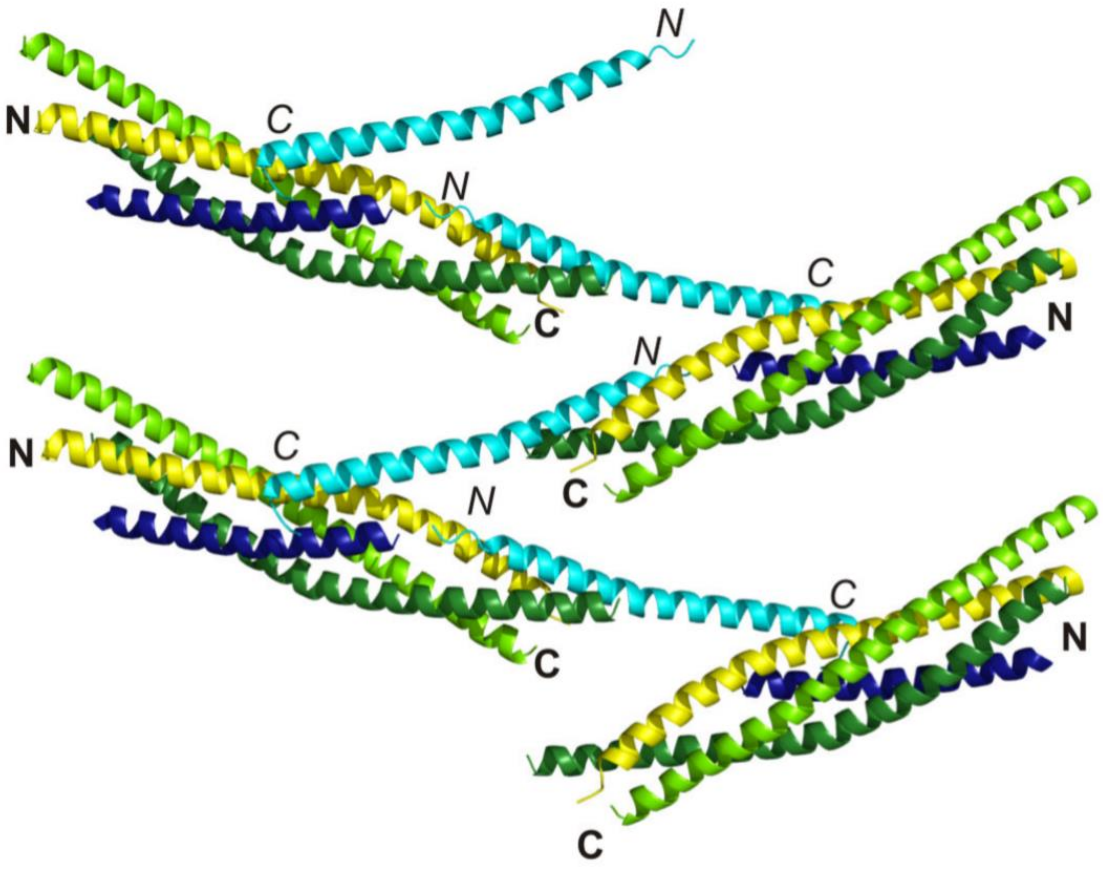

Figure 5 Cpx-SNARE zigzag array model. Nat Struct Mol Biol. 2011 Jul 24;18(8):927-33

The accessory helix domain and the central helix domain of one Cpx (residues 26-73, in cyan) cross-link two adjacent SNAREs. Syntaxin (residues 190-250) is in yellow. SNAP25 is in lime for N-terminal SNARE motif (residues 10-74) and green for C-terminal SNARE motif (residues 141-203). VAMP2 (residues 29-60) is in blue. Eventually, Cpx proteins and partially-zippered SNARE proteins can form a zigzag array structure.

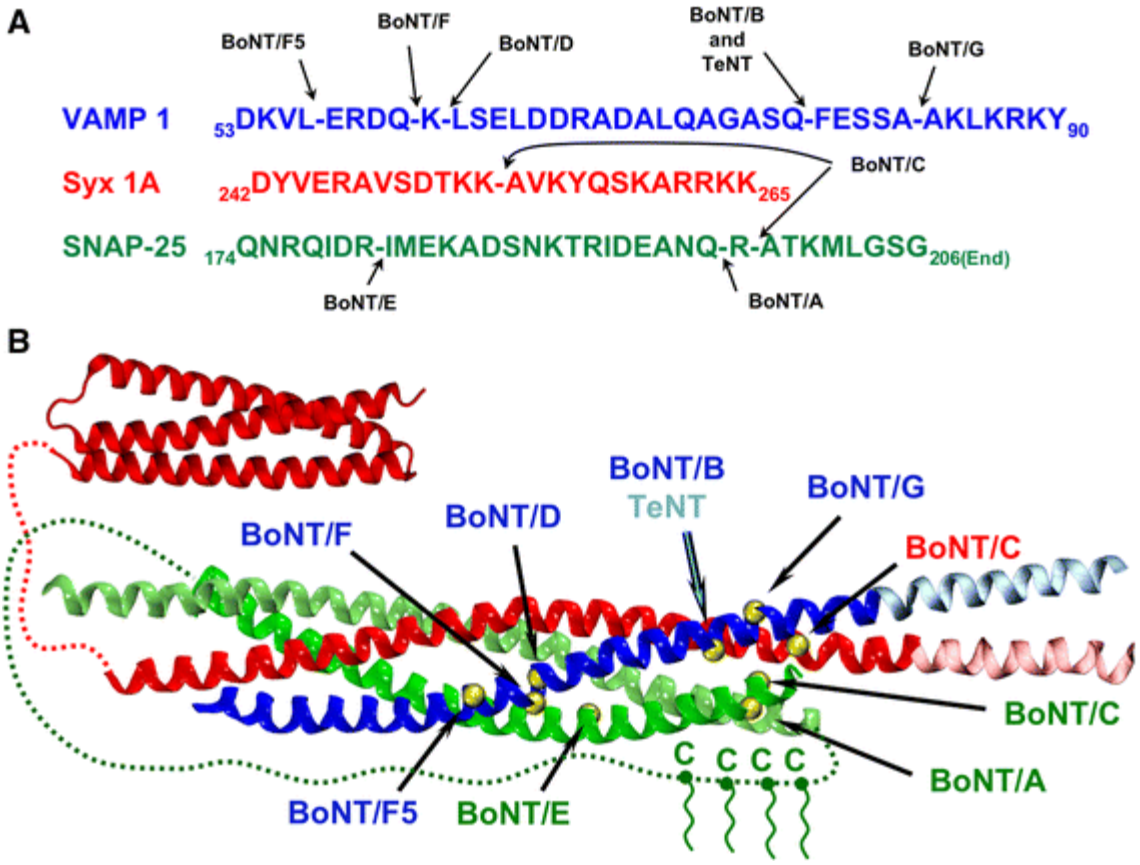

Figure 6 BoNTs selectively and specifically cleave different SNARE proteins at different sites. Cell. Mol. Life Sci. (2014) 71:793–811.

(A) There are seven major BoNT serotypes (donated BoNT A through G). BoNT A and BoNT E cleave SNAP-25 (green); BoNT type B, BoNT D, BoNT F and BoNT G only cleave VAMP (blue); and BoNT C cleaves both SNAP25 and syntaxin (red). BoNTs cleave different SNARE proteins at different residues. (B) BoNTs cleavage sites shown in the backbone ribbon drawing of the SNARE complex.

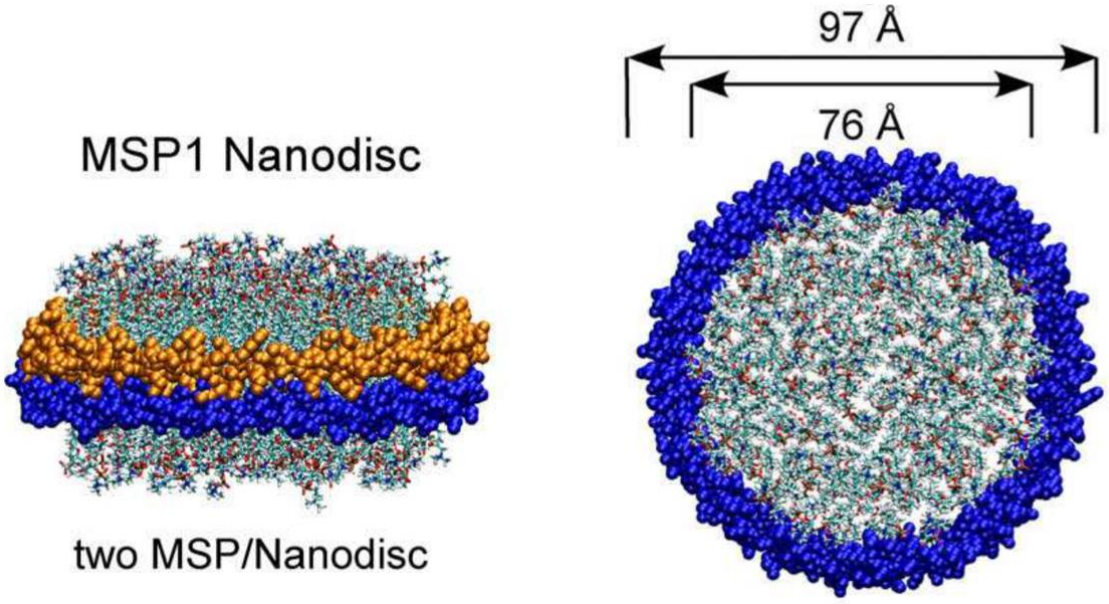

Figure 7 The structure of a Nanodisc. FEBS letters. 2010 May 3;584(9):1721-7.

In the nanodisc, the lipid bilayer is encircled by two membrane scaffolding proteins (MSPs, in blue and in gold). The diameter of an ApoA1 nanodisc is around 10nm. Left: side view of a nanodisc. Right: top view of a nanodisc.

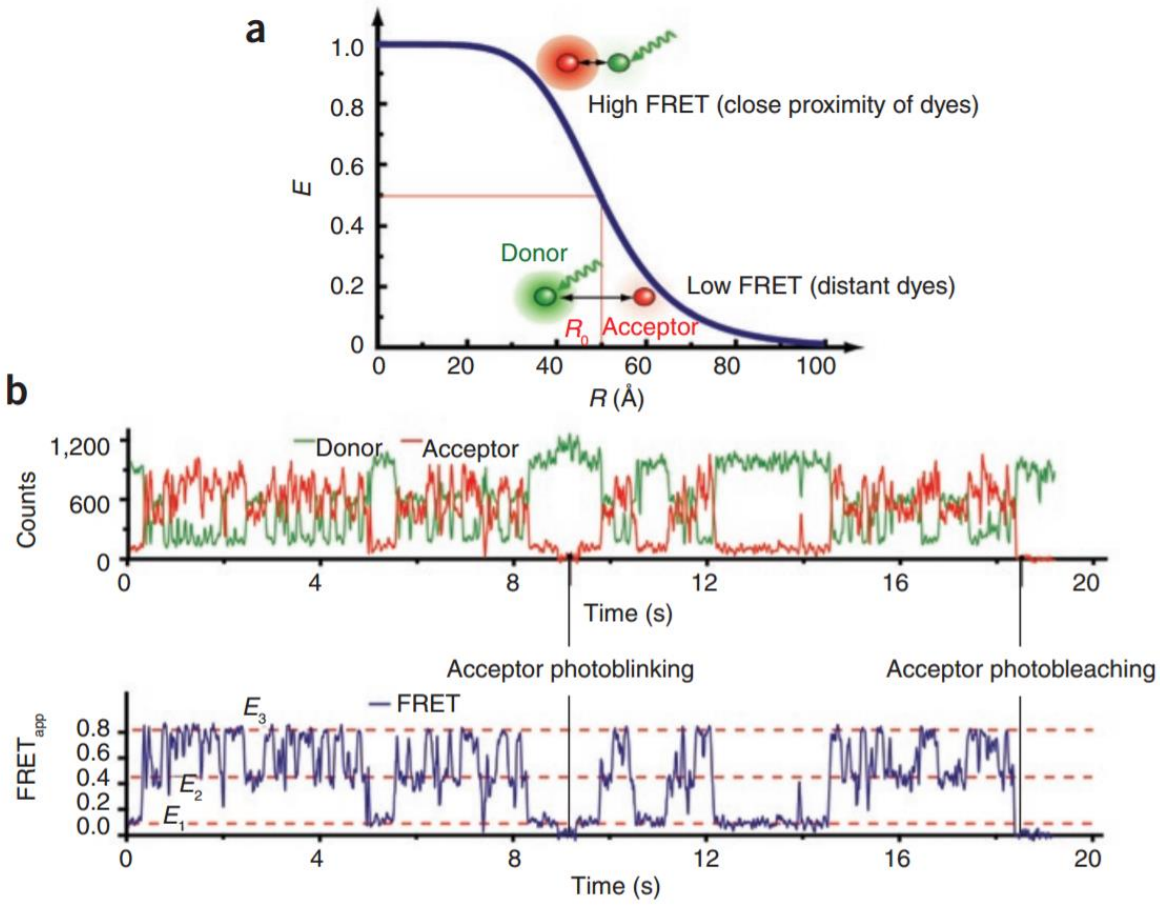

Figure 8 Single-molecule FRET dynamics. Nat Methods. 2008 Jun;5(6):507-16.

(a) The efficiency (*E*) transferred during FRET is dependent on the donor-acceptor inter-fluorophore distance (*R*). Single-molecule FRET can distinguish the distance changes according to the low and high FRET efficiency changes. (b) A representative fluctuating FRET trace from smFRET data. SmFRET provides us information of the real-time, transient asynchronous dynamics of individual molecules.

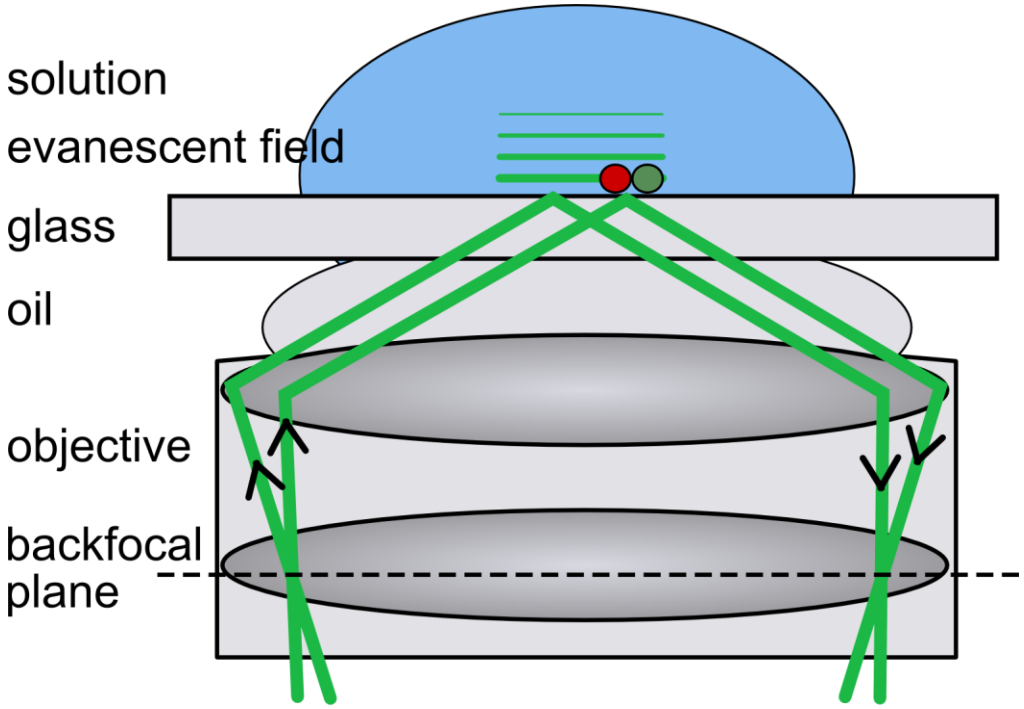

Figure 9 Total internal reflection microscopy generates evanescent field
https://www.wur.nl/en/show/Superresolution-Microscopy.htm

Total internal reflection microscopy generates the evanescent field (usually less than 200nm in depth). The evanescent field can selectively illuminate fluorescent molecules adjacent to the glass slide-solution interface.

CHAPTER 2: COMPLEXIN SPLITS THE MEMBRANE-PROXIMAL REGION OF A SINGLE SNAREPIN

Modified from a paper published in *Biochemical Journal (2016) 473(14), 2219-2224.*

Linxiang Yin*, Jaewook Kim*, and Yeon-Kyun Shin*[1]

*Roy J. Carver Department of Biochemistry, Biophysics, and Molecular Biology, Iowa State University, Ames, IA 50011, U.S.A.

[1]Corresponding author.

Abstract

Complexin (Cpx) is thought to be a major regulator of SNARE-dependent membrane fusion. Although the inhibition of membrane fusion by complexin has been frequently reported, its structural basis has been elusive and an anticipated disruption of the SNARE core has never been observed. Here, to mimic the natural environment, we assembled a single SNAREpin between two nanodisc membrane patches. Single molecule FRET detects a large conformational change, specifically at the C-terminal half, while no conformational change is observed at the N-terminal half. Our results suggest that complexin splits the C-terminal half of the SNARE core at least 10 Å, whereby inhibiting further progression of SNARE zippering and membrane fusion.

Introduction

In the neuron, soluble N-ethylmaleimide-sensitive factor attachment protein receptors (SNAREs) mediate vesicle fusion that releases neurotransmitters to the synaptic cleft. Vesicle-anchored (v-) SNARE associates with target membrane-anchored (t-) SNARE to form a complex that facilitates fusion of two membranes [1,2]. If unregulated, however, vesicle fusion would be spontaneous and random. Complexin (Cpx) is a small, soluble SNARE binding protein [3,4] that is believed to suppress such spontaneous fusion [4–7]. When evoked, a major Ca^{2+}-sensor synaptotagmin 1 (Syt1) triggers fast fusion [8,9], perhaps by lifting the Cpx clamp [10–12].

Presumably, Cpx may achieve the inhibition of spontaneous membrane fusion by blocking SNARE complex formation. However, the structural basis for such an inhibitory function of Cpx is hotly debated [13–17]. An X-ray structure shows that Cpx binds to the surface groove of the SNARE core, which is a four-helix bundle [18–20], in a conformation that stabilizes the structure instead of disrupting it [21]. Another X-ray structure shows that Cpx crosslinks two adjacent SNARE cores [22]. However, caveats of this study are that it was performed with a truncated v-SNARE in which a bulk of the C-terminal residues that have been proposed to compete with Cpx was removed and also the Cpx that was used was mutated to act as a super clamp. It is not yet elucidated that the wild type Cpx can form this crosslinking structure. Alternatively, Cpx is shown to be capable of displacing v-SNARE from the core structure but the results are purely computational and have not been verified experimentally [23].

Given the confusing results, one might wonder if the recombinant soluble SNARE core is a good model system to investigate the function of Cpx. In the absence of two opposing membranes, the isolated SNARE core is likely to represent the post fusion conformation. Thus,

previous structural studies of Cpx might be depicting the post fusion conformation with the isolated SNARE core rather than its involvement in the fusion process.

There is compelling evidence that cognate SNAREs zipper, starting from membrane distal N-terminal region and proceeds toward the membrane-proximal C-terminal region [24,25]. Consistent with this hypothesis, an intermediate in which the N-terminal half is zippered while the C-terminal half is frayed has been recently characterized [26–28]. One might wonder if this half-zippered SNARE complex is the primary target of Cpx and other regulators.

In this work, we investigated, using single molecule FRET, the effect of Cpx binding to a single *trans*-SNAREpin trapped in the nanodisc sandwich. Our results demonstrate that Cpx has the capacity to split t- and v-SNAREs at the C-terminal half while maintaining the core structure at the N-terminal, whereby Cpx inhibits SNARE complex formation and membrane fusion.

Materials and Methods

Plasmid Construct and Site-Directed Mutagenesis

DNA sequences encoding Syntaxin 1A (Syn1A, amino acids 1–288 with three cysteines replaced by alanines), SNAP-25 (amino acids 1–206 with four native cysteines replaced by alanines), VAMP2 (amino acids 1–116 with C103 replaced by alanines), soluble VAMP2 (amino acids 1–96), rat complexin 1 (Cpx, amino acids 1–134), N-terminal truncated Cpx (Cpx 27-134, amino acids 27–134) and N-terminal mutated Cpx (M5E/K6E, amino acids 1-134, M5 and K6 replaced with E) were inserted into the pGEX-KG vector as N-terminal GST fusion proteins. A

modified ApoA1 (amino acids, 27-267) was inserted into pNFXeX vector as an N-terminal His-tagged protein.

All cysteine mutants, including Syn1A I203C, Syn1A V241C, VAMP2 Q33C, VAMP2 A72C, soluble VAMP2 A72C and Cpx M5E/K6E were generated by the Quick Change site-directed mutagenesis. All DNA sequences were confirmed by the Iowa State University DNA Sequencing Facility.

Protein expression purification and fluorophore labeling

All recombinant proteins were expressed in *Escherichia coli* BL21 (DE3) cells. Cells were first grown in LB medium at 37 ℃, 200 rpm to an optical absorbance of 0.6-0.8 with 600 nm. 0.4 mM IPTG was added to induce the protein production. For Syn1A I203C, Syn1A V241C, VAMP2 Q33C, VAMP2 A72C, cells were further grown at 16 ℃, 100 rpm for another 14-16 hours. For soluble VAMP2 A72C, apoA1 and Cpx, cells were grown at 20 ℃, 100 rpm for another 14-16 hours after induction.

For GST-tagged proteins, cell pellets were resuspended in 15 mL of PBST (PBS, pH 7.4, containing 0.2 v% Triton X-100) for membrane proteins and 15 mL of PBS (pH 7.4) for the soluble proteins with final concentrations of 1 mM 4-(2-aminoethyl)-benzenesulfonyl fluoride (AEBSF) and 4mM DTT.

Cells were lysed by sonication in ice bath and centrifuged at 14,000rpm for 30 min at 4 °C. Except for apoA1, the supernatant was incubated with 2 mL GST beads at 4 °C for 2 hours. The proteins were then eluted by 0.02unit/μl thrombin in cleavage buffer (PBS, pH 8.0, containing 2 mM DTT) with/without 0.8 wt% n-octyl-D-glucopyranoside (OG) for membrane and soluble

proteins, respectively. ApoA1 was purified with the same protocol except for using the Ni-NTA column. Purified proteins were examined with 15% (wt/vol) SDS-PAGE, and the purity was at least 85% for all proteins and the concentrations was measured with RC DC kit (BioRad).

Single cysteine mutants of syntaxin-1a (I203C, V241C), soluble VAMP2 (A72C） and VAMP-2 (Q33C, A72C) were desalted with a PD MiniTrap G-25 column (GE Healthcare) to eliminate free DTT and then incubated with a 10× molar excess of maleimide-derivative fluorophore Cy5 (indodicarbocyanine) or Cy3 (indocarbocyanine), respectively overnight at 4°C. The labeled protein was purified using the PD MiniTrap G-25 column and free dye was further separated from the protein sample using centrifugal filters (Amicon). The labelling efficiency of each SNARE protein was measured spectrophotometrically (Beckman). Further details can be found in our previous paper [26].

Lipid reconstitution and purification of SNARE-incorporated nanodiscs

To generate homogeneously sized nanodiscs, POPC, DOPS, cholesterol, PIP2, and biotin-PEG-DSPE (Avanti Polar Lipids) lipid mixture with a molar ratio of 62.9:15:20:2:0.1 was used for t-nanodiscs and *cis*-SNAREpin nanodiscs. The v-nanodiscs were comprised of POPC, DOPS and cholesterol with a molar ratio of 75:5:20. The lipid mixture was initially dried with the nitrogen gas and incubated under vacuum for 6-8 hours and then resuspended with HEPES buffer (25 mM HEPES, pH 7.4, 150 mM KCl) to a final concentration of 50 mM.

Then 5 μL of 50mM resuspended lipid mixture was first dissolved in sodium cholate such that the final concentration of sodium cholate was 50 mM after apoA1 and SNARE proteins were added. Then the t-SNARE binary complex (syntaxin-1a and SNAP-25 with a molar ratio of 1:2,

pre-incubated at room temperature for 1 hour), *cis*-ternary SNARE complex (syntaxin-1a, SNAP-25 and VAMP2 or soluble VAMP2 with a molar ratio of 1:2:1, pre-incubated at 4°C overnight) or VAMP2 and apoA1 were added to the detergent-solubilized lipid mixture. The molar ratio of lipids, apoA1 and SNARE(s) was 300:5:1. After incubating for 20 mins, the self-assembly of SNARE-incorporated nanodiscs was initiated via rapid removal of sodium cholate by adding 50% (w/v) SM-2 Bio-Beads (Bio-Rad). The t-, v- or *cis*-nanodiscs were then purified through gel filtration using a Superdex^{TM} 200 GL 10/300 column (GE Healthcare).

Preparation of *trans*- and *cis*-SNAREpin nanodisc on the imaging surface for TIR

The imaging surface was prepared by coating the quartz surface with a solution of methoxypolyethylene glycol and biotin-PEG molecules (100:1). Flow chambers were assembled between the quartz slide and coverslip. Streptavidin (0.2 mg/ml was introduced into and washed from the flow chamber for subsequent nanodisc immobilization via biotin-streptavidin conjugation.

For experiments with *trans*-SNAREpin nanodiscs, t-nanodiscs were immobilized on the surface and the unbound t-nanodiscs were washed out. Then v-nanodiscs were introduced into the flow chamber and incubated for 45 min to allow formation of a *trans*-SNAREpin between two nanodiscs (Figure 1). The unbound v-nanodiscs were then washed out.

For experiments with WT and Cpx mutants, a 2 μM solution of the appropriate Cpx was injected into the flow chamber prior to the v-nanodisc injection and incubated for 10 min at room temperature (~25 °C). Subsequent solutions were prepared such that the Cpx or Cpx mutant concentration was maintained throughout the experiments.

For experiments with *cis*-SNAREpins, a premixed solution of *cis*-SNAREpin nanodiscs and Cpx was prepared and injected into the flow chamber and unbound nanodiscs were washed out. 2 μM concentrations of Cpx was maintained throughout the experiments.

The imaging of the samples was performed at room temperature with the oxygen scavenger system (0.4% (w/v) glucose (Sigma), 4 mM Trolox (Calbiochem), 1 mg/ml glucose oxidase (Sigma), 0.04 mg/ml catalase (Calbiochem)) in HEPES buffer with/without 2 μM Cpx. Further details can be found in our previous paper [26].

Data analysis of TIR image recordings

We analyzed the traces from the TIR recordings using a home-made software. The first 10-20 frames were recorded with excitation by red laser (635 nm) in order to identify spots with t-nanodisc with Cy5. Then the light is switched to the green laser (532 nm) to select the *trans*-SNAREpin nanodisc sandwich or *cis*-SNAREpin nanodisc with both Cy3 (donor) and Cy5 (acceptor), which are characterized by the co-localized spots on both the acceptor and donor signal channel.

From the selected spots, the acceptor and donor time traces were analyzed to obtain the FRET histograms. Because we seldom observed any significant transitions in the FRET value with our time resolution (200 ms per frame), we assigned a single FRET value (mean) for each *trans*- or *cis*-SNAREpin nanodisc (Figure 2b). We averaged FRET efficiency within the period in which both dyes were photon emitting. The rarely observed transitioning or fluctuating spots were not included in the histograms (Figure 2c).

Results

Cpx splits the C-terminal region of a single SNAREpin in the nanodisc sandwich.

In order to understand the involvement of Cpx during the fusion process, we investigate single *trans*-SNAREpin in the chasm of two membranes using single-molecule (sm) FRET [26]. First, we prepared labeled proteins, the fluorescence donor Cy3 was attached site-specifically to an engineered cysteine on v-SNARE VAMP2 while the acceptor Cy5 was attached to t-SNARE syntaxin 1a. We prepared two sets of dye pairs, one at the N-terminal residues (NN pair, Figure 1a and 1b) and the other at the C-terminal residues (CC pair, Figure 1c and 1d) to separately monitor the conformational changes in the N- terminal region from those in the C-terminal region.

The Cy3-labeled VAMP2 was incorporated into one population of the nanodisc (v-nanodisc). Meanwhile, the Cy5-labeled syntaxin 1A was premixed with recombinant SNAP-25 and incorporated into another population of the nanodisc (t-nanodisc). The v- and t-nanodiscs were separately purified with FPLC. The protein concentration was adjusted in order to ensure that most nanodiscs had a single SNARE protein, which was later verified with photobleaching (Figure 2a).

The t-nanodiscs, doped with biotin-PEG-DSPE, were introduced into the flow cell and immobilized onto the PEGylated imaging surface. The v-nanodiscs were then injected into the flow cell to allow for the formation of the *trans*-SNAREpin in the middle of the nanodisc sandwich. The co-localized dots on the microscope image which have both the acceptor (Cy5) and donor signals (Cy3) were selected and the FRET efficiencies for the individual nanodisc pairs were analyzed (Figure 1 and 2b).

For the NN pair, the population is distributed around the FRET efficiency E=0.75, consistent with short distance between the acceptor and the donor, which may reflect the robust

helical structure at the N-terminal region. When 2 μM Cpx is added to this sample, no appreciable change in the population distribution of the FRET histogram is observed, indicating that Cpx has little effect on the SNARE conformation at the N-terminal region (Figure 1a and b).

For the CC pair, however, we observe two distinctly separated distributions, one peaked at E=0.2 and the other at E=0.8, with nearly equal counts (Figure 1c). The high FRET population reflects the fully zippered species while those at low FRET are from the half-zippered intermediate. It appears that these two species are energetically balanced to borne out near equal populations. We observe transitions between two states in a small number of time traces (<2%), indicating that it is likely to be a slow equilibrium (Figure 2c).

Surprisingly, when Cpx is added into the sample with the CC pair a single distribution peaked at E=0.5 emerges. The population at low FRET and those at high FRET are both pulled into the middle (Figure 1d). Average distance changes from high FRET to middle FRET and from low FRET to middle FRET are estimated to be approximately 10-15 Å. Such rearrangements of the distribution reflect a significant conformational change for both fully zippered and half-zippered conformations. In particular, the disappearance of the high FRET distribution indicates that t- and v-SNAREs in the C-terminal region split at least 10 Å on average, most likely due to the insertion of Cpx into the SNARE core.

The *cis*-SNARE complex shows no splitting by Cpx.

It has been previously shown that Cpx binds to the surface groove of the isolated SNARE core without causing structural disruption [21]. As controls, we investigate the effect of Cpx binding to *cis*-SNARE complexes. We prepared two types of *cis*-complexes; one sample with VAMP2, syntaxin 1a and SNAP25 anchored to the nanodisc with the transmembrane domains of

VAMP2 and syntaxin 1a (Figure 3a). In another sample, we prepared a nanodisc with soluble VAMP2, such that the *cis*-SNAREpin is anchored to the nanodisc with one transmembrane helix (Figure 3b). In both cases, in the absence of Cpx, we observe a single high FRET population with some minor populations in the low FRET region, consistent with fully zippered SNARE complex. Even when Cpx is added to samples we do not observe any appreciable change in the FRET distribution, indicating that no splitting between t- and v-SNAREs occurs in the presence of Cpx. Thus, the results show that, for the *cis*-SNAREpin, Cpx is incapable of inserting into the SNARE core and that *trans*-binding of v- and t-SNAREs to opposite membranes is necessary for Cpx insertion into the SNARE core. We observe a slight increase in the low FRET population when both transmembrane helices are present (Figure 3a and 3c) compared with just one, reflective of relative dynamic movement of the two transmembrane helices in the nanodisc membrane. Also, the high FRET peak of the *cis*-complex is shifted to a higher FRET value (Figure 3a), compared to the *trans*-complex (Figure 1c), which is indicative of a more compact structure.

The N-terminal region of Cpx plays a role in restructuring the *trans*-SNAREpin.

It was previously shown that Cpx mutants M5E/K6E, in which two N-terminal positions 5 and 6 are altered, and Cpx27-134, in which N-terminal 26 residues were deleted, both suppress spontaneous fusion significantly [29,30]. We investigate these mutants with our SNARE zippering assay to look for the structural basis for the enhanced fusion-suppressing activity of the Cpx mutants.

When the Cpx double mutant M5E/K6E is added to the nanodisc sandwich, harboring the SNAREpin with the CC pair, we observe the disappearance of the high FRET population and the appearance of the middle FRET population as it was observed for wild-type (WT) Cpx. However,

the low FRET population did not shift towards the middle FRET region in contrast to what was observed for WT Cpx (Figure 4). Thus, the results show that while the mutant still maintains the ability to insert into and split the SNARE core, it loses some capacity to induce a conformational change that causes the v-SNARE to come closer to the t-SNAREs. We find that the effect of Cpx27-134 is very similar to that of Cpx M5E/K6E (Figure 4a and 4b). Thus, the results show that the N-terminal sequence of Cpx plays a role in inducing a conformational change in the v-SNARE VAMP2 to keep v- and t-SNAREs closer than that in the half-zippered intermediate.

Discussion

In this work, we demonstrate that Cpx has the capacity to insert into and split the SNARE core, specifically in the C-terminal region, which may serve as a mechanism to inhibit SNARE zippering and membrane fusion. Such splitting is observed only when the SNAREpin is attached in *trans*- to two opposed membrane patches but it is not seen when SNAREpin is attached to one nanodisc, either by one or two transmembrane domains. Thus, our results show that the repulsive force between two membranes is necessary for the proper Cpx function and two opposed membranes are an integral part of the regulatory machinery for synaptic vesicle fusion.

A previous EPR study revealed that the low FRET species corresponds to the half-zippered SNARE intermediate in which C-terminal half of the VAMP2 SNARE motif is completely unstructured with an average distance of 65 Å. Our results show that Cpx has the ability to pull the extreme ends of v- and t-SNAREs to be approximately 50 Å. We speculate that it involves a conformational change in C-terminal half of VAMP2, most likely from a random coil to a α-helix. A hypothetical model that represents such con-formational changes is depicted in Figure 1(d).

While our data suggests that Cpx might insert into a single SNARE core it is possible that Cpx might be able bring together the two opposing lipid membranes to a point where the half zippered *trans*-SNAREpin exhibits mid-FRET (CC pair) but the steric hindrance of Cpx could cause the high-FRET population to be shifted lower, converging into a single mid-FRET population. We also note that Rothman and coworkers proposed the possibility of Cpx binding to one SNAREpin and inserting, in *trans*-, to a neighboring SNAREpin [22]. We do not observe such *trans*- insertion in our single molecule SNARE zippering assay. But, our experiments operate under very low concentrations (100 pM range). The fusion site between synaptic vesicles and the plasma membrane bears a clouded environment. Therefore, we cannot rule out the possibility of such cross-binding occurring in synaptic vesicle fusion.

Care must be taken when relating Cpx induced conformational changes in the SNARE core to the evoked release. In evoked release, the three-way interactions among Cpx, Syt1, and SNAREs would determine the efficiency and the time scales of vesicle fusion. Therefore, more work is definitely necessary to comprehend to fully understand the Cpx phenotypes in evoked fusion. Whether Cpx inhibits spontaneous fusion or whether clamping of vesicle fusion by Cpx is necessary for synchronization or not are hotly debated controversial issues [13–15]. Certainly, further work is needed to sort out the Cpx function in synaptic vesicle fusion. Studies of the interaction between Cpx and SNAREpin will serve as a good starting point towards understanding the exquisite regulatory mechanism of synaptic vesicle fusion.

Author Contributions

Yeon-Kyun Shin and Linxiang Yin designed experiments. Linxiang Yin performed all experiments. Jaewook Kim wrote the computer program for the data analysis. Yeon-Kyun Shin, Linxiang Yin and Jaewook Kim wrote the paper.

Acknowledgements

This work was supported by the National Institutes of Health [grant number R01 GM051290 (to Y.-K.S.)].

References

1 Sudhof, T. C. and Rothman, J. E. (2009) Membrane fusion: grappling with SNARE and SM proteins. Science. **323**, 474–477.

2 Wickner, W. and Schekman, R. (2008) Membrane fusion. Nat. Struct. Mol. Biol. **15**, 658–664.

3 Ishizuka, T., Saisu, H., Odani, S. and Abe, T. (1995) Synaphin: a protein associated with the docking/fusion complex in presynaptic terminals. Biochem. Biophys. Res. Commun. **213**, 1107–1114.

4 McMahon, H. T., Missler, M., Li, C. and Sudhof, T. C. (1995) Complexins: Cytosolic proteins that regulate SNAP receptor function. Cell. **83**, 111–119.

5 Maximov, A., Tang, J., Yang, X., Pang, Z. P. and Südhof, T. C. (2009) Complexin controls the force transfer from SNARE complexes to membranes in fusion. Science. **323**, 516–521.

6 Hobson, R. J., Liu, Q., Watanabe, S. and Jorgensen, E. M. (2011) Complexin maintains vesicles in the primed state in C. elegans. Curr. Biol. **21**, 106–113.

7 Huntwork, S. and Littleton, J. T. (2007) A complexin fusion clamp regulates spontaneous and synaptic growth. Nat. Neurosci. **10**, 1235–1237.

8 Fernández-Chacón, R., Königstorfer, A., Gerber, S. H., García, J., Matos, M. F., Stevens, C. F., Brose, N., Rizo, J., Rosenmund, C. and Südhof, T. C. (2001) Synaptotagmin I functions as a calcium regulator of release probability. Nature. **410**, 41–49.

9 Chapman, E. R. (2008) How does synaptotagmin trigger neurotransmitter release? Annu. Rev. Biochem. **77**, 615–641.

10 Giraudo, C. G., Eng, W. S., Melia, T. J. and Rothman, J. E. (2006) A clamping mechanism involved in SNARE-dependent exocytosis. Science. **313**, 676–680.

11 Tang, J., Maximov, A., Shin, O. H., Dai, H., Rizo, J. and Sudhof, T. C. (2006) A Complexin/Synaptotagmin 1 Switch Controls Fast Synaptic Vesicle Exocytosis. Cell. **126**, 1175–1187.

12 Schaub, J. R., Lu, X., Doneske, B., Shin, Y. and Mcnew, J. A. (2006) Hemifusion arrest by complexin is relieved by Ca2+–synaptotagmin I. Nat. Struct. Mol. Biol. **13**, 748–750.

13 Xue, M., Stradomska, A., Chen, H., Brose, N., Zhang, W., Rosenmund, C. and Reim, K. (2008) Complexins facilitate neurotransmitter release at excitatory and inhibitory synapses in mammalian central nervous system. Proc. Natl. Acad. Sci. U. S. A. **105**, 7875–7880.

14 Yang, X., Cao, P. and Südhof, T. C. (2013) Deconstructing complexin function in activating and clamping Ca2+-triggered exocytosis by comparing knockout and knockdown phenotypes. Proc. Natl. Acad. Sci. U. S. A. **110**, 20777–20782.

15 Trimbuch, T. and Rosenmund, C. (2016) Should I stop or should I go? The role of complexin in neurotransmitter release. Nat. Rev. Neurosci. **17**, 118–125.

16 Trimbuch, T., Xu, J., Flaherty, D., Tomchick, D. R., Rizo, J. and Rosenmund, C. (2014) Re-examining how complexin inhibits neurotransmitter release: SNARE complex insertion or electrostatic hindrance? Elife. **3**, e02391.

17 Krishnakumar, S. S., Li, F., Coleman, J., Schauder, C. M., Pincet, F., Rothman, J. E. and Reinisch, K. M. (2015) Re-visiting the trans insertion model for complexin clamping. Elife. **4**, e04463.

18 Poirier1, M. A., , Wenzhong Xiao, J. C. M., Chan1, C., Shin, Y.-K. and Bennett, and M. K. (1998) The synaptic SNARE complex is a parallel four- stranded helical bundle. Nat. Struct. Biol. **5**, 765–769.

19 Stein, A., Weber, G., Wahl, M. C. and Jahn, R. (2009) Helical extension of the neuronal SNARE complex into the membrane. Nature. **460**, 525–528.

20 Sutton, R. B., Fasshauer, D., Jahn, R. and Brunger, A. T. (1998) Crystal structure of a SNARE complex involved in synaptic resolution exocytosis at 2. 4 A˚ resolution. Nature.**395**, 347–353.

21 Chen, X., Tomchick, D. R., Kovrigin, E., Arac, D., Machius, M. and Su, T. C. (2002) Three-Dimensional Structure of the Complexin / SNARE Complex. Neuron. **33**, 397–409.

22 Kümmel, D., Krishnakumar, S. S., Radoff, D. T., Li, F., Giraudo, C. G., Pincet, F., Rothman, J. E. and Reinisch, K. M. (2011) Complexin cross-links prefusion SNAREs into a zigzag array. Nat. Struct. Mol. Biol. **18**, 927–933.

23 Giraudo, C. G., Garcia-Diaz, A., Eng, W. S., Chen, Y., Hendrickson, W. A., Melia, T. J. and Rothman, J. E. (2009) Alternative zippering as an on-off switch for SNARE-mediated fusion. Science. **323**, 512–516.

24 Sørensen, J. B., Wiederhold, K., Milosevic, I. and Groot, B. L. De. (2006) Sequential N- to C-terminal SNARE complex assembly drives priming and fusion of secretory vesicles. EMBO J. **25**, 955–966.

25 Fiebig, K. M., Rice, L. M., Pollock, E. and Brunger, A. T. (1999) Folding intermediates of SNARE complex assembly. Nature. **6**, 117–123.

26 Shin, J., Lou, X., Kweon, D., Shin, Y. and Korea, S. (2015) Multiple conformations of a single SNAREpin between two nanodisc membranes reveal diverse pre-fusion states. Biochem. J. **459**, 95–102.

27 Gao, Y., Zorman, S., Gundersen, G., Xi, Z., Ma, L., Sirinakis, G., Rothman, J. E. and Zhang, Y. (2012) Single Reconstituted Neuronal SNARE Complexes Zipper in Three Distinct Stages. Science. **337**, 1340–1344.

28 Min, D., Kim, K., Hyeon, C., Cho, Y. H., Shin, Y. and Yoon, T. (2013) Mechanical unzipping and rezipping of a single SNARE complex reveals hysteresis as a force-generating mechanism. Nat. Commun. **4**, 1705–1710.

29 Xue, M., Reim, K., Chen, X., Chao, H.-T., Deng, H., Rizo, J., Brose, N. and Rosenmund, C. (2007) Distinct domains of complexin I differentially regulate neurotransmitter release. Nat. Struct. Mol. Biol. **14**, 949–958.

30 Xue, M., Craig, T. K., Xu, J., Chao, H.-T., Rizo, J. and Rosenmund, C. (2010) Binding of the complexin N terminus to the SNARE complex potentiates synaptic-vesicle fusogenicity. Nat. Struct. Mol. Biol. **17**, 568–575.

Figures with Titles and Legends

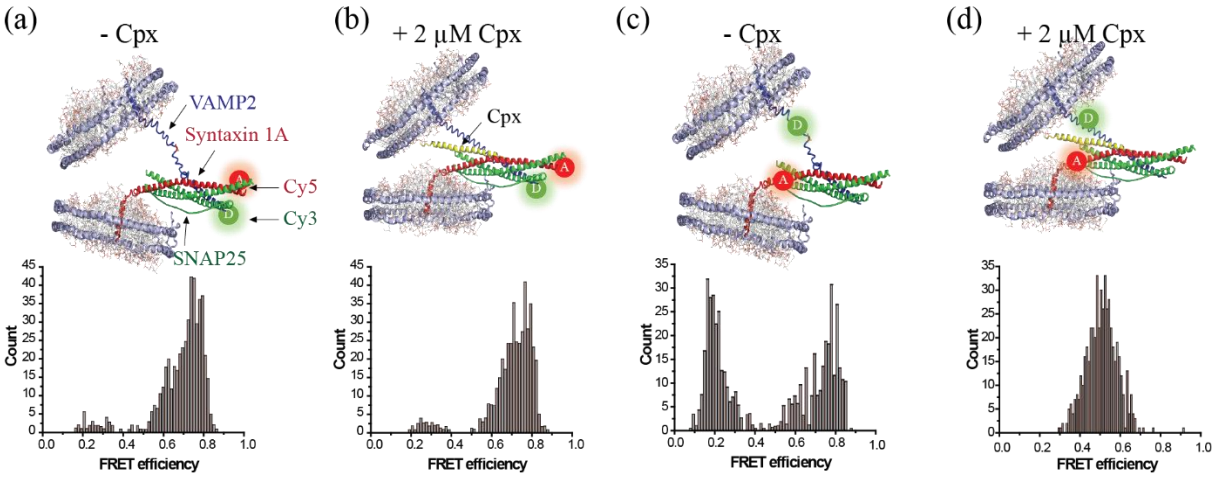

Figure 1 Cpx splits the C-terminal region of a single SNAREpin in the nanodisc sandwich.

(a) Nanodisc sandwich harboring a single SNAREpin with the FRET pair at the N-terminal region (NN). VAMP2 Q33C-Cy3 and syntaxin 1a I203C-Cy5 are used for NN. The majority of the population is distributed in the high FRET region. (b) 2 μM Cpx does not affect the FRET distribution of NN. (c) Nanodisc sandwich harboring a SNAREpin with the FRET pair at the C-terminal region (CC). VAMP2 A72C-Cy3 and syntaxin 1a V241C-Cy5 were used to make CC. The distribution shows two distinct populations in the high and in the low FRET regions, but little in the mid FRET region. (d) 2 μM Cpx pulls both the low and high FRET populations towards the mid FRET region. All experiments were independently conducted at least 4 times. Total of 499, 446, 502 and 524 traces was analyzed for (a), (b), (c), and (d), respectively.

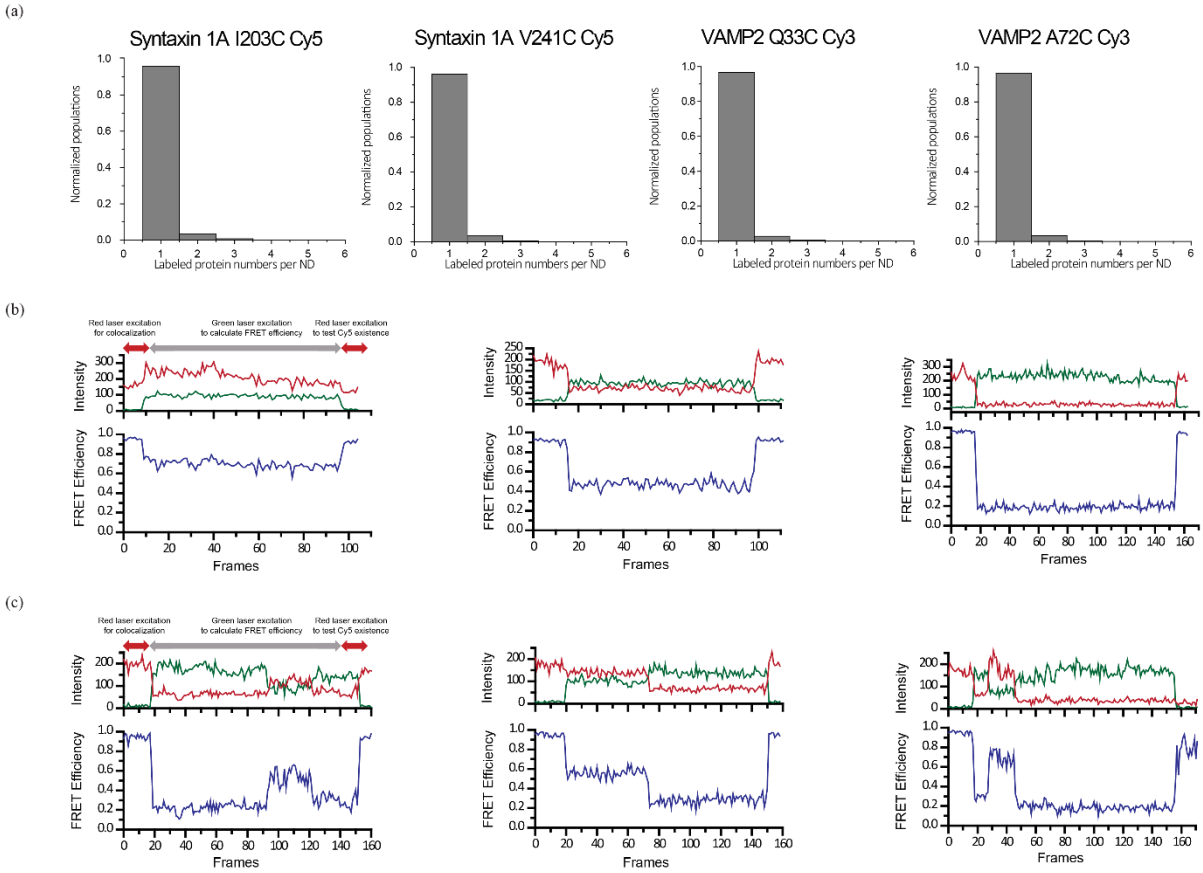

Figure 2 Single-molecule FRET for nanodisc sandwiches with SNAREs.

(a) Photobleaching experiment to confirm number of labeled SNARE proteins in a single nanodisc. Distribution of Syntaxin 1a I203C Cy5, Syntaxin 1a V241C Cy5 VAMP2 A72C Cy3 and VAMP2 Q33C Cy3, from left to right. (b) Representative FRET traces from nanodisc sandwiches for high, middle and low FRET, from left to right. (c) Representative fluctuating FRET traces from nanodisc sandwiches for low-high-low, high-low and low-high-bleached FRET, from left to right. Such traces are rarely observed (<2%). The samples were initially excited with the red laser in order to find co-localized FRET pairs. The FRET efficiency of the specimen was calculated from the region depicted by grey arrows.

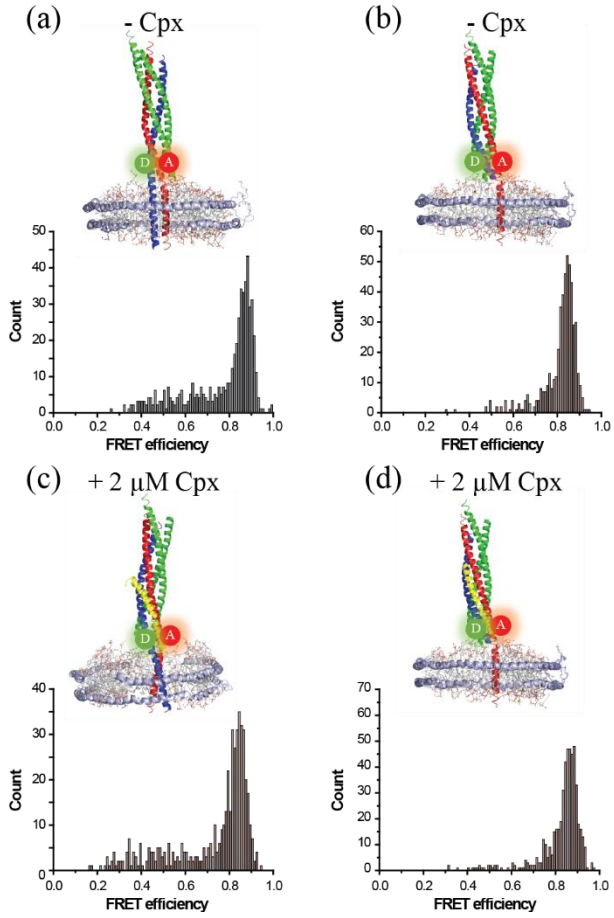

Figure 3 The cis-SNARE complex shows no splitting by Cpx.

The cis-SNAREpin with the CC FRET pair with one transmembrane domain (a) or two (b), respectively. (c), (d) 2 μM Cpx does not affect the cis-SNARE complex. All experiments were independently conducted at least 4 times. Total of 516, 499, 489 and 517 traces was analyzed for (a), (b), (c), and (d), respectively.

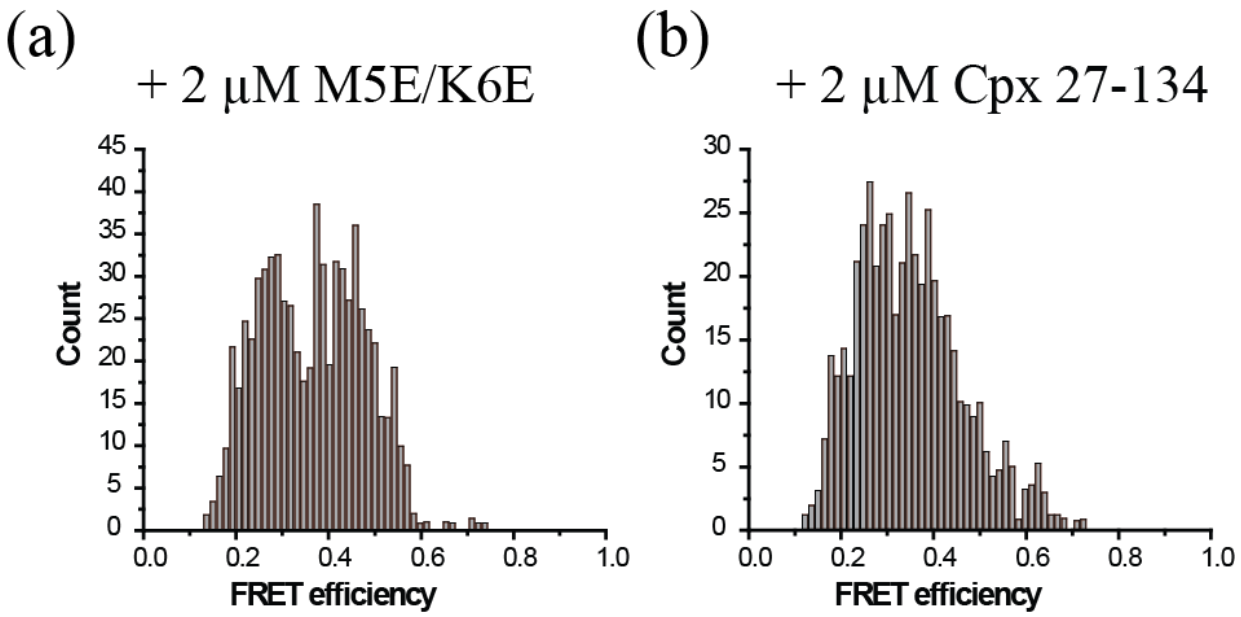

Figure 4 The N-terminal region of Cpx plays a role in restructuring the trans-SNAREpin.

Both N-terminal Cpx mutants (a) M5E/K6E and (b) Cpx 27-134 can pull the high FRET population down to mid FRET for CC. However, they are incapable of pushing the low FRET population to the mid FRET region. All experiments were independently conducted 4 times. Total of 704 and 494 traces was analyzed for (a) and (b), respectively.

CHAPTER 3: BOTULINUM TOXINS A AND E INFLICT DYNAMIC DESTABILIZATION ON T-SNARE TO IMPAIR SNARE ASSEMBLY AND MEMBRANE FUSION.

Modified from a paper published in *Structure (2017) 25 (11), 1679-1686. e5*

Ryan Khounlo[1,2], Jaewook Kim[1,2], Linxiang Yin[1,2], and Yeon-Kyun Shin[1,3,*]

[1]Roy J. Carver Department of Biochemistry, Biophysics & Molecular Biology, Iowa State University, Ames, IA 50011, USA

[2]These authors contributed equally

[3]Lead Contact

Abstract

Botulinum toxins (BoNT) A and E block neurotransmitter release by specifically cleaving the C-terminal ends of SNAP-25, a plasma membrane SNARE protein. Here, we find that SNAP-25A and E, the cleavage products of BoNT A and E respectively, terminate membrane fusion via completely different mechanisms. Combined studies of single molecule FRET and single vesicle fusion assays reveal that SNAP-25E is incapable of supporting SNARE pairing and thus, vesicle docking. In contrast, SNAP-25A facilitates robust SNARE pairing and vesicle docking with somewhat reduced SNARE zippering, which leads to severe impairment of fusion pore opening. The EPR results show that the discrepancy between SNAP-25A and E might stem from the extent of the dynamic destabilization of the t-SNARE core at the N-terminal half which plays a pivotal role in nucleating SNARE complex formation. Thus, the results provide insights into the structure/dynamics-based mechanism by which BoNT A and E impair membrane fusion.

Introduction

Synaptic communication involves neurotransmitter release from the neuron to the synaptic cleft. The release of neurotransmitters requires synaptic vesicle docking onto the target plasma membrane, formation of a fusion pore, and complete fusion of two membranes. It is widely believed that this membrane fusion process is mediated by soluble N-ethylmaleimide-sensitive factor attachment protein receptors (SNAREs). The SNARE proteins consist of VAMP2 on the synaptic vesicle (v-SNARE) and syntaxin 1A and SNAP-25 on the target membrane (t-SNAREs). The cognate v- and t-SNAREs, when brought into proximity, form a highly stable ternary SNARE complex that is thought to drive fusion of two membranes (Jahn and Scheller, 2006; Rizo and Rosenmund, 2008; Sudhof and Rothman, 2009; Wickner and Schekman, 2008).

More specifically, the highly conserved SNARE motifs, one from syntaxin 1A, two from SNAP- 25 and one from VAMP2, assemble into a parallel four-helix bundle (Fasshauer et al., 1998; Poirier et al., 1998; Stein et al., 2009; Sutton et al., 1998). It has been proposed that SNARE complex formation is a multi-step process where zippering starts from the membrane-distal N-terminal region and progresses towards the membrane-proximal C-terminal region (Gao et al., 2012; Min et al., 2013; Shin et al., 2014; Sorensen et al., 2006). However, the coupling mechanism between zippering steps and membrane remodeling steps has been elusive (Lou and Shin, 2016).

Prior to their interaction with VAMP2, syntaxin 1A and SNAP-25 form a binary 1:1 t-SNARE complex on the plasma membrane (Fasshauer and Margittai, 2004; Fiebig et al., 1999; Rizo and Rosenmund, 2008). It has been shown that VAMP2 has a significantly higher affinity to the t- SNARE complex compared to the individual t-SNAREs (Calakos et al., 1994). Moreover,

only with the t-SNARE complex, not with individual t-SNAREs, does VAMP2 assemble into the SNARE complex and elicit synaptic exocytosis. The importance of the t-SNARE complex may be further emphasized with the fact that some botulinum toxins (BoNT) inhibit synaptic exocytosis by enzymatically cleaving individual t-SNAREs (Gerona et al., 2000; Rossetto et al., 2014).

BoNTs are a class of protein toxins with eight distinct serotypes produced from clostridia. BoNT consists of four distinct domains that function to bind to the nerve terminals, translocate into the cytosol, and cleave SNAREs via the metalloprotease activity (Lacy et al., 1998). While all BoNT serotypes induce flaccid paralysis by inhibiting neurotransmitter release at the neuromuscular junction, individual isoforms target different SNAREs and cleave them at different positions (Rossetto et al., 2014).

Both BoNT A and E site-specifically cleave SNAP-25 at the C-terminal SNARE motif leaving 9 and 26 residues shortened versions SNAP-25A and SNAP-25E, respectively (Rossetto et al., 2014; Schiavo et al., 1993). This cleavage is sufficient to reduce or abolish membrane fusion. While BoNT E completely abolishes neurotransmitter release, BoNT A seems to have a milder effect considering some membrane fusion is rescued with elevated levels of Ca2+ (Gerona et al., 2000; Lundh et al., 1977). This may imply that BoNT E and A impair membrane fusion at different steps. Thus, an understanding of the impact of the cleavage on the structure and dynamics of the SNARE complexes could provide valuable insights into the mechanism by which SNAREs mediate membrane fusion.

In order to cohesively investigate the effect of BoNT A and E cleavage on SNARE complex formation and membrane fusion, we probed the structure and dynamics of t-SNAREs using electron paramagnetic resonance (EPR), followed by observing SNARE zippering with single

molecule fluorescent resonance energy transfer (smFRET). We finally used single vesicle fusion assays to dissect the individual membrane fusion steps. Our results show that the BoNT A and E, although otherwise similar except that BoNT E cuts 17 residues more from SNAP-25 than BoNT A, impairs membrane fusion through entirely different mechanisms. While SNAP-25E blocks SNARE complex formation and vesicle docking, SNAP-25A allows robust vesicle docking, but reduces SNARE zippering and significantly impairs membrane fusion. The EPR results show that such big differences might stem from the extent of the dynamic destabilization of the t-SNARE core at the N-terminal half which plays a pivotal role in nucleating SNARE complex formation.

Results

Dynamic structure of the 1:1 binary t-SNARE complex of syntaxin 1A and SNAP-25

Although the structures of the ternary SNARE complex have been thoroughly investigated in both solution and membrane mimetics (Poirier et al., 1998; Shin et al., 2014; Stein et al., 2009), the t- SNARE complex is less well defined. Considering that the t-SNARE complex serves as a precursor to the ternary SNARE complex, further insights into the structure could shed light on the mechanistic steps in the ternary SNARE complex formation.

There are two forms of the t-SNARE complex: the non-productive 2:1 (syntaxin 1A: SNAP-25) complex and the productive, on-pathway 1:1 complex (Fasshauer and Margittai, 2004; Xiao et al., 2001). The 2:1 t-SNARE complex has been previously investigated with EPR (Xiao et al., 2001; Zhang et al., 2002). The structure is a parallel four-helix bundle, basically identical to the ternary SNARE complex, but with the second syntaxin 1A SNARE motif replacing VAMP2. In

contrast, the structure of the 1:1 t-SNARE complex has been elusive, most likely due to the dynamic nature of the structure.

Based on their smFRET experiments in live cells, An and Almers have previously proposed that the N-terminal SNARE motif of SNAP-25 (SN), within the 1:1 t-SNARE complex, forms a robust helical complex with syntaxin 1A while the C-terminal SNARE motif of SNAP-25 (SC) is detached from the complex and freely diffuses in solution (An and Almers, 2004). To verify this model, we first probed the dynamics of SN in the 1:1 complex using site-directed spin labeling EPR. This technique was chosen because the lineshape is highly sensitive to the motion of the nitroxide spin label, which is a reflection of the local structural environment. In one case, we attached the nitroxide to an engineered single cysteine at position 42 in the N-terminal region of SN and in another case, the nitroxide was attached at position 74 in the C-terminal region of SN (Figure 1A). Prior to complex formation, EPR spectra from both spin labeled mutants showed narrow lineshapes, prototypical of a freely diffusing random coil. However, when SNAP-25 was complexed with syntaxin 1A in the 1:1 stoichiometry, we observed extensive line-broadening in both cases (Figure 1B). This suggests that SN underwent a conformational change from a random coil to a helical structure at both N-terminal and C-terminal regions upon formation of the t-SNARE complex.

We still observed some narrow components in the EPR spectra, which represent signals from an unstructured polypeptide. The percentage of the narrow spectral components was quantitatively determined with the spectral subtraction method (Figure 1C) (Thorgeirsson et al., 1996). We found that the narrow components were approximately 5-10% of the composite spectra (Figure 1D). These numbers are consistent with the previously reported dissociation equilibrium of the 1:1 binary t-SNARE complex, where K_d ~0.4 μM (Weninger et al., 2008). One could argue

that the narrow component may have been due to the predominant existence of the 2:1 complex in the 1:1 mixture. However, if this were the case, a much larger narrow component would be observed due to the significant fraction of SNAP-25 remaining as monomers.

We then investigated the structure and dynamics of SC in the 1:1 complex using EPR. We generated five single cysteine mutants: G168C, T173C, N175C, N196C, and L203C of SC. These mutants were specifically selected to be around the central conserved residue Q174 (zero layer); two were positioned on the N-terminal half and three were positioned on the C-terminal half (Figure 1A). As monomers, all spin labeled SNAP-25 mutants displayed a narrow EPR spectra similar to what was observed with the SN, indicative of a freely diffusing polypeptide chain with little secondary or tertiary structure. However, when bound to syntaxin 1A all positions except 203C exhibited a composite two component spectra with one broad component reflecting the structured species and another narrow component reflecting the unstructured species (Figure 1E and F). We did not observe much spectral change with 203C, consistent with the previous finding that the C-terminal end is frayed for the 1:1 complex (Zhang et al., 2016).

Quantitative spectral subtraction analysis revealed that approximately 40% of SC was unstructured (Figure 1F), which was 4 times more than what was expected from the dissociation equilibrium between syntaxin 1A and SNAP-25. Taking into account the global association-dissociation equilibrium, we estimate that approximately 30% of SC remains unstructured when SNAP-25 is complexed with syntaxin 1A (Figure 1F). Thus, the results show that a significant fraction of SC (~30%) is unstructured while SN is complexed with syntaxin 1A. The results are partially consistent with the dynamic structure proposed by An and Almers in that SC has the tendency to dissociate from the complex (An and Almers, 2004). However, our observations

suggest that the majority of SC (~70%) is still bound to syntaxin 1A and SN and together they form a three−helix bundle (Figure 1G).

Cleavage of SC by botulinum toxins increases the dynamics of SC

Having characterized the 1:1 t-SNARE complex with EPR, we investigated the impact of the proteolytic cleavage of SC by BoNT A and E. To this end, we prepared recombinant SNAP-25 mutants of reduced lengths, SNAP-25A (aa. 1-197) and SNAP-25E (aa. 1-180). For SNAP-25A and SNAP-25E, we attached nitroxide spin labels at the same positions as those of the wild-type described in the previous section (Figure 2A).

For spin labeled positions 42 and 74 on SN, not much difference in the spectral line shape between wild-type SNAP-25 and the shortened mutants was observed. Further quantitative spectral subtraction analysis confirmed that the amounts of the narrow spectral components reflecting the global dissociation of the t-SNARE complex remained within ± 5% (Figure 2B). This suggests that BoNT A or E-induced cleavage of SNAP-25 does not alter the stability of SN in the t-SNARE complex.

However, when we examined the EPR spectra from SNAP-25E, the broad spectral components reflecting the structured conformation was reduced significantly (Figure 2C). Quantitative spectral subtraction analysis showed that the bound fraction was decreased for SNAP-25E as much as ~55% for the spin labeled positions in SC (Figure 2D). Thus, our results show that the cleavage of 26 residues of SC causes the dynamic destabilization of the already dynamic t-SNARE complex.

In contrast, the dynamic destabilization that was brought about by the cleavage of SC by BoNT A appeared to be milder than what was observed with the cleavage by BoNT E (Neal et al., 1999). The effect is pronounced on positions 175 and 196, which are located in the C-terminal half of SC. In contrast, the change is not visible in the N-terminal half. Thus, the EPR analysis shows that while BoNT E affects the dynamics of the entire SC motif, the effect of BoNT A cleavage is confined within the C-terminal half of SC.

Cleavage of SC by BoNT E impairs ternary SNARE complex formation

The EPR results suggest that although the SN in the t-SNARE complex was bound robustly to the syntaxin 1A, the SC was partially bound and destabilized. This destabilization was significantly increased for SNAP-25E, while the change was confined only within the C-terminal half for SNAP- 25A. We then asked how the increased dynamics of the t-SNARE complexes due to the BoNT cleavage affects the formation of the ternary SNARE complex or SNARE zippering.

To answer this question, we observed SNARE zippering at the membrane proximal region of a single trans-SNARE complex assembled between two nanodiscs (Figure 3A) with smFRET. Experimentally, we site-specifically labeled VAMP2 A72C and syntaxin 1A V241C with the fluorescence donor Cy3 and the fluorescence acceptor Cy5, respectively. We then prepared two populations of nanodiscs with the labeled proteins, one reconstituted with Cy3-labeled VAMP2 (v- nanodisc) and the other with the t-SNARE complex (t-nanodisc). The t-SNARE complex was prepared by premixing Cy5-labeled syntaxin 1A with either SNAP-25, SNAP-25A, or SNAP-25E. The t-nanodiscs were mixed with v-nanodiscs to allow the formation of the trans-SNARE complex and then immobilized onto the polyethylene glycol (PEG)-covered quartz imaging surface via streptavidin and biotin-PEG-DSPE conjunction. After washing out free nanodiscs with sufficient

buffer, the smFRET efficiencies of the single nanodisc pairs were analyzed from the fluorescence image. We found, using photobleaching counting, that most nanodiscs (~90%) have single fluorescent dyes (Figure S1). The results show that more than 90% of t-nanodiscs had the 1:1 t-SNARE complex. We only analyzed the nanodisc pairs that have single acceptor and donor dyes, which was verified with photobleaching after the FRET measurements.

When we counted the number of co-localized donor and acceptor signals, which represented nanodisc-to-nanodisc docking, there was no apparent difference between the wild-type SNAP-25 and SNAP-25A. However, we observed a dramatic decrease of docking, as much as a factor of 1/5, with SNAP-25E (Figure 3B).

We took a closer look into the docked nanodisc sandwich and further examined FRET efficiencies coming from the nanodisc pairs. For wild-type SNAP-25, the histogram showed both a low and a high FRET population, which was consistent with the results from our previous study (Shin et al., 2014; Yin et al., 2016). For SNAP-25E, the high FRET population completely disappeared with some small remaining populations at low FRET (Figure 3C). Our observations were quantitatively confirmed by analyzing the high FRET fraction of the total docked nanodisc pairs (Figure 3D). Although the overall low and high FRET distribution is similar to that of the wild-type, SNAP-25A had ~20% of the high FRET population shifted towards the low FRET region, which indicates that SNARE zippering was mildly hampered due to the cleavage. Thus, the results show that for SNAP-25E, both t- and v-SNARE pairing and SNARE zippering are severely hampered. However, for SNAP-25A the changes are rather mild.

For comparison, we examined the post-fusion state by preparing the cis-SNARE complex in a nanodisc. The cis-SNARE complex was prepared using VAMP2 without the transmembrane

domain such that the complex is anchored to the nanodisc via the transmembrane helix from syntaxin 1A (Figure 3E). Consistent with the previous results, we observed severely diminished v- and t-SNARE pairing for SNAP-25E, while no apparent difference between SNAP-25A and wild-type (Figure 3F and G). FRET histograms displayed a dominant high FRET population which peaked at the FRET efficiency E = 0.90 for wild-type SNAP-25 and SNAP-25A, but SNAP-25E did not show any dominant population (Figure 3G and H). Thus, the results suggest that the t-SNARE complex prepared with SNAP-25E is unable to form a well-structured ternary SNARE complex even in the cis conformation.

Cleavage of SC by botulinum toxins decreases/abolishes Ca^{2+}-triggered vesicle fusion

The results from the smFRET experiments show that the t-SNARE complex composed of SNAP-25E and syntaxin loses its ability to bind to VAMP2. However, with SNAP-25A, we observed only a mild decrease in SNARE zippering. This is intriguing because previous in vivo studies have shown that both BoNT A and E both elicit the effective inhibition of synaptic exocytosis (Gerona et al., 2000). This raises the possibility that cleavage by BoNT E inhibits the synaptic vesicles at the vesicle docking step, while BoNT A inhibits synaptic exocytosis at a later membrane fusion step.

To test this possibility, we examined Ca2+-triggered SNARE-mediated membrane fusion in the presence of auxiliary factors synaptotagmin 1 and complexin. Synaptotagmin 1 is a major Ca2+ sensor that triggers SNARE-mediated membrane fusion with the Ca2+ signal (Brose et al., 1992; Fernandez-Chacon et al., 2001), while complexin is believed to finely regulate membrane fusion (Tang et al., 2006; Xue et al., 2007). Using the in vitro single-vesicle content-mixing assay,

we examined how the SNAP-25A and E affect docking and membrane fusion at the single vesicle level.

Experimentally, we prepared two populations of vesicles representing the synaptic vesicles and the target membrane. The t-vesicles, reconstituted with syntaxin 1A and SNAP-25, were injected into the flow chamber and tethered on the PEGylated imaging surface through streptavidin-biotin conjugation. The v-vesicles, encapsulating 20 mM sulforhodamine B (SRB) and reconstituted with both VAMP2 and synaptotagmin 1, were injected into the flow chamber to allow vesicle docking. After docking, a buffer wash was used to remove any unbound v-vesicles. Throughout the process, the concentration of complexin was maintained at 100 nM, which has been recently shown to confer physiologically relevant Ca2+ sensitivity (Kim et al., 2016). After the docked vesicle-vesicle pairs were prepared, Ca2+ was injected into the flow chamber to trigger membrane fusion (Figure 4A). Fluorescence dequenching of SRB caused a stepwise increase in the fluorescence intensity of the v-vesicles, which was used to identify content-mixing from individual vesicle pairs (Figure 4A and B).

As expected, while the number of docked vesicles was similar for t-vesicles prepared with the wild-type and those with SNAP-25A, we observed almost no docking with SNAP-25E (Figure 4C). This agreed well with the aforementioned smFRET experiments. When we flew in 10 μM Ca2+, approximately 45% of the docked vesicles-vesicle pairs showed fusion with the wild-type, similar to our previous results (Kim et al., 2016). The first-order time constant of the content mixing kinetics was 5 seconds in the kinetic measurement that was carried out on the timeframe of 1 minute. In sharp contrast, we observed no fusion with both SNAP-25A and SNAP-25E (Figure 4D). Taken together, the results suggest that BoNT E blocks synaptic membrane fusion by

prohibiting docking, while BoNT A stops fusion after docking, but prior to the fusion pore opening.

A previous in vivo study reported that the inhibition of the release by BoNT A can be rescued via treatment with high Ca2+ concentrations (~200 μM) (Gerona et al., 2000; Lundh et al., 1977). To test whether our in vitro system faithfully recapitulates the in vivo results, we performed the single vesicle content-mixing assay using 500 μM Ca2+. Indeed, the fusion activity with t-vesicles prepared with SNAP-25A was rescued up to ~60% of the wild-type. However, membrane fusion was still completely abolished with SNAP-25E even at 500 μM Ca2+ (Figure 4E).

To further dissect steps where membrane fusion was inhibited, we performed the single vesicle- to-vesicle lipid mixing assay (Figure 4F). The experiment was prepared identically to the content- mixing assay except for incorporating lipid dyes instead of content dyes. By doing so, we are able to characterize the physical state of the docked vesicle pairs just prior to Ca2+ injection. We observed a homogenous FRET histogram centered at E = ~0.4 with the wild-type SNAP-25, indicating that hemifusion may be the dominant species prior to the Ca2+ injection. However, with SNAP-25A the FRET histogram is spread over a wider range and is skewed towards low FRET values (Figure 4G). Meanwhile, the docked vesicle pairs were extremely rare with SNAP-25E to the extent that we were unable to obtain an accurate FRET histogram. Thus, the results suggest that for the wild-type, the vesicles are prepared in the hemifused state ready to fuse upon Ca2+ injection (Kweon et al., 2017). In contrast, SNAP-25A is incapable of priming the fusion complex, while SNAP- 25E is unable to even mediate vesicle docking.

Discussion

It is well established that BoNTs inhibit neurotransmitter release from the neuron by site-specifically cleaving SNAREs (Rossetto et al., 2014; Neale et al., 1999). However, the underlying molecular mechanisms by which the BoNT-shortened SNAREs fail to elicit neurotransmitter release are not clearly understood.

In this work, we investigated the effects of SNAP-25 cleavage by BoNT A and E on the initial interactions with syntaxin 1A with EPR, on subsequent interactions and zippering with the vesicle v-SNARE VAMP2 using single-molecule FRET, and on specific membrane fusion steps with the single vesicle-vesicle docking and fusion assay.

By employing a combination of these techniques, we were able to comprehensively dissect how cleavage of SNAP-25, by BoNT A and E, impacts SNARE-mediated membrane fusion from the very early steps of SNARE assembly through the final steps of membrane fusion. In comparison to the wild-type SNAP-25, the EPR results show that the cleavage of 26 residues at the C-terminal end by BoNT E significantly destabilizes the C-terminal SNARE motif (SC). Importantly, the destabilization infiltrates into the N-terminal half which serves as the nucleating core for the interaction with VAMP2. Consequently, we observed the dramatic decrease of SNARE complex formation and vesicle docking, which resulted in almost no membrane fusion even at high Ca^{2+} concentrations.

While the EPR spectra show that SNAP-25E destabilizes the entire SC motif, SNAP-25A appears to have a milder effect and the destabilization was confined within the C-terminal half of SC. Our results suggest that the structural integrity of the N-terminal core of the t-SNARE complex is still preserved despite the deletion of the 9 residues at the C-terminus. In addition, the smFRET

results with SNAP-25A show that the docking probability remains unchanged with the FRET distribution shifted mildly towards low FRET values, indicative of somewhat impaired SNARE zippering. However, the single vesicle fusion assay shows complete inhibition of fusion with physiologically relevant 10 μM Ca^{2+}. Taken together, our results suggest that BoNT A tampers with membrane fusion just prior to the fusion pore formation step, in sharp contrast to BoNT E which inhibits at the very early step of SNARE complex formation.

It is remarkable that, despite only being a 17 residues difference in length, SNAP-25A and E terminate membrane fusion at completely different steps along the fusion pathway. While SNAP- 25A is able to support robust docking, SNAP-25E loses its ability to interact with VAMP2 almost completely, seriously impairing vesicle docking. Our results are in line with the previous observation in the presynapse that the size of the readily releasable vesicle pool for the BoNT A-treated neuron, determined by the high K^+ treatment, is similar to the control, while that for the BoNT E-treated neuron is significantly reduced (Neal et al., 1999). Furthermore, our results show that the C-terminal part of SC plays an important role in maintaining the stability of the N-terminal core of the t-SNARE complex, which is necessary for the interaction with VAMP2. For SNAP-25A, the t-SNARE core is able to tolerate the loss of C-terminal 9 residues. However, the loss of 26 residues in SNAP-25E is sufficiently large to disrupt the stability of the N-terminal core of the t-SNARE complex.

Now one might ask why SNAP-25A is able to lead the membrane fusion process up to docking, but utterly fail thereafter. We observed some decrease of the high FRET population with SNAP- 25A, indicating some impaired SNARE zippering for SNAP-25A. However, it appeared that the shift was only mild and one might wonder if this is sufficient to explain the major blockage of membrane fusion. One possible scenario could be that, although not significant individually,

this effect could be amplified due to the expected cooperativity among the multiple SNARE complexes that are believed to participate at the active zone (Montecucco et al., 2005). We also note that the membrane proximal C-terminal region of the SNARE complex plays an important role when interacting with synaptotagmin 1 and complexin (Chen et al., 2002; Gerona et al., 2000; Kim et al., 2012). Thus, we cannot rule out the possibility that the loss of 9 residues in SNAP-25A hampers the necessary interaction with the accessory proteins.

In the past, clostridial neurotoxins, including BoNT A and E, have played a crucial role in revealing SNAREs as the core fusion machinery for neurotransmitter release (Gerona et al., 2000; Lundh et al., 1977; Pirazzini M et al., 2017). In this study, we performed a comprehensive analysis of their impact on the structure and dynamics of SNARE complex and consequential effects on membrane fusion steps. The results from this study reveal new insights into the mechanism by which SNARE complex formation is coupled to individual fusion steps.

Author Contributions

R.K., J.K., and L.Y. contributed equally to the data collection, analysis, and interpretation of the experiments along with the drafting and revising the manuscript. R.K. contributed to the EPR, J.K. to the single vesicle fusion, and L.Y. to the smFRET experiments. Y.-K.S. was responsible for the design of the experiments and writing the manuscript.

Acknowledgements

This work was supported by the grant from the National Institute of Health R01 GM051290.

References

An, S.J., and Almers, W. (2004). Tracking SNARE complex formation in live endocrine cells. Science *306*, 1042-1046.

Brose, N., Petrenko, A.G., Sudhof, T.C., and Jahn, R. (1992). Synaptotagmin: a calcium sensor on the synaptic vesicle surface. Science *256*, 1021-1025.

Calakos, N., Bennett, M.K., Peterson, K.E., and Scheller, R.H. (1994). Protein-protein interactions contributing to the specificity of intracellular vesicular trafficking. Science *263*, 1146-1149.

Chen, X., Tomchick, D.R., Kovrigin, E., Arac, D., Machius, M., Sudhof, T.C., and Rizo, J. (2002). Three- dimensional structure of the complexin/SNARE complex. Neuron *33*, 397-409.

Fasshauer, D., Eliason, W.K., Brunger, A.T., and Jahn, R. (1998). Identification of a minimal core of the synaptic SNARE complex sufficient for reversible assembly and disassembly. Biochemistry *37*, 10354- 10362.

Fasshauer, D., and Margittai, M. (2004). A transient N-terminal interaction of SNAP-25 and syntaxin nucleates SNARE assembly. J Biol Chem *279*, 7613-7621.

Fasshauer, D. (2006). Sequential N- to C-terminal SNARE complex assembly drives priming and fusion of secretory vesicles. EMBO J *25*, 955-966.

Fernandez-Chacon, R., Konigstorfer, A., Gerber, S.H., Garcia, J., Matos, M.F., Stevens, C.F., Brose, N., Rizo, J., Rosenmund, C., and Sudhof, T.C. (2001). Synaptotagmin I functions as a calcium regulator of release probability. Nature *410*, 41-49.

Fiebig, K.M., Rice, L.M., Pollock, E., and Brunger, A.T. (1999). Folding intermediates of SNARE complex assembly. Nature Structural Biology *6*, 117-123.

Gao, Y., Zorman, S., Gundersen, G., Xi, Z., Ma, L., Sirinakis, G., Rothman, J.E., and Zhang, Y. (2012). Single Reconstituted Neuronal SNARE Complexes Zipper in Three Distinct Stages. Science *337*, 1340-1343.

Gerona, R.R., Larsen, E.C., Kowalchyk, J.A., and Martin, T.F. (2000). The C terminus of SNAP25 is essential for Ca(2+)-dependent binding of synaptotagmin to SNARE complexes. J Biol Chem *275*, 6328-6336.

Jahn, R., and Scheller, R.H. (2006). SNAREs--engines for membrane fusion. Nat Rev Mol Cell Biol *7*, 631- 643.

Kim, J., Zhu, Y.C., and Shin, Y.K. (2016). Preincubation of t-SNAREs with Complexin I Increases Content- Mixing Efficiency. Biochemistry *55*, 3667-3673.

Kim, J.Y., Choi, B.K., Choi, M.G., Kim, S.A., Lai, Y., Shin, Y.K., and Lee, N.K. (2012). Solution single-vesicle assay reveals PIP2-mediated sequential actions of synaptotagmin-1 on SNAREs. Embo J *31*, 2144-2155.

Kweon, D., Kong B, Shin YK. (2017) Hemifusion in Synaptic Vesicle Cycle. Front Mol Neurosci.10:65.

Lacy, D.B., Tepp, W., Cohen, A.C., DasGupta, B.R., and Stevens, R.C. (1998). Crystal structure of botulinum neurotoxin type A and implications for toxicity. Nat Struct Biol *5*, 898-902.

Lou, X.C., and Shin, Y.K. (2016). SNARE zippering. Biosci Rep *36*, 7.

Lundh, H., Leander, S., and Thesleff, S. (1977). Antagonism of the paralysis produced by botulinum toxin in the rat. The effects of tetraethylammonium, guanidine and 4-aminopyridine. J Neurol Sci *32*, 29-43.

Min, D., Kim, K., Hyeon, C., Cho, Y.H., Shin, Y.K., and Yoon, T.Y. (2013). Mechanical unzipping and rezipping of a single SNARE complex reveals hysteresis as a force-generating mechanism. Nature Communications *4*, 10.

Montecucco, C., Schiavo, G., and Pantano, S. (2005). SNARE complexes and neuroexocytosis: how many, how close? Trends Biochem Sci *30*, 367-372.

Neale, E.A., et al. (1999) Botulinum neurotoxin A blocks synaptic vesicle exocytosis but not endocytosis at the nerve terminal. J Cell Biol. 147(6):1249-60

Pirazzini M, et al. (2017) Botulinum Neurotoxins: Biology, Pharmacology, and Toxicology. Pharmacol Rev. 69(2):200-235.

Poirier, M.A., Xiao, W.Z., Macosko, J.C., Chan, C., Shin, Y.K., and Bennett, M.K. (1998). The synaptic SNARE complex is a parallel four-stranded helical bundle. Nature Structural Biology *5*, 765-769.

Rizo, J., and Rosenmund, C. (2008). Synaptic vesicle fusion. Nat Struct Mol Biol *15*, 665-674.

Rossetto, O., Pirazzini, M., and Montecucco, C. (2014). Botulinum neurotoxins: genetic, structural and mechanistic insights. Nat Rev Microbiol *12*, 535-549.

Schiavo, G., Santucci A, Dasgupta BR, et al. (1993) Botulinum neurotoxins serotypes A and E cleave SNAP-25 at distinct COOH-terminal peptide bonds. FEBS Lett. 335(1):99-103.

Shin, J., Lou, X., Kweon, D.-H., and Shin, Y.-K. (2014). Multiple conformations of a single SNAREpin between two nanodisc membranes reveal diverse pre-fusion states. Biochemical Journal *459*, 95-102.

Sorensen, J.B., Wiederhold, K., Muller, E.M., Milosevic, I., Nagy, G., de Groot, B.L., Grubmuller, H., and Stein, A., Weber, G., Wahl, M.C., and Jahn, R. (2009). Helical extension of the neuronal SNARE complex into the membrane. Nature *460*, 525-U105.

Sudhof, T.C., and Rothman, J.E. (2009). Membrane Fusion: Grappling with SNARE and SM Proteins. Science *323*, 474-477.

Sutton, R.B., Fasshauer, D., Jahn, R., and Brunger, A.T. (1998). Crystal structure of a SNARE complex involved in synaptic exocytosis at 2.4 angstrom resolution. Nature *395*, 347-353.

Tang, J., Maximov, A., Shin, O.-H., Dai, H., Rizo, J., and Sudhof, T.C. (2006). A complexin/synaptotagmin 1 switch controls fast synaptic vesicle exocytosis. Cell *126*, 1175-1187.

Thorgeirsson, T.E., Russell, C.J., King, D.S., and Shin, Y.K. (1996). Direct determination of the membrane affinities of individual amino acids. Biochemistry *35*, 1803-1809.

Weninger, K., Bowen, M.E., Choi, U.B., Chu, S., and Brunger, A.T. (2008). Accessory proteins stabilize the acceptor complex for synaptobrevin, the 1:1 syntaxin/SNAP-25 complex. Structure *16*, 308-320.

Wickner, W., and Schekman, R. (2008). Membrane fusion. Nat Struct Mol Biol *15*, 658-664.

Xiao, W., Poirier, M.A., Bennett, M.K., and Shin, Y.K. (2001). The neuronal t-SNARE complex is a parallel four-helix bundle. Nat Struct Biol *8*, 308-311.

Xue, M., Reim, K., Chen, X., Chao, H.T., Deng, H., Rizo, J., Brose, N., and Rosenmund, C. (2007). Distinct domains of complexin I differentially regulate neurotransmitter release. Nat Struct Mol Biol *14*, 949-958. Yin, L., Kim, J., and Shin, Y.K. (2016). Complexin splits the membrane-proximal region of a single SNAREpin. Biochem J *473*, 2219-2224.

Zhang, F., Chen, Y., Kweon, D.H., Kim, C.S., and Shin, Y.K. (2002). The four-helix bundle of the neuronal target membrane SNARE complex is neither disordered in the middle nor uncoiled at the C-terminal region. J Biol Chem *277*, 24294-24298.

Zhang, X., Rebane AA, Ma L, et al. (2016) Stability, folding dynamics, and long-range conformational transition of the synaptic t-SNARE complex. Proc Natl Acad Sci USA. 113(50):E8031-E8040

Experimental Model and Subject Details

All the experiments were performed in vitro.

Plasmid construction and mutagenesis

DNA sequence encoding: syntaxin 1A (amino acids 1-288 with three native cysteines replaced by alanines), SNAP-25 (amino acids 1-206 with four native cysteines replaced by alanines), SNAP- 25A (amino acids 1-198), SNAP-25E (amino acids 1-180), VAMP2 (amino acids 1-116 with 1 cysteine replaced by alanines), soluble VAMP2 (amino acids 1-96), complexin (Cpx, amino acids 1-134) were inserted into the pGEX-KG vector as GST fusion proteins. Synaptotagmin 1 (amino acids 50-421 with four cysteines replaced by alanines) was inserted into pET-28b vector as C- terminal His-tagged proteins. Modified apoA1 (amino acids, 1-258) was inserted into pNFXeX vector as a N-terminal His-tagged protein. All cysteine mutants, including SNAP-25 A42C, SNAP- 25 A74C, SNAP-25 G168C, SNAP-25 T173C, SNAP-25 N175C, SNAP-25 N196C, and SNAP-25 L203C were generated by the QuickChange site-directed mutagenesis kit and confirmed by DNA sequencing (Iowa State University DNA Sequencing Facility).

Protein Purification

All recombinant proteins were expressed in Escherichia coli BL21 (DE3) bacterial strain cells. Cells were first grown in LB medium at 37°C with shaking at 200 rpm until optical density reached 0.6-0.8 (600 nm). Isopropyl-β-D-thiogalactopyranoside (IPTG) (0.4 mM final concentration) was added to induce protein expression. After induction cells were further incubated at 16°C, shaking at 100 rpm for another 14-16 h.

For GST-tagged proteins, cells were pelleted and resuspended in 15 mL of PBST (PBS, pH 7.4, containing 0.2 Triton X-100) for membrane proteins and 15 ml of PBS (pH 7.4) for the soluble proteins with final concentrations of 1 mM 4-(2- aminoethyl)- benzenesulfonyl fluoride (AEBSF) and 4 mM DTT. Cells were lysed by sonication on ice and centrifuged at 25,000 g for 30 min at 4°C. The cleared supernatant was nutated with 2 ml of GST beads for 1 hour at 4°C. His-tagged synaptotagmin 1 and ApoA1 were purified using the same protocol except for using the Ni-NTA column.

After intense washing, the bound proteins were then eluted by 0.02 unit/μL thrombin in cleavage buffer (PBS, pH 8.0, containing 2 mM DTT) with/without 0.8 noctyl-D-glucopyranoside (OG) for GST-tagged membrane and soluble proteins, respectively. For His-tagged proteins, elution was carried out with buffer of 25 mM HEPES, 400 mM KCl, 500 mM imidazole and 0.8% OG. Purified proteins were examined by SDS-PAGE (15%, w/v) and the purity was at least 85% for all proteins. The protein concentration was determined using RC DC kit.

Site-directed spin and fluorophore labeling

For site-directed spin labeling of single cysteine mutants for EPR, the protein were incubated with 5 mM dithiothreitol (DTT) for 1 hour at 4°C. The protein was then subjected to the PD-10 size exclusion column and incubated for 16 hours at 4°C with 10-fold molar excess of 1-Oxyl-2,2,5,5- tetramethylpyrroline-3-methyl methanethiosulfonate (MTSSL). The proteins were then subjected to another PD-10 size exclusion column to remove any excess spin labels.

For site-directed fluorophore labeling of single cysteine mutants, the proteins were desalted with a PD MiniTrap G-25 column to eliminate free DTT and then incubated with a 10-fold molar excess of maleimide-derivative fluorophore indodicarbocyanine (Cy5) or indocarbocyanine (Cy3),

respectively, overnight at 4 ◦C. The labelled protein was purified using the PD MiniTrap G- 25 column and free dye was further separated from the protein sample using centrifugal filters (3kDa, Amicon Millipore Corporation, Bedford, MA). The labeling efficiency of each SNARE protein was measured spectrophotometrically (NanoDrop 2000c Spectrophotometer, Thermo Fisher Scientific, Waltham, MA). Further details can be found in our recent paper (Yin et al., 2016).

EPR data collection

EPR spectra were obtained using a Bruker ESP 300 spectrometer (Bruker, Germany) equipped with a low-noise microwave amplifier (Miteq, Hauppauge, NY) and loop gap resonator (Medical Advances, Milwaukee, WI). The modulation amplitude was set at no greater than one-fourth of the line width. Spectra were collect at room temperature in the first-derivative mode.

SNARE-incorporated nanodiscs preparation

The following lipids were used to generate nanodiscs. t-nanodiscs were prepared with 1,2-dioleoyl-sn-glycero-3-phospho-L-serine (DOPS), 1-palmitoyl-2-oleoyl-snglycero-3-phosphocholine (POPC), phosphatidylinositol-4,5-bisphosphate (PIP2, from porcine brain), cholesterol, and biotin-PEG-DSPE with a molar ratio of 62.9:15:20:2:0.1. The v-nanodiscs are composed of POPC, DOPS, and cholesterol with molar ratios of 75:5:20. Lipid film was made by drying the lipid mixtures with air and further incubation in house vacuum for 16-18 hours. The lipid film was then resuspended in HEPES buffer (25 mM HEPES, pH 7.4, and 150 mM KCl) to a final concentration of 50 mM. We then took 5 μL of the resuspended lipid mixture and dissolved it in sodium cholate such that the final concentration of sodium cholate would become 50 mM after the addition of apoA1 and SNARE proteins. Then, the binary t-SNARE complex (syntaxin

1A and SNAP proteins with a molar ratio of 1:2, pre-incubated at room temperature for 1 h) for t-nanodisc and VAMP2 for v-nanodiscs were added along with apoA1 into their respective detergent-solubilized lipid mixture. The final molar ratio of lipids, apoA1, and SNARE(s) was 300:5:1. After a 20min incubation period, the reconstitution of protein into nanodiscs was initiated by rapid removal of detergent with 50% (w/v) SM-2 Bio-Beads. Homogenously sized t- and v-nanodiscs were purified by gel filtration using a SuperdexTM 200 GL 10/300 column (GE Healthcare Life Sciences, Piscataway, NJ).

Preparation of *trans*-/*cis*-SNAREpin nanodiscs

The PEGylated imaging surface (25 x 75 x 1.0 mm) was prepared as previously described (Yin et al., 2016). The flow chambers were assembled with strips of double-sided tape placed between the quartz slide and coverslip. Streptavidin (0.2 mg/mL) was incubated in the flow chamber for 10 min and washed out prior to subsequent nanodisc immobilization.

The experiments using trans-SNAREpin nanodiscs, t-nanodiscs, and v-nanodiscs were pre-incubated at room temperature for 45 minutes with a molar ratio of 1:5 to allow the formation of a trans- SNAREpin between two nanodiscs. The unbound nanodiscs were then washed out. The experiments with cis-SNAREpin nanodiscs, t-nanodiscs, and soluble VAMP2 were pre-incubated at room temperature for 45 minutes with a molar ratio of 1:5 to allow the formation of a cis-SNAREpin in one nanodisc. The unbound t-nanodiscs and soluble VAMP2 were then washed out.

SmFRET collection

The imaging of the samples was performed at room temperature with the oxygen scavenger system [0.4% glucose (Sigma Aldrich, St. Louis, MO), 4 mM Trolox, 1 mg/mL glucose oxidase, 0.04 mg/ml catalase in HEPES buffer.

Proteoliposome Reconstitution

For the single vesicle content mixing assay, molar ratios of lipids used for vesicle preparation were 15:63:20:2:0.1 (DOPS: POPC: Cholesterol: PIP2: biotin-PEG-DSPE) for the t-vesicles, and 5:75:20 (DOPS: POPC: Cholesterol) for the v-vesicles, respectively. We added 1% 1,1'- Dioctadecyl-3,3,3',3'-Tetramethylindocarbocyanine Perchlorate (DiI) and 1,1'-Dioctadecyl-3,3,3',3'-Tetramethylindodicarbocyanine, 4-Chlorobenzenesulfonate (DiD) to the v- and t-vesicles, respectively, for the single vesicle lipid mixing assay (Thermo Fisher Scientific, Waltham, MA). The lipids were dried in a glass tube with nitrogen gas and stored overnight in a vacuum desiccator. The lipid film was resuspended with HEPES buffer (25mM HEPES, 100 mM KCl, pH 7.4) whereas, in the single vesicle content mixing assay, v-vesicle lipid film was resuspended with HEPES buffer containing 20 mM SRB (Thermo Fisher Scientific, Waltham, MA). After 10 times freeze-thaw cycles between hot water and liquid nitrogen, we used an extruder to make unilamellar vesicles with polycarbonate filter (100 nm pore size, Avanti Polar Lipids, Alabaster, AL). The binary t-SNARE complex, pre-mixed at room temperature for 30 min, were mixed with liposomes (10 mM in total lipid concentration) while VAMP2 and Syt1 were reconstituted with SRB (20 mM)-containing liposomes for ~10 min. We used a 200:1 lipid/protein molar ratio for both t- and v-vesicles. The mixture was diluted with HEPES buffer (3 times the lipid/protein mixture volume) and then dialyzed in 2 L dialysis buffer at 4°C overnight. For the v-

vesicles, free SRB was removed using the PD-10 desalting column (GE Healthcare Life Sciences, Piscataway, NJ) after dialysis.

Single vesicle content-mixing data collection

The imaging surface was prepared identically to the nanodisc smFRET experiments. We introduced a mixture containing 125 μM t-vesicles with 100 nM Cpx in HEPES buffer into the flow chamber. Once t-vesicles were immobilized on the PEGylated surface, the unbound t-vesicles were washed using HEPES buffer containing 100 μM Cpx. Then mixture of 100 nM Cpx and v-vesicles (20 mM SRB) in HEPES buffer was injected and incubated for 10 min for vesicle-vesicle docking. The unbound v-vesicles were washed out using HEPES buffer containing 100 nM Cpx. We imaged the vesicle-vesicle pairs as we injected Ca2+ into the flow chamber.

Single vesicle lipid-mixing data collection

The single vesicle lipid mixing experiment was performed identical to the content-mixing assay with exception of Ca2+. Data from docked vesicle-vesicle pairs were obtained taking multiple images from randomly selected areas in the flow chamber. The immobilized spots were analyzed and we measured the FRET efficiencies of individual vesicle pairs and plotted onto a histogram.

EPR data analysis

The Bruker Xepr software was used to collect all EPR spectra (Figure 1b, 1e, 2b, and 2c). The spectral subtraction method involves obtaining the EPR spectra of the monomer and the composite at the same position. The monomer was subtracted from the composite in order to

determine the amount of monomer present (Figure 1c). This was used to quantitatively determine the population of mobile and immobile spin labeled proteins (Figure 1d, 1f, and 2d).

SmFRET data analysis

Images were recorded using smFRET Package software that was a gift from the Taekjip Ha lab. While recording, the first 10-20 frames were excited by a red laser (635 nm) so the t-nanodisc could be identified. We then switched to the green laser (532 nm) to identify v- and t-pairing from the nanodiscs. The co-localized spots, which have both the acceptor and donor signal channel, were then selected and analyzed.

From the selected spots, the acceptor and donor time traces were analyzed to obtain the FRET histograms (Figure 3c and 3g). As mentioned in our previous work (Yin et al., 2016), we seldom observed any significant transitions in the FRET value using 100 msec time resolution. Thus, we assigned a single FRET value (mean) for each co-localized spot. The assigned FRET value was obtained from the period in which both dyes were photon emitting. Significant FRET values were quantified using the student's t-test. The t-test was performed using the GraphPad software (Figure 3b, 3d, 3f, and 3h).

Single vesicle content/lipid mixing analysis

Images were obtained using the same software as the smFRET data analysis. However, the data was analyzed using a home built software developed in MATLAB R2014b. For the single vesicle content mixing assay, a stepwise jump in the fluorescence intensity was monitored as an indication of content-mixing (Figure 4b). The fusion percentage was the average number of fused vesicles over the total number of docked vesicles in 3 separate recordings (Figure 4d and 4e). For

the single vesicle lipid mixing assay, the FRET distribution was calculated in the same way as the smFRET data analysis (Figure 4g).

Data resources

The following DNA and protein sequences have been deposited in UniProt under the corresponding ID codes.

- Syntaxin 1A: UniProt P32851
- SNAP-25: UniProt P60881
- VAMP2: UniProt P63045
- Synaptotagmin: UniProt P21707
- Complexin: UnitProt P63041

Software resources

- The following software can be found at the corresponding links.
- Bruker Xepr used to collect and analyze EPR spectra:
- https://www.bruker.com/products/mr/epr/epr-software/xepr/overview.html
- smFRET Package software used to image and analyze FRET distributions was a gift from the Taekjip Ha lab. Information on how to obtain the software can be directed to our lead author.
- GraphPad Software used to perform the student t-test:

- https://www.graphpad.com/quickcalcs/ttest1.cfm
- The MATLAB R2014b software was built in house and analyze content mixing assays. Information on how to obtain the software can be directed to our lead author.

Figures with Titles and Legends

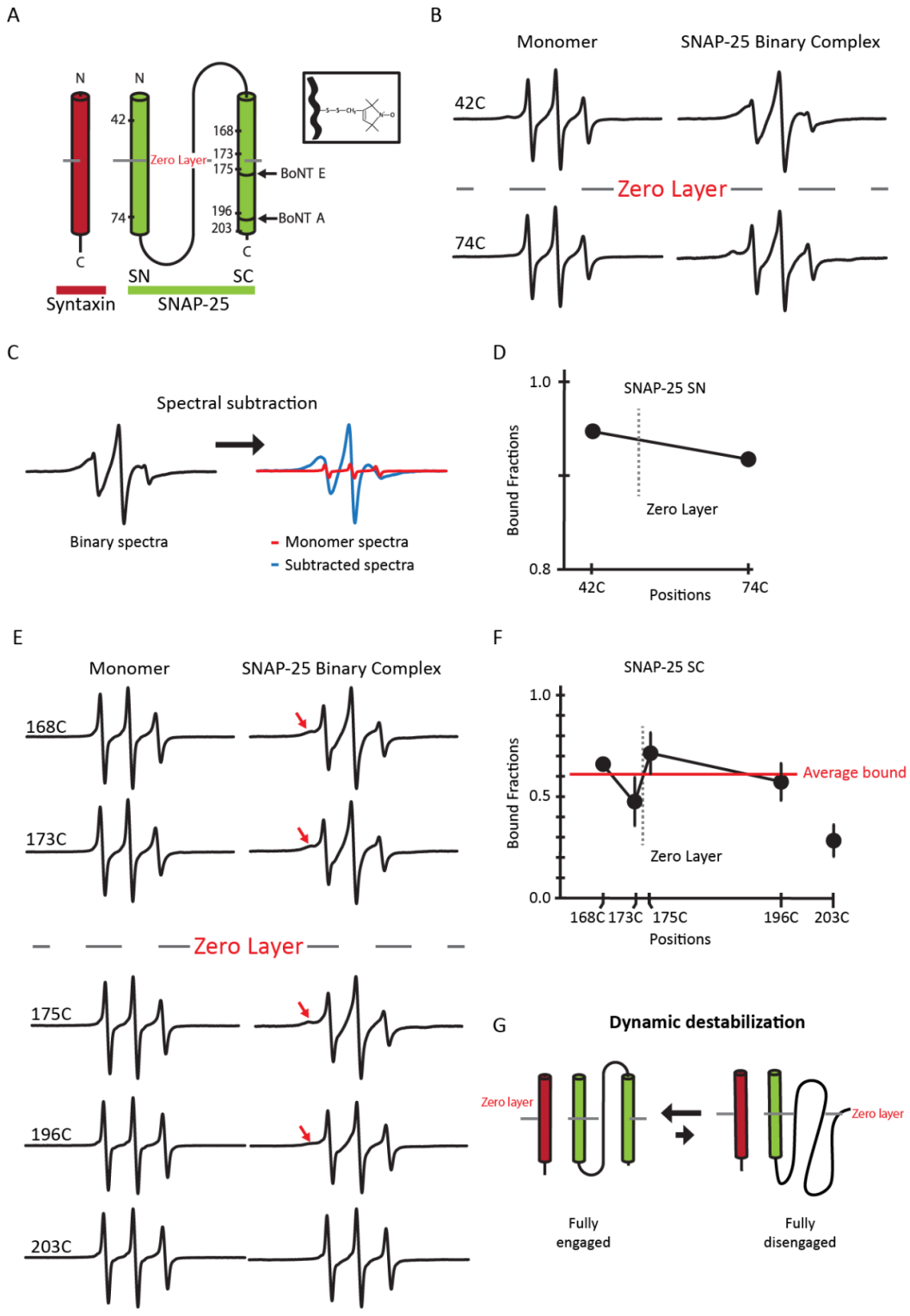

Figure 1 EPR spectra and analysis of spin-labeled SNAP-25 as monomers and part of the 1:1 binary t-SNARE complex.

(A) Schematic representation of the site-directed spin labeling EPR of the t-SNARE complex with syntaxin 1A (red) and SNAP-25 (green). SNAP-25 is denoted with spin labeled positions and BoNT A and E cleavage sites. The conserved zero layer is represented by a dashed line. The inset depicts chemical structure of the spin label (MTSSL) attached to the cysteine side chain. (B) Room temperature EPR spectra for A42C and A74C in the SN domain in monomeric SNAP-25 or in the t-SNARE complex. (C) Representative EPR spectral subtraction analysis. The composite binary EPR spectrum (black) was subtracted by the monomer spectra (red) to obtain the broad, interacting spectral component (blue). (D) Bound fraction of the labeled positions (SN domain) in the t-SNARE complex obtained from the spectral subtraction analysis. The data are shown as means ± SD. (E) Room temperature EPR spectra for the labeled positions in the SC domain in monomeric SNAP-25 or in the t-SNARE complex. The red arrow indicates areas of EPR lineshape broadening. (F) Bound fraction of the labeled positions (SC domain) in the t-SNARE complex obtained from the spectral subtraction analysis. The average bound fraction (red) of spin labeled positions G168C, T173C, N175C, and N196C is 0.61. Position 203 was excluded when calculating the mean due to its position being near the end the SC domain which is known to be frayed and unstructured. The data are shown as means ± SD. (G) Model of dynamic equilibrium of the SNAP-25.

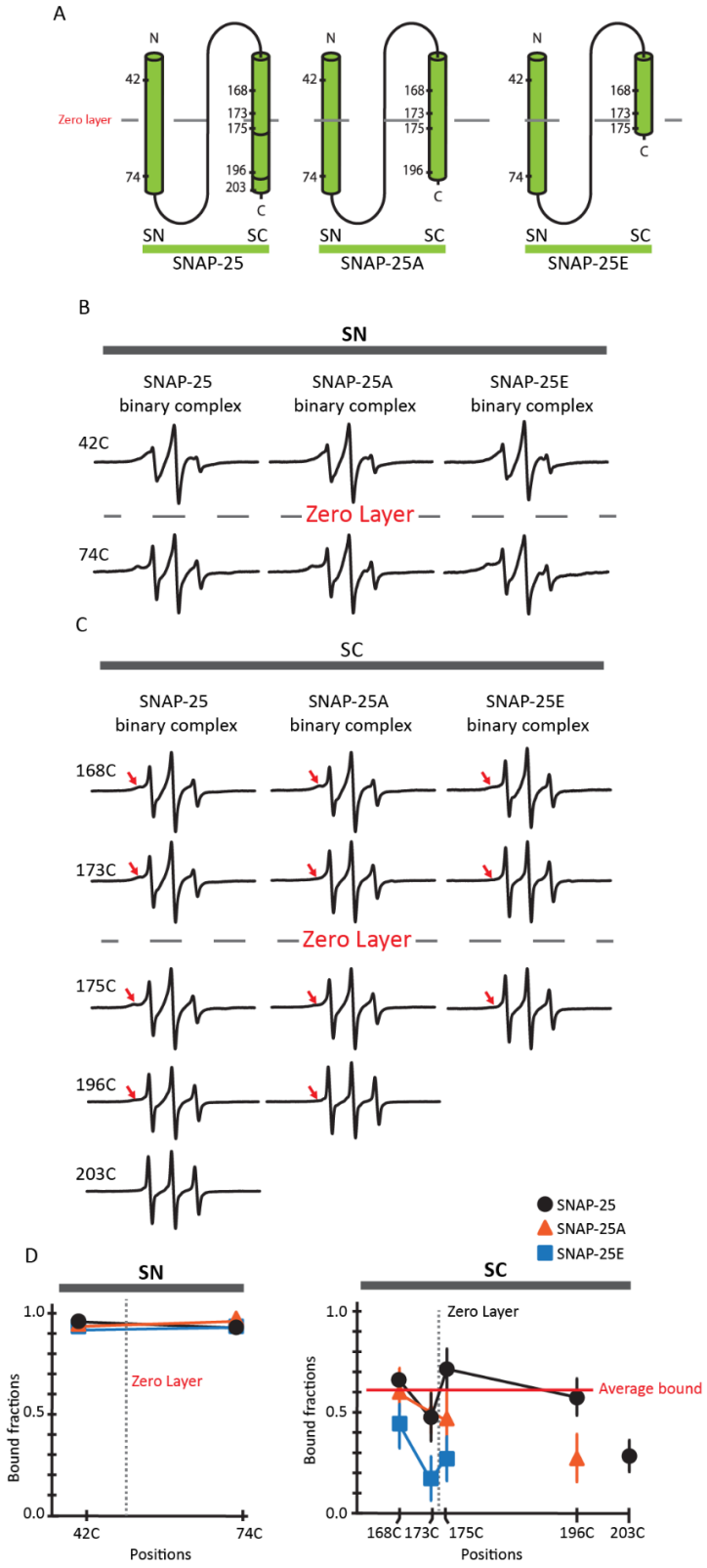

Figure 2 EPR spectra and analysis of spin-labeled SNAP-25, SNAP-25A, and SNAP-25E as monomers or part of the 1:1 binary t-SNARE complex.

(A) Schematic representation of the site-directed spin labeling positions of SNAP-25, SNAP-25A and SNAP-25E. The zero layer is denoted by a dashed line. (B) Room temperature EPR spectra of SNAP-25, SNAP-25A and SNAP- 25E spin labeled variants on the SN motif as monomers or part of the t-SNARE complex. (C) EPR spectra of SNAP-25, SNAP-25A, and SNAP-25E spin labeled variants on the SC motif as monomers or part of the t-SNARE complex. The red arrows point to the broad component of the EPR spectra. (D) Bound fraction of the labeled positions in the t-SNARE complex obtained from spectral subtraction analysis for SC and SN motifs are shown in the left and right graph, respectively. The data for SNAP-25 (black circle), SNAP-25A (orange triangle), and SNAP-25E (blue rectangle) are shown as means ± SD.

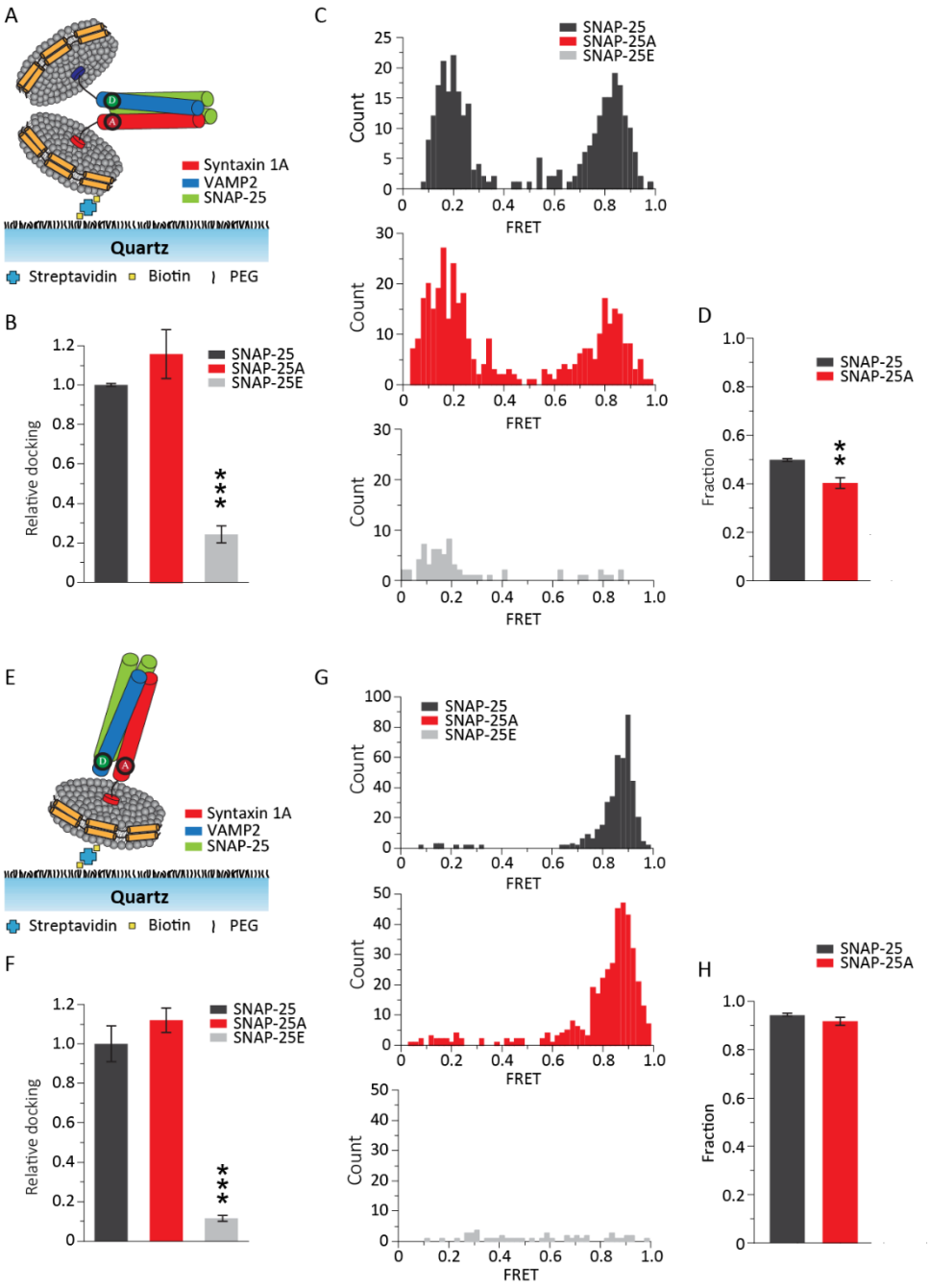

Figure 3 SmFRET analysis of the ternary trans- and cis-SNARE complex using nanodiscs.

(A) Schematic of a nanodisc sandwich harboring a single trans-SNARE complex with the FRET pair at the C-terminal region (CC). VAMP2 A72C-Cy3 and syntaxin 1A V241C-Cy5 were used for CC. (B) Relative docked nanodisc sandwiches for SNAP-25A and SNAP-25E normalized to SNAP-25 are shown as means ± SD. Docking was significantly reduced with SNAP-25E. (C)

Histogram of the FRET efficiency distribution for SNAP-25 (top), SNAP-25A (middle) and SNAP-25E (bottom). The distribution showed two distinct populations in the high and in the low FRET regions for SNAP-25 and SNAP-25A. The distribution for SNAP-25E is not well organized. Total of 307, 380 and 69 traces was analyzed for SNAP-25, SNAP-25A and SNAP-25E respectively. (D) The fraction of the high FRET population from the trans-SNARE complex. Approximately half of the population is distributed in the high FRET region for SNAP-25 and SNAP-25A. (E) Schematic a single cis-SNARE complex (CC) anchored to a single nanodisc by the syntaxin 1A transmembrane domain. (F) Relative co-localized Cy3-Cy5 spots for SNAP-25A and SNAP-25E normalized to SNAP-25. Co-localized spots are significantly reduced with SNAP- 25E. Data are shown as means ± SD. (G) Histogram of the FRET efficiency distribution for SNAP- 25 (top), SNAP-25A (middle) and SNAP-25E (bottom). The distribution showed one distinct population in the high FRET regions for SNAP-25 and SNAP-25A. The distribution for SNAP- 25E was not well organized. Total of 422, 411 and 47 traces was analyzed for SNAP-25, SNAP- 25A and SNAP-25E respectively. (H) The fraction of the high FRET population from the cis-SNARE complex. In (B), (D), (F) and (H), the data are shown as means ± SD (*$p < 0.05$, **$p < 0.01$, and ***$p < 0.005$ by Student's t-test; n = 3 independent experiments).

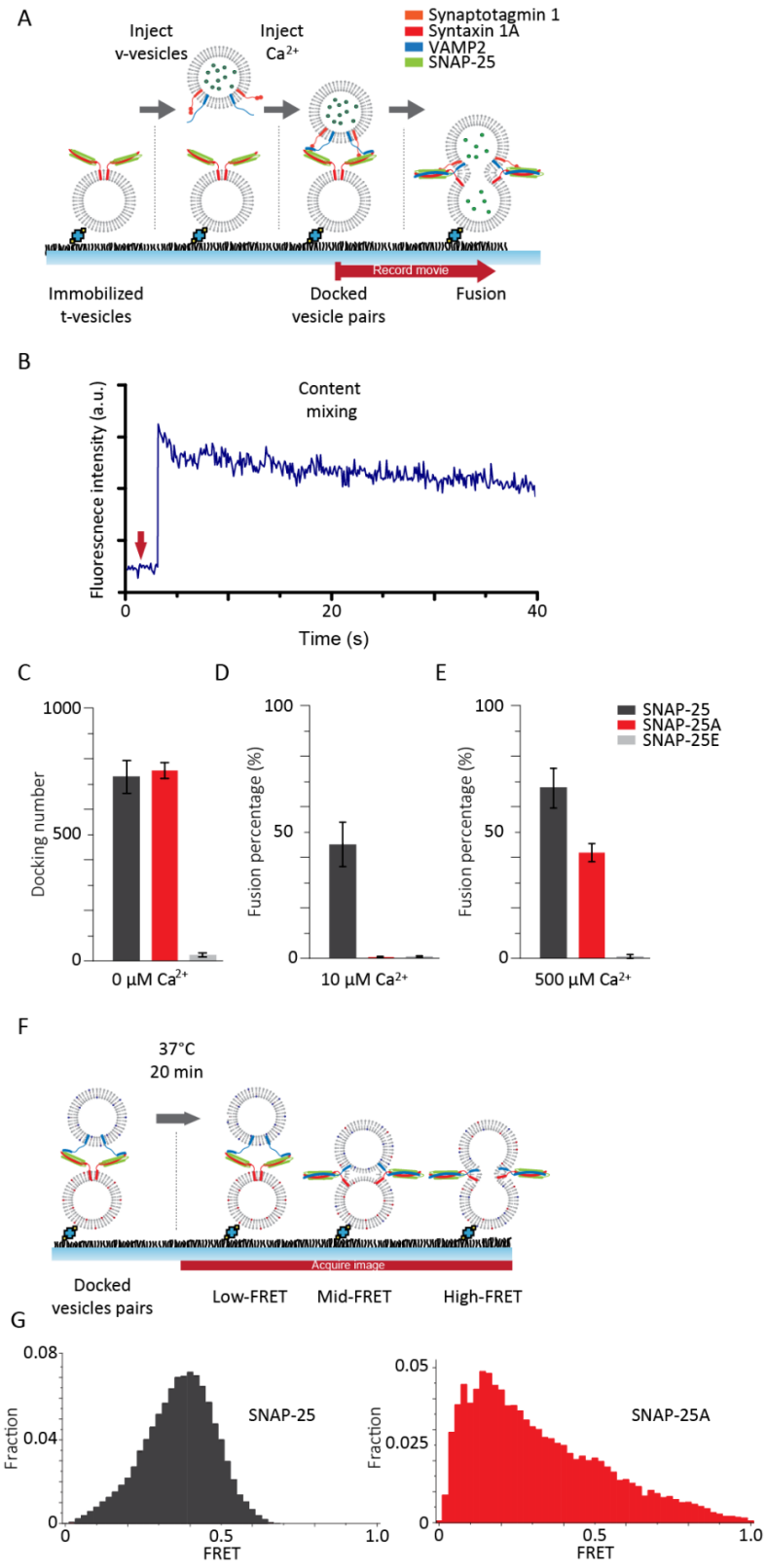

Figure 4 SNAP-25A is unable to trigger SNARE-mediated membrane fusion with 10 μM Ca^{2+}.

(A) Schematic of the in vitro single-vesicle content-mixing assay. After the t-vesicles are immobilized on the imaging surface, unbound t-vesicles were washed out and subsequent docking and washing of unbound v-vesicles were also performed. Once the v-vesicles and t-vesicles are docked, we injected Ca2+ into the flow chamber to evoke content-mixing which are detected by a sudden step-wise increase of fluorescent intensity. The flow chamber maintained constant 100 nM Cpx concentration throughout the experiment. (B) A representative fluorescent intensity time trace is shown in blue. The stepwise increase indicates content-mixing. The red arrow indicates the time Ca2+ was added to the flow chamber. (C) Bar graph of the average number of docked vesicles-vesicle pairs from 3 recordings. Bar graph of the average fusion percentage from 3 recordings are shown for (D) 10 μM Ca2+ and for (E) 500 μM Ca2+. (F) Schematics of the in vitro single-vesicle lipid-mixing assay. The single-vesicle lipid-mixing assay was identical to the content-mixing assay prior to Ca2+ injection with the exception of using DiI and DiD instead of SRB. (G) The FRET distribution between the docked vesicle-vesicle pairs for prepared with SNAP-25 and SNAP-25A are shown left and right, respectively.

Supplementary Information

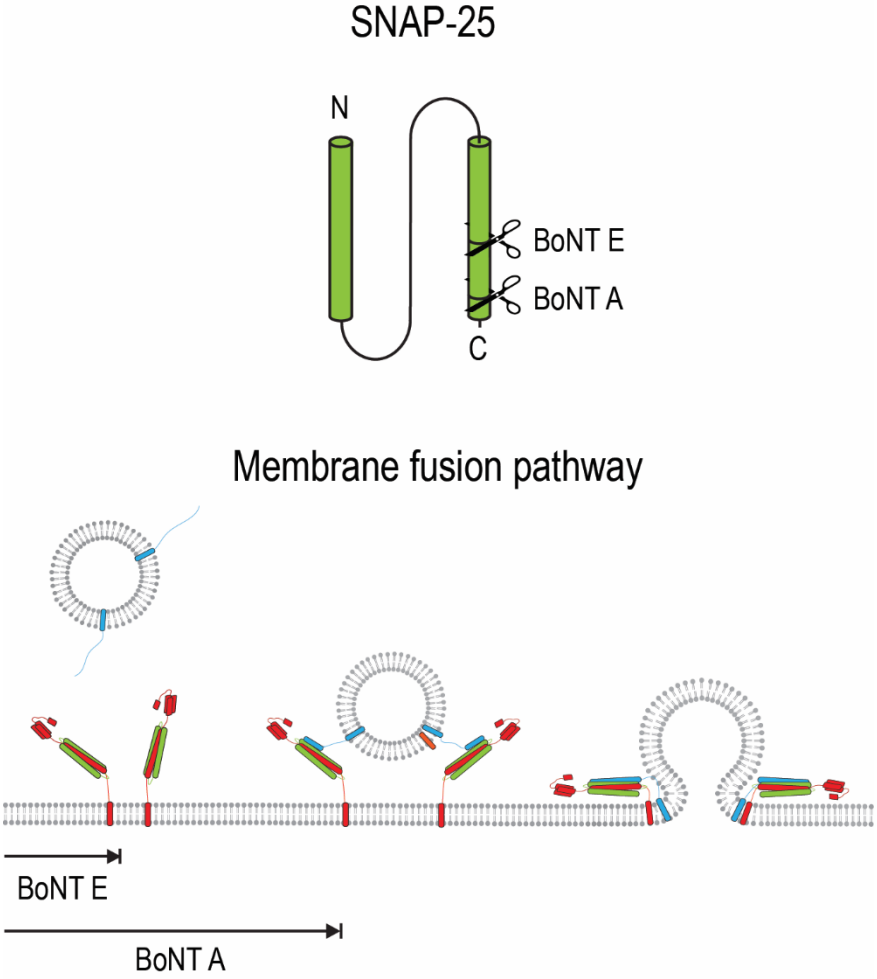

Graphical Abstract

In this work, Khounlo et al. show that cleavage of SNAP-25 by BoNT A and E terminates SNARE-mediated membrane fusion at different stages. EPR shows that this discrepancy stems from structural destabilization of the N-terminal half of t-SNARE.

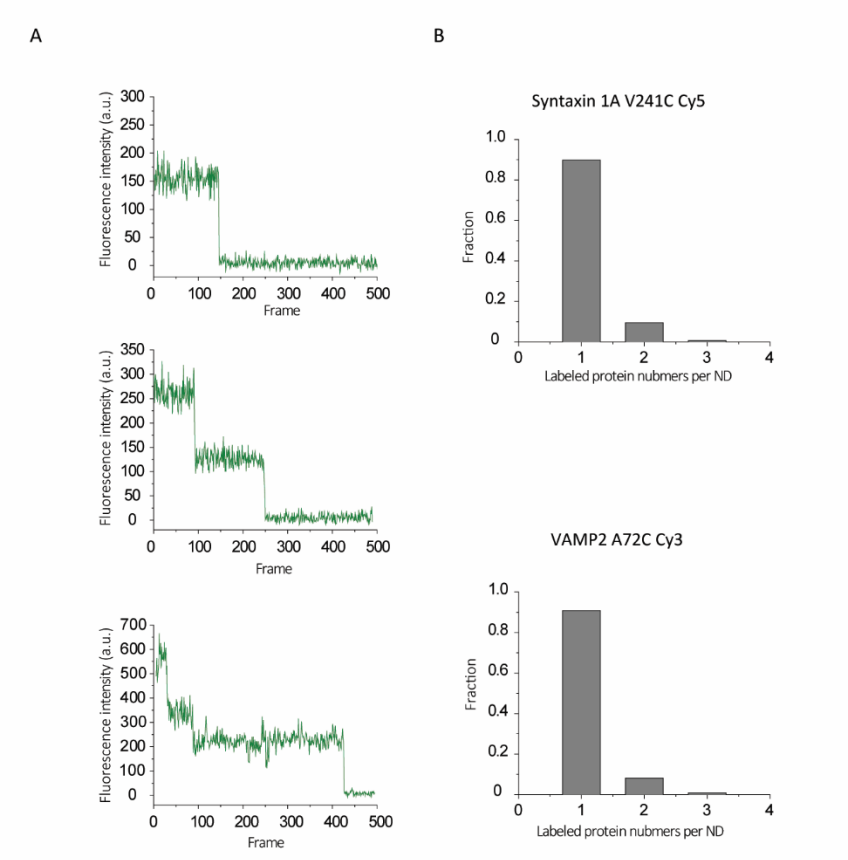

Figure S1 (related to Figure 3). Photobleaching steps to confirm the number of labeled SNARE proteins in a single nanodisc.

(A) Fluorescence intensity time traces showed single or multiple photobleaching steps (green lines). The number of steps was counted to confirm the number of labeled SNARE proteins per nanodisc. Typical photobleaching traces showing one, two and three steps of photobleaching, from top to bottom. (B) Distribution of the number of labeled SNARE proteins embedded in a single nanodisc, syntaxin 1A V241C Cy5 and VAMP2 A72C–Cy3, from top to bottom.

CHAPTER 4: SNAP-25 C-TERMINAL SNARE MOTIF UPSTREAM LAYERS AND DOWNSTREAM LAYERS PLAY CRUCIAL BUT DISTINCT ROLES DURING SNARE COMPLEX FORMATION

A manuscript in preparation

Linxiang Yin*, and Yeon-Kyun Shin*[1]

*Roy J. Carver Department of Biochemistry, Biophysics, and Molecular Biology, Iowa State University, Ames, IA 50011, U.S.A.

[1]Corresponding author.

Abstract

The SNARE complex is the central fusion machinery during neurotransmitter release. During SNARE complex formation, the binary 1:1 syntaxin 1A: SNAP-25 acceptor complex binds to VAMP2 to form a four-helix bundle held together by 16 (numbered -7 to +8) highly conserved layers of interacting amino acid side chains. In the tri-party SNARE complex, SNAP-25 is an essential component and is also the target of botulinum toxins (BoNTs) A and E. The exact effects of those layers in SNAP-25 during SNARE complex formation and why naturally selected BoNT E and A site-specially choose to cleave SNAP-25 at the C-terminal SNARE motif (SC) residues 180 and 197 remain poorly understood. Here, using single-molecule FRET, we systematically examine the binary and ternary SNARE complex structures with a series of SNAP-25 truncations introduced at SC layers. We show that, in the binary SNARE complex, SC downstream '+2' to '+6' layers increase tightly zippered SC upstream layers in a gradual manner and these tightly zippered SC upstream layers serve as a landing platform for VAMP2 binding that initiates the ternary SNARE complex formation. Interestingly, the ternary SNARE complex C-terminal can still zipper even without the last 22 SNAP25 C-terminal end residues, indicating the SC downstream layers mainly stabilize the binary SNARE complex structure rather than bind VAMP2 and stabilize the ternary complex. These data also provide insights into why BoNT E and A choose to target SNAP-25 at the C-terminal residues 180 and 197.

Introduction

In the presynaptic nerve terminal, SNARE proteins mediate synaptic vesicle fusion that releases neurotransmitters. SNARE proteins consist of plasma membrane-anchored syntaxin 1A and SNAP-25 and the vesicle membrane protein VAMP2 (Söllner et al., 1993; Südhof, 2004; Südhof & Rothman, 2009). It is widely believed that syntaxin 1A and SNAP-25 first form a binary 1:1 SNARE complex on the target plasma membrane (t-SNARE) (Fasshauer & Margittai, 2004; Pobbati, Stein, & Fasshauer, 2006; Weninger, Bowen, Choi, Chu, & Brunger, 2008). The 1:1 t-SNARE complex then binds to VAMP2 on the synaptic vesicle membrane (v-SNARE) to form a twisted four-helix bundle ternary SNARE complex. Such ternary SNARE complex can bridge the plasma membrane and vesicle membrane, thus overcoming the repulsive forces between these two negatively charged membranes. As the vesicular membranes fully fuse with the plasma membrane, this membrane-connecting *trans*-SNARE complex adopts a *cis*-SNARE complex structure, in which all three SNAREs are located on the same side of the membrane (Jahn & Scheller, 2006; Südhof & Rothman, 2009).

In the *cis*-SNARE complex, the four SNARE-motifs adopt a parallel four-helical bundle coiled-coil conformation (Poirier et al., 1998; Sutton, Fasshauer, Jahn, & Brunger, 1998). In the interior of the tightly packed alpha-helical coiled-coil, SNARE contains highly conserved 16 (numbered -7 to +8) layers of interacting amino acid side chains. Layer 0 located in the center of the bundle is maintained by the ionic interactions so it is also referred to as the ionic layer. Seven upstream layers (layers -7 to -1) and eight downstream layers (layers +1 to +8) of layer 0 are maintained primarily by hydrophobic interactions (Sutton et al., 1998)(as in Figure 1). The function of these layers of SNAP-25 has not been systematically studied.

BoNT type A and E can cleave SNAP-25 and shorten the last 9 and 26 residues from SNAP25 C-terminus (Rossetto, Pirazzini, & Montecucco, 2014; Schiavo et al., 1993). The efficiency and potency of SNAP-25 targeting neurotoxins BoNT A and E highlight the crucial roles of the C-terminus layers of SNAP-25 during SNARE function. BoNT is produced by a gram-positive anaerobic bacterium *Clostridium botulinum* (Lacy, Tepp, Cohen, Dasgupta, & Stevens, 1998). There are seven major serotypes of BoNTs (types A-G) (Peng et al., 2013). BoNTs inhibit SNARE complex formation by site-specifically cleaving SNARE proteins (Rossetto et al., 2014). Previous studies have shown that BoNT E but not BoNT A can trigger neuron degeneration. Syntaxin 1A and SNAP-25 are essential to maintaining neuronal survival for membrane recycling and only a minute amount of residue level of syntaxin 1A and SNAP-25 after exposed to BoNT E at lower concentrations is still able to prevent neurodegeneration (Peng et al., 2013). The delicate different effects of these two BoNTs on neuronal survival as well as why these naturally selected toxins targeting SNAP-25 at the C-terminal SNARE motif (SC) residues 180 and 197 are intriguing questions to explore.

To address these questions, we pursued the approach of generating a series of SNAP-25 truncation at the SC layers. We monitored the structures and directly observed the real-time dynamics of the binary and ternary SNARE complexes with these truncations using smFRET. Our results show that SC '-7' to '+1' layers can only form a basal level of the unstructured binary complex with syntaxin 1A. SC downstream layers (from +2 to +6) gradually accumulate the t-SNARE population containing tightly zippered SC upstream layers while at the same time maintain the basal level of the unstructured t-SNARE complex population. Strikingly, VAMP2 binding to the 1:1 t-SNARE complex is also close to background level with just SC '-7' to '+1' layers and increases from SC downstream '+2' to '+6' layers in a progressive manner. Of note, the

ternary SNARE complex C-terminal syntaxin 1A and VAMP2 can still form a tightly zippered structure without most of the SC downstream layers (from +3 to +7). Our results demonstrate that SC upstream layers (layers -7 to -1) and downstream layers (layers +2 to +6) play crucial but distinct roles during the binary and ternary SNARE complex formation.

Results

SC downstream layers gradually accumulated the well-structured 1:1 t-SNARE complex population.

The ternary SNARE complex contains four SNARE-motifs with a parallel four-alpha-helix bundle conformation (Figure 1). Syntaxin 1A and VAMP2 each contribute one SNARE motif while SNAP-25 contributes two: the N-terminal SNARE motif (SN) and the C-terminal SNARE motif(SC) (Sutton et al., 1998). Prior to the ternary SNARE complex formation, the t-SNARE complex formation is likely a slow and rate-limiting step of SNARE assembly (Pobbati et al., 2006; Walter, Wiederhold, Bruns, Fasshauer, & Sørensen, 2010; Zhang et al., 2016). In physiological conditions, one molecule of SNAP-25 associates with one molecule of syntaxin 1A to form the 1:1 t- SNARE complex (Weninger et al., 2008). There is also an off-pathway product of syntaxin 1A: SNAP-25 SNARE complex with a 2:1 stoichiometry formed *in vitro* (Fasshauer & Margittai, 2004; Margittai, Fasshauer, Pabst, Jahn, & Langen, 2001; Xiao, Poirier, Bennett, & Shin, 2001). However, such 2:1 t-SNARE complex cannot bind to VAMP2 to initiate the membrane fusion (James, Kowalchyk, Daily, Petrie, & Martin, 2009; Pobbati et al., 2006). In our study, we focused on the functional 1:1 t-SNARE complex.

The slowly preformed 1:1 t- SNARE complex in the target membrane can tightly associate with VAMP2 in the vesicular membrane, thus boost the SNARE zippering and membrane fusion proceeded in a robust and speedy manner (Zhang et al., 2016). Compared with the extraordinarily stable, even SDS-resistant ternary SNARE complex (Otto, Hanson, & Jahn, 1997), the 1:1 t-SNARE complex is more dynamic. SNAP-25 binds to syntaxin 1A through SN with high affinity, forming a tight helical structure with syntaxin 1A (Khounlo, Kim, Yin, & Shin, 2017). SNAP-25 with an N-terminal truncation (amino acids 39-206) cannot initiate a binary or a ternary SNARE complex formation (Fasshauer & Margittai, 2004). SC can either associate tightly with syntaxin 1A or detach from syntaxin 1 A (Khounlo et al., 2017). Several versions of VAMP2 fractions used in recent *in vitro* studies have the capacity to facilitate SNARE zippering and enhance membrane fusion (Pobbati et al., 2006; Shin, Lou, Kweon, & Shin, 2015). The underlying molecular mechanisms might be these VAMP2 fractions have a 1:1 t- SNARE complex stabilizing effect (Pobbati et al., 2006).

Considering the dynamic nature of the 1:1 t-SNARE complex, technically, smFRET in combination with nanodiscs is an ideal way to directly monitor the structure of the 1:1 t-SNARE complex within its native plasma membrane lipid environment. To directly observe the effects of SC layers on the 1:1 t-SNARE complex folding, conformations and dynamics, we first designed six recombinant SNAP-25 truncations introduced at different SC layers (from layer +2 to layer +7) based on the SNARE complex X-ray crystal structure. These SNAP-25 truncations were referred to as SNAP-25 deletions at layer n (SNAP-25 dLn, n=2-7, as can be seen in Figure 2A).

We then introduced a cysteine mutation N175C in these SNAP-25 truncations for fluorophore labeling. We site-specifically labeled these SNAP-25 truncations that harbor an N175C mutation and syntaxin 1A V241C with FRET donor Cy3 and acceptor Cy5. We then

incorporated labeled syntaxin 1A into nanodiscs. During nanodisc assembly, we used very low syntaxin 1A to lipid as well as the membrane scaffolding protein apoA1 ratio to make sure most nanodiscs contained at most one labeled syntaxin 1A. The nanodisc formation was confirmed by negative stain electron microscopy imaging (Figure S1). The syntaxin 1A containing nanodiscs were first incubated with 10 times more Cy3 labeled SNAP-25 truncation to allow the 1:1 t-SNARE complex formation. The mixture was flowed into a microfluidic channel and immobilized onto the streptavidin-decorated quartz slide surfaces via the nanodisc lipid biotin-PEG-DSPE and streptavidin conjugation (Figure 2B). After washing out the unbound nanodiscs and free proteins thoroughly, FRET donor and acceptor signals were recorded and FRET efficiencies were analyzed.

We found high FRET, low FRET and fluctuating FRET traces in all cases (Figure 2C), confirming the dynamic characteristics of the 1:1 t-SNARE complex. The fluctuating traces were mainly from low FRET traces and only a minute percentage were from high- and low- FRET transitions. In syntaxin 1A and SNAP-25 dL2 binary complex, the high FRET population is close to background level. Just a basal level of the low FRET unstructured binary complex was formed, indicating SC was mainly detached from syntaxin 1A (Figure 2D). In the syntaxin 1A and SNAP-25 dL3 binary complex, a certain amount of high FRET population emerged, indicating the well-structured t-SNARE complex was formed from SC downstream layer '+2'. SNAP-25 dL4, dL5, dL6, and dL7 have the increasingly well-structured t-SNARE complex with syntaxin 1A. This indicates that the well-structured t-SNARE complex was formed from SC downstream layer '+2' and accumulated all the way towards layer '+6' in a progressive manner. SNAP-25 dL7 and SNAP-25 WT had comparable ability to form the well-structured t-SNARE complex (Figure 2D). We calculated the percentage of the high FRET population from the 1:1 t-SNARE complex, and found

that it increased dramatically from around 10% with SNAP-25 dL2 all the way to around 80% with SNAP-25 dL7 (Figure 2E).

SC downstream layers gradually increased the VAMP2 pairing to the 1:1 t-SNARE complex.

To further characterize the effects of SC layers on the ternary SNARE complex folding and formation, we used five recombinant SNAP-25 with deleted SC at different layers (from layer +2 to layer +7) based on the SNARE complex X-ray crystal structure (Figure 3A). We site-specifically labeled VAMP2 A72C and syntaxin 1A V241C with FRET donor Cy3 and acceptor Cy5. The SNAP-25 truncations were not labeled so they were not introduced with cysteine mutation. We then incorporated syntaxin 1A into nanodiscs. Syntaxin 1A nanodiscs and 10 times more of syntaxin 1A amount of SNAP-25 truncation were pre-incubated to form the 1:1 t-SNARE complex, which were then immobilized onto the imaging surface. Unbound components were removed after buffer washing. The Cy3 labeled VAMP2 was then loaded to form the ternary SNARE complex (Figure 3B).

We only observed very stable high FRET traces in all cases (Figure 3C and 3D), indicating the formation of tightly zippered ternary SNARE complex. Similarly, VAMP2 binding to the binary SNARE complex ratio had close to negligible background level with just SNAP-25 dL2. With SNAP-25 dL3, dL4, dL6 and dL7, VAMP2 has increasingly well-structured ternary SNARE complex formed with syntaxin 1A. We also calculated the docking of VAMP2 to the binary SNARE complex of SNAP-25 truncations and compared it with that of SNAP-25 WT (Figure 3E). VAMP2 relative binding to the binary SNARE complex increased from 2% with SNAP-25 dL2 to almost 100% with SNAP-25 dL7 in a progressive manner. The binary complex formed by syntaxin

1A and SNAP-25 dL7 or SNAP-25 WT had comparable capabilities to form the well-structured ternary SNARE complex.

In the ternary SNARE complex C-terminal, only tightly zippered structure between syntaxin 1A and VAMP2 was formed even in the absence of the SC downstream layers (from +3 to +7). The results indicated that SC upstream layers functioned as the landing platform for VAMP2 binding that initiated the ternary SNARE complex assembly even in the absence of most layers of the SC downstream (Figure 3D).

Discussion

We have systematically examined the function of SC layers of SNAP-25 during SNARE assembly. The results illuminate the crucial but distinct roles of SC upstream layers and downstream layers in the binary and ternary SNARE complex formation. For the binary SNARE complex, SN with SC upstream layers as well as the ionic layer seems incapable to form a well-structured t-SNARE complex with syntaxin 1A. The well-structured binary complex formation is initiated after layer '+1' and increases progressively to layer '+6'. SNAP-25 has comparable effects to form the well-structured t-SNARE complex with or without the last two layers at the C-terminal end. We found both high FRET, low FRET and fluctuating FRET states in all cases, which underlines that the 1:1 t-SNARE complex is intrinsically dynamic, even with full-length wild-type SNAP-25. There is a dynamic equilibrium between the unstructured and well-structured binary complex population. The SC downstream layers can shift the equilibrium toward the well-structured binary complex population in the SC upstream layers in a gradual manner.

Our results indicate a delicate alpha-helix nucleation process in the SC layers (Figure 4). The SC upstream layers with the ionic layer themselves are not able to nucleate an alpha-helical structure that binds syntaxin 1A and SN. The SC downstream layers (from +2 to +6) gradually help SC upstream layers with alpha helix nucleation. The SC downstream last two layers (from +7 to +8) are not involved in further facilitating SC alpha helix nucleation. This is consistent with a recent study that the 1:1 t-SNARE complex is frayed in the C-terminal end (Zhang et al., 2016). We also noticed a basal level of the unstructured binary complex with syntaxin 1A in all cases. Such basal level of SNAP-25 docked to syntaxin 1A is very likely just stabilized by the syntaxin 1A and SN interaction. Since such interaction is not influenced by the SC layers and structure, we observed the similar amount of basal levels of the unstructured t-SNARE complex population with all SNAP-25 truncations. However, The SC downstream layers (from +2 to +6) enable SC the possession of increasingly higher alpha-helix nucleation ability and alpha-helical structure binding affinity, which render SNAP-25 a more tight and stable syntaxin 1A binding capability. The percentage of the well-structured population from the 1:1 t-SNARE complex increases from around 10% with SNAP-25 dL2 gradually to around 80% with SNAP-25 dL7 and SNAP-25 (Figure 2E). Even though the binary SNARE complex is dynamic, physiologically with wild-type SNAP-25, most (around 80%) 1:1 t-SNARE adopt a well-structured tightly-zippered SC upstream layers conformation. Such ratio is deemed high enough for VAMP2 binding during neurotransmitter release.

During the ternary SNARE complex formation, we found that the unstructured syntaxin 1A: SNAP-25 dL2 1:1 binary complex is almost incapable of binding VAMP2. VAMP2 binding to the binary SNARE complex increases from SC downstream layer '+2' to layer '+6' progressively. The last two layers at the C-terminal end are not able to further increase VAMP2 docking. In the

ternary SNARE complex C- terminal, VAMP2 can tightly associate with the binary SNARE complex even without the SC downstream layers (from +3 to +7). The trends of binary complex high FRET population ratio and the VAMP2 docking to the binary complex with these SNAP-25 truncations are strikingly similar, suggesting that the well-structured SC upstream layers serve as a landing template for VAMP2 binding. Such binding can initiate the ternary SNARE complex formation even without SC downstream most layers. Once the ternary complex assembly is initiated in the N-terminal, the interactions between the syntaxin 1A, SN, and VAMP2 three SNARE motifs are able to form a very stable alpha-helical structure in the C-terminal even without most downstream layers of SC.

It is very interesting to notice that both the binary complex high FRET population ratio and VAMP2 docking to the binary complex start at layer '+2', the BoNT E cleavage site. Both the binary complex high FRET population ratio increase and VAMP2 docking to the binary complex increase stop at layer '+7', the BoNT A cleavage site (Schiavo et al., 1993). Previous studies have shown that syntaxin 1A together with SNAP-25 are necessary to maintain neuronal survival (Peng et al., 2013). A very low amount of residue level of syntaxin 1A and SNAP-25 after limited exposure to BoNT type E is still able to prevent neurodegeneration. Just monomeric largely unstructured syntaxin 1A or just SNAP-25 is not able to rescue the neurodegeneration. This indicates that the well-structured 1:1 syntaxin 1A and SNAP-25 binary complex is involved in preventing neurodegeneration (Peng et al., 2013). In our study, we found that SNAP-25 proteins truncated after layer '+2' are still capable to form a well-structured 1:1 syntaxin 1A and SNAP-25 binary complex. Thus, the layer '+2' is a delicately chosen cleavage site by naturally selected neurodegeneration inducing BoNT E.

SN associates with syntaxin 1A with high affinity (Khounlo et al., 2017). SC upstream layers themselves are not able to associate with syntaxin 1A tightly without the help of SC downstream layers. This provides an ideal targeting region for SNARE-mediated membrane fusion inhibiting toxins BoNT A and E. Even with wild-type SNAP-25, there are still ~20% SC are detached from syntaxin 1A. This provides the potential for SNARE-dependent membrane fusion facilitators to further stabilize the 1:1 t-SNARE complex, according to a previous study (Weninger et al., 2008). From an energy point of view, the 1:1 t-SNARE complex is a slowly-preformed complex (Zhang et al., 2016). The free energy released to mediate the membrane fusion for SNARE is mainly during the ternary SNARE rather than the t-SNARE complex assembly (Gao et al., 2012; Min et al., 2013). A dynamic rather than a tightly folded 1:1 t-SNARE complex is less energy-consuming during SNARE complex disassembly and recycling. Our study reveals SNAP-25 upstream and downstream layers play critical but distinct roles during SNARE assembly and contribute to this highly energy-efficient and delicately-regulated membrane fusion machine.

Methods

Plasmid construction and mutagenesis.

DNA sequences encoding syntaxin 1A (amino acids 1–288, with three native cysteines replaced by alanines), SNAP-25 (amino acids 1–206, with four native cysteines replaced by alanines), and soluble VAMP2 (amino acids 1–96) were cloned into the pGEX-KG vector as N-terminal GST fusion proteins. A modified apolipoprotein A1 (apoA1, amino acids, 27–267) was inserted into a pNFXeX vector as an N-terminal His-tagged protein.

SNAP-25 truncations were produced by nonsense mutations resulting in the premature termination of proteins. All the nonsense mutation introduced into SNAP-25 and all cysteine mutants were generated by the QuikChange site-directed mutagenesis (Stratagene). The primers used were as follows:

Table 1 The oligonucleotide sequences of the primers.

Primers	Oligonucleotides
SN180 truncation forward primer	GGGCAATGAGATTGACACCCAGAATCGCCAGATCGACAGGTAG
SN180 truncation reverse primer	CTACCTGTCGATCTGGCGATTCTGGGTGTCAATCTCATTGCCC
SN184 truncation forward primer	CCCAGAATCGCCAGATCGACAGGATCATGGAGAAGTAG
SN184 truncation reverse primer	CTACTTCTCCATGATCCTGTCGATCTGGCGATTCTGGG
SN187 truncation forward primer	CCCAGAATCGCCAGATCGACAGGATCATGGAGAAGGCTGATTCCTAG
SN187 truncation reverse primer	CTAGGAATCAGCCTTCTCCATGATCCTGTCGATCTGGCGATTCTGGG
SN191 truncation forward primer	CTGATTCCAACAAAACCAGATAGGATGAAGCCAACCAACGTGC
SN191 truncation reverse primer	GCACGTTGGTTGGCTTCATCCTATCTGGTTTTGTTGGAATCAG
SN194 truncation forward primer	GGAGAAGGCTGATTCCAACAAAACCAGAATTGATGAATAG
SN194 truncation reverse primer	CTATTCATCAATTCTGGTTTTGTTGGAATCAGCCTTCTCC

SNAP-25 N175C and other primers used can be found in our recently published paper (Khounlo et al., 2017). All DNA sequences were confirmed by sequencing in the Iowa State University DNA Sequencing Facility.

Protein expression and purification

All recombinant proteins were expressed in *Escherichia coli* strain BL21 (DE3). Cells were first grown in LB medium at 37°C with shaking at 200 rpm until optical density was 0.7-0.8 (600 nm). Isopropyl-β-D-thiogalactopyranoside (IPTG) (0.4 mM final concentration) was then added to the LB medium to induce protein expression.

For SNARE proteins, cells were induced at 16°C with shaking at 100 rpm for 14-16 h. For ApoA1 protein, cells were induced at 30°C with shaking at 100 rpm for 6 h. Cells were then pelleted and resuspended in 15 mL of PBST (PBS, pH 7.4, containing 0.2% Triton X-100) for full length syntaxin 1A and 15 ml of PBS (pH 7.4) for all other proteins with final concentrations of 1 mM 4-(2- aminoethyl)- benzenesulfonyl fluoride (AEBSF) and 4 mM DTT. Re-suspended cells immersed in an ice bath were lysed by sonication and then centrifuged at 25,000 g for 40 min at 4°C. The supernatant was nutated with 2 ml GST beads for SNARE proteins and 2 ml Ni-NTA beads for ApoA1 protein for 1 hour at 4°C. The unbound fractions were then washed away by intense washing. The bound SNARE proteins were then eluted by 0.02 unit/μL thrombin in cleavage buffer (PBS, pH 8.0, containing 2 mM DTT) with/without 0.8% octyl-D-glucopyranoside (OG) for GST-tagged syntaxin 1A and all other SNARE proteins, respectively. The bound His-tagged ApoA1 proteins were eluted with imidazole elution buffer (PBS, pH 7.4, containing 300 mM imidazole). The purity of proteins was determined by SDS-PAGE gel (15%, w/v) and the purity was at least 85% for all proteins. The protein concentration was determined by absorption at 750nm using the RC DC kit assay.

Site-specific labeling of proteins with the fluorescent dye Cy3 or Cy5 (maleimide-derivative fluorophore indodicarbocyanine (Cy5) or indocarbocyanine (Cy3))

For site-specific labeling of single cysteine mutant proteins, the proteins were incubated with 4 mM DTT for 30 mins and then desalted with a PD MiniTrap G-25 column to get rid of excess free DTT. Right after desalting, the proteins were incubated with a 10-fold molar excess of Cy5 or Cy3, respectively, overnight at 4°C. The labeled proteins were purified using the PD MiniTrap G- 25 column and free dyes were further eliminated from the proteins using centrifugal filters (3kDa, Amicon Millipore Corporation, Bedford, MA). The labeling efficiency of each labeled SNARE protein was measured spectrophotometrically (NanoDrop 2000c Spectrophotometer, Thermo Fisher Scientific, Waltham, MA). Further details can be found in our recently published papers ((Khounlo et al., 2017; Yin, Kim, & Shin, 2016)).

Lipid reconstitution and SNARE-Incorporated Nanodiscs Preparation

1,2- dioleoyl-sn-glycerol-3-phospho-L-serine (DOPS), 1-palmitoyl-2-oleoyl-sn-glycerol-3- phosphocholine (POPC), phosphatidylinositol-4,5-bisphosphate (PIP2, from porcine brain), cholesterol, and biotin-PEG-DSPE with a molar ratio of 62.9:15:20:2:0.1 in chloroform solution were mixed to form the lipid mixture. The lipid mixture was dried with air and further incubated in vacuum to eliminate free chloroform for 16-18 hours to form the lipid film. The lipid film was then resuspended and diluted in HEPES buffer (25 mM HEPES, pH 7.4, with 150 mM KCl) to achieve a final lipid concentration of 50 mM. 5 μL of the resuspended lipid mixture was dissolved in detergent sodium cholate such that the final concentration of sodium cholate would become 50 mM after the addition of membrane scaffolding protein apoA1 and SNARE proteins. Syntaxin 1A or the binary t-SNARE complex (syntaxin 1A and SNAP-25 proteins with a molar ratio of 1:2, pre-incubated at room temperature for 1 hour with nutation) along with apoA1 were added into

the detergent sodium cholate solubilized lipid mixture solution. The final molar ratio of lipids, apoA1, and SNARE(s) was 300:5:1. After a 16min incubation period, the SNARE membrane protein containing nanodisc formation was initiated by rapid removal of detergent with 50% (w/v) SM-2 Bio-Beads. Nanodiscs were then separated from free proteins and aggregates by gel filtration using a SuperdexTM 200 GL 10/300 column (GE Healthcare Life Sciences, Piscataway, NJ).

Negative stain transmission electron microscopy (TEM) study of nanodiscs

The carbon grid was first processed in a discharge equipment to make the grid surface hydrophilic. Then the nanodisc solution was pipetted onto the carbon grid surface for a 30 seconds period deposition. After eliminating excess nanodisc and buffer by using a piece of filter paper, the uranyl acetate solution was added onto the top of the nanodisc sample area for another 30 seconds. After removing excess uranyl acetate solution and thorough air-drying the carbon grid, electron microscopy images were collected by Tracey P. Stewart of The Microscopy and NanoImaging Facility (MNIF) of the Office of Biotechnology at Iowa State University

SmFRET signal collection

The PEGylated quartz slides imaging surface (25 x 75 x 1.0 mm) was deeply-cleaned and prepared as previously described ((Khounlo et al., 2017; Roy, Hohng, & Ha, 2008; Yin et al., 2016)). The microfluidic channels were assembled and sealed between the quartz slide and coverslip with double-sided tape and five-minute epoxy. Streptavidin (0.2 mg/mL) was incubated in the flow chamber for 2 mins and then washed out thoroughly prior to subsequent nanodisc immobilization. The t-nanodiscs were formed by pre-incubating syntaxin 1A nanodisc and SNAP-25 proteins at room temperature for 45 minutes with a molar ratio of 1:10. The t-nanodiscs

were injected into the microfluidic channels, and unbound fractions were then washed out. For ternary SNARE complex formation, VAMP2 was further loaded to bind the t-nanodiscs on the slide surface. The unbound VAMP2 was then washed out by buffer washing.

All image recordings were performed by using smFRET software smCamera (https://cplc.illinois.edu/software/) that was a gift from the Dr.Taekjip Ha lab. The TIRF imaging was carried out at room temperature with the oxygen scavenger system (0.4% glucose (Sigma Aldrich, St. Louis, MO), 4 mM Trolox, 1 mg/mL glucose oxidase, 0.04 mg/ml catalase in HEPES buffer) except for the photobleaching experiments. All data were recorded at an imaging rate of 10 s−1 (100 ms integration time). At the beginning of each experiment, a 1-2 s (10-2 frames) movie was recorded with an alternation of 532- and 635-nm excitation. At the end of each experiment, a 1-2 s (10-2 frames) movie was recorded with an alternation of 635- and 532-nm excitation. This alternating laser excitation (ALEX) scheme (Kapanidis et al., 2005) allowed us to separate the fluorescence contributions of the green and red dyes, thus enabling us to identify the SNARE complexes that contain co-localized one donor and one acceptor dyes.

SmFRET data analysis

Using smFRET software smCamera, the acquired single-molecule videos were processed to identify and extract the acceptor and donor fluorescence intensity time traces of individual molecules. For those extracted traces for further analysis, no more than one bleaching step for both the donor and acceptor dyes was used; and traces containing a constant total fluorescence intensity from the donor and acceptor fluorophores before photobleaching were selected. The assigned FRET value was obtained from the first 6 frames period in which the green laser was on and both dyes were photon emitting. From the selected spots, the acceptor and donor time traces were

analyzed to compile the FRET histograms (Figure 2 and Figure 3). For the predominant peaks shown in FRET histograms, peak fitting was performed using the program Origin Pro (OriginLab, Northampton, MA).

Author Contributions

Linxiang Yin and Yeon-Kyun Shin designed experiments. Linxiang Yin performed all experiments. Linxiang Yin and Yeon-Kyun Shin wrote the paper.

Acknowledgement

The authors would like to acknowledge Dr. Taekjip Ha and the Ha lab members for providing smFRET software smCamera and technical assistance. This work was supported by a grant from the NIH (R01 GM051290).

References

Fasshauer, D., & Margittai, M. (2004). A transient N-terminal interaction of SNAP-25 and syntaxin nucleates SNARE assembly. *Journal of Biological Chemistry*, *279*(9), 7613–7621. http://doi.org/10.1074/jbc.M312064200

Gao, Y., Zorman, S., Gundersen, G., Xi, Z., Ma, L., Sirinakis, G., … Zhang, Y. (2012). Single reconstituted neuronal SNARE complexes zipper in three distinct stages. *Science*, *337*(6100), 1340–1344.

Jahn, R., & Scheller, R. H. (2006). SNAREs - engines for membrane fusion. *Nature Reviews Molecular Cell Biology*, *7*(9), 631–643. http://doi.org/10.1038/nrm2002

James, D. J., Kowalchyk, J., Daily, N., Petrie, M., & Martin, T. F. J. (2009). CAPS drives trans-SNARE complex formation and membrane fusion through syntaxin interactions. *Proceedings of the National Academy of Sciences*, *106*(41), 17308–17313.

Kapanidis, A. N., Laurence, T. A., Lee, N. K., Margeat, E., Kong, X., & Weiss, S. (2005). Alternating-laser excitation of single molecules. *Accounts of Chemical Research*, *38*(7), 523–533. http://doi.org/10.1021/ar0401348

Khounlo, R., Kim, J., Yin, L., & Shin, Y. (2017). Botulinum toxins A and E inflict dynamic destabilization on t-SNARE to impair SNARE assembly and membrane fusion. *Structure*, *25*, 1–8. http://doi.org/10.1016/j.str.2017.09.004

Lacy, D. B., Tepp, W., Cohen, A. C., Dasgupta, B. R., & Stevens, R. C. (1998). Crystal structure of botulinum neurotoxin type A and implications for toxicity. *Nature Structural Biology*, *5*(10), 898–902.

Margittai, M., Fasshauer, D., Pabst, S., Jahn, R., & Langen, R. (2001). Homo- and heterooligomeric SNARE complexes studied by site-directed spin labeling. *Journal of Biological Chemistry*, *276*(16), 13169–13177. http://doi.org/10.1074/jbc.M010653200

Min, D., Kim, K., Hyeon, C., Cho, Y. H., Shin, Y., & Yoon, T. (2013). Mechanical unzipping and rezipping of a single SNARE complex reveals hysteresis as a force-generating mechanism. *Nature Communications*, *4*, 1705. http://doi.org/10.1038/ncomms2692

Otto, H., Hanson, P. I., & Jahn, R. (1997). Assembly and disassembly of a ternary complex of synaptobrevin , syntaxin , and SNAP-25 in the membrane of synaptic vesicles. *Proceedings of the National Academy of Sciences*, *94*(12), 6197–6201.

Peng, L., Liu, H., Ruan, H., Tepp, W. H., Stoothoff, W. H., Brown, R. H., … Dong, M. (2013). Cytotoxicity of botulinum neurotoxins reveals a direct role of syntaxin 1 and SNAP-25 in neuron survival. *Nature Communications*, *4*, 1472. http://doi.org/10.1038/ncomms2462

Pobbati, A. V, Stein, A., & Fasshauer, D. (2006). N- to C-terminal SNARE complex assembly promotes rapid membrane fusion. *Science*, *313*(5787), 673–676. http://doi.org/10.1126/science.1129486

Poirier, M. A., Wenzhong, X., Macosko, J. C., Chan, C., Yeon-Kyun, S., & Bennett, M. K. (1998). The synaptic SNARE complex is a parallel four- stranded helical bundle. *Nature Structural Biology*, *5*(9), 765–769.

Rossetto, O., Pirazzini, M., & Montecucco, C. (2014). Botulinum neurotoxins: genetic, structural and mechanistic insights. *Nature Reviews Microbiology*, *12*(8), 535–549. http://doi.org/10.1038/nrmicro3295

Roy, R., Hohng, S., & Ha, T. (2008). A practical guide to single-molecule FRET. *Nature Methods*, *5*(6), 507–516. http://doi.org/10.1038/NMETH.1208

Schiavo, G., Santuccib, A., Dasguptac, B. R., Mehtad, P. P., Jontesd, J., Benfenati, F., … Montecucco, C. (1993). Botulinurn neurotoxins serotypes A and E cleave SNAP-25 at distinct COOH-terminal peptide bonds. *FEBS Letters*, *335*(1), 99–103.

Shin, J., Lou, X., Kweon, D., & Shin, Y. (2015). Multiple conformations of a single SNAREpin between two nanodisc membranes reveal diverse pre-fusion states. *Biochemical Journal*, *459*(1), 95–102. http://doi.org/10.1042/BJ20131668.Multiple

Söllner, T. H., Whiteheart, S. W., Brunner, M., Erdjument-Bromage, H., Geromanos, S., Tempst, P., & Rothman, J. E. (1993). SNAP receptors implicated in vesicle targeting and fusion. *Nature*, *362*(6418), 318–324.

Südhof, T. C. (2004). The synaptic vesicle cycle. *Annual Review of Neuroscience*. http://doi.org/10.1146/annurev.neuro.26.041002.131412

Südhof, T. C., & Rothman, J. E. (2009). Membrane fusion: Grappling with SNARE and SM proteins. *Science*, *323*(5913), 474–477. http://doi.org/10.1126/science.1161748

Sutton, R. B., Fasshauer, D., Jahn, R., & Brunger, A. T. (1998). Crystal structure of a SNARE complex involved in synaptic exocytosis at 2.4 Å resolution. *Nature*, *395*(6700), 347–353. http://doi.org/10.1038/26412

Walter, A. M., Wiederhold, K., Bruns, D., Fasshauer, D., & Sørensen, J. B. (2010). Synaptobrevin N-terminally bound to syntaxin-SNAP-25 defines the primed vesicle state in regulated exocytosis. *Journal of Cell Biology*, *188*(3), 401–413. http://doi.org/10.1083/jcb.200907018

Weninger, K., Bowen, M. E., Choi, U. B., Chu, S., & Brunger, A. T. (2008). Accessory proteins stabilize the acceptor complex for synaptobrevin , the 1 : 1 syntaxin / SNAP-25 complex. *Structure*, *16*(2), 308–320. http://doi.org/10.1016/j.str.2007.12.010

Xiao, W., Poirier, M. A., Bennett, M. K., & Shin, Y. (2001). The neuronal t-SNARE complex is a parallel four-helix bundle. *Nature Structural Biology*, *8*(4), 308–311.

Yin, L., Kim, J., & Shin, Y. (2016). Complexin splits the membrane-proximal region of a single SNAREpin. *Biochemical Journal*, *473*(14), 2219–2224. http://doi.org/10.1042/BCJ20160339

Zhang, X., Rebane, A. A., Ma, L., Li, F., Jiao, J., Qu, H., … Zhang, Y. (2016). Stability, folding dynamics, and long-range conformational transition of the synaptic t-SNARE complex. *Proceedings of the National Academy of Sciences*, *113*(50), E8031–E8040. http://doi.org/10.1073/pnas.1605748113

Figures with Titles and Legends

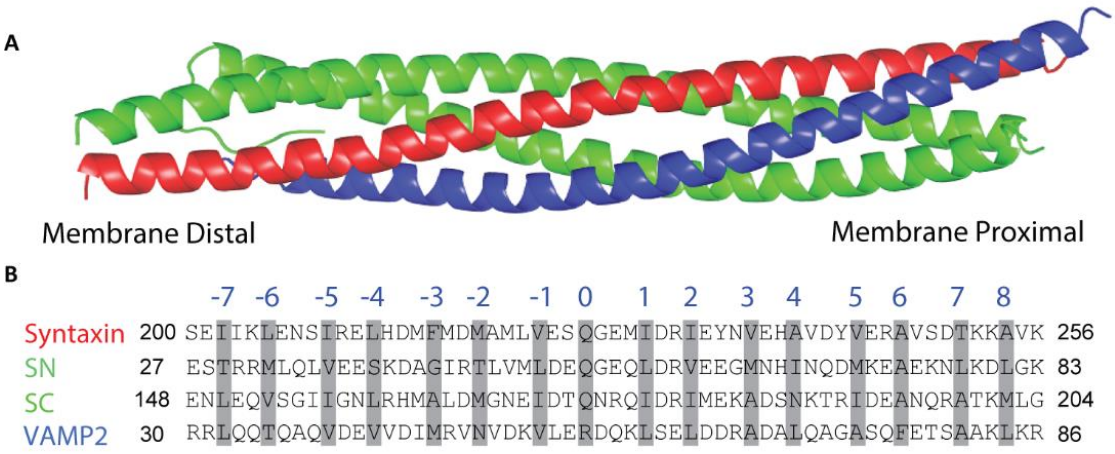

Figure 1 Structure of the Cis-Ternary SNARE Complex and the SNARE Motifs Sequences and 16 Layers.

(A) The cis-ternary SNARE complex X-ray crystal structure rendered by PyMol. Syntaxin 1A and VAMP2 are in red and blue, respectively. The N-terminal SNARE motif of SNAP-25 (SN) and C-terminal SNARE motif of SNAP-25 (SC) are in green. (B) Amino acid sequences of the four SNARE motifs in cis-SNARE complex. The 16 layers (labeled on the top) are indicated by grey bars.

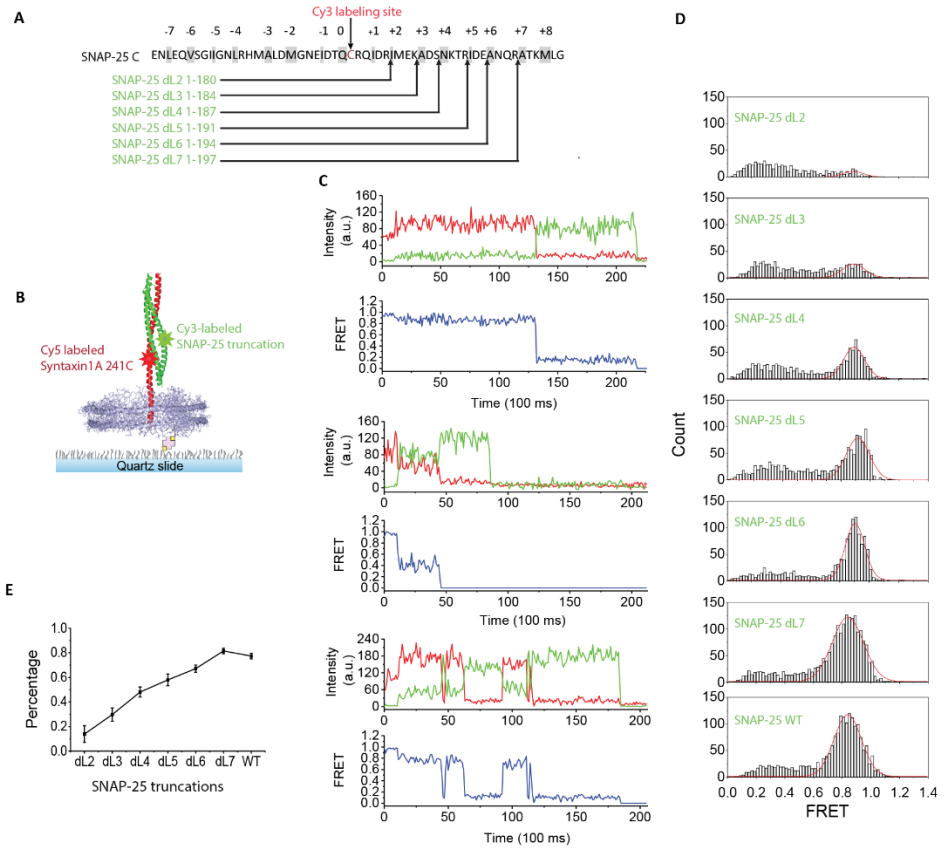

Figure 2 SmFRET Analysis of the 1:1 T-SNARE Complexes with a Series of SNAP-25 Truncations in the Nanodisc.

(A) Schematic of a series of SNAP-25 truncations with a single cysteine mutation (N175C) for Cy3 labeling. In the C-terminal SNARE motif of SNAP-25 (SNAP-25 C) sequence, layers are indicated by grey bars. The residue that was mutated to cysteine are highlighted in red and the truncation sites are indicated by upward pointing arrows. (B) Schematic diagram for monitoring the structure of a 1:1 t-SNARE complex incorporated into a single nanodisc using total internal reflection smFRET imaging. In the 1:1 t-SNARE complex, full-length syntaxin 1A 241C (red) was labeled with Cy5, and SNAP-25 truncation 175C (green) was labeled with Cy3. The Cy3 and Cy5 dyes are in green and red, respectively. The nanodisc, doped with biotin-PEG-DSPE lipid (biotin,

light yellow; PEG, grey), was immobilized on streptavidin (pink)-decorated quartz slide surfaces via the biotin-streptavidin interaction. (C) Representative fluorescence (donor, green; acceptor, red), and FRET (blue) time traces from the 1:1 t-SNARE complex for high-, low- FRET and fluctuating states. Single step photo-bleaching events and typical counter switches between donor and acceptor during FRET were observed in the traces. (D) Histograms of the FRET efficiency distribution for the 1:1 t-SNARE complexes with different SNAP-25 truncations (green). The predominant peaks shown in the histograms were fitted with Gaussians (red). Total of 101, 133, 182, 230, 211, 339, and 312 traces was included for the histograms, from top to bottom. (E) The percentage of the high FRET population from the 1:1 t-SNARE complexes. The data are shown as means ± SD.

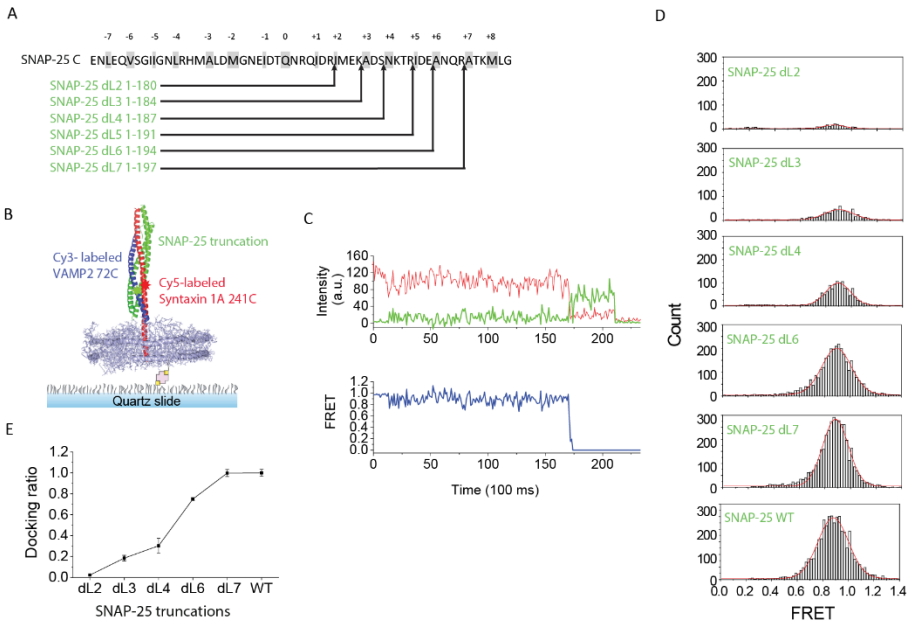

Figure 3 SmFRET Analysis of the Ternary SNARE Complexes with a Series of SNAP-25 Truncations in the Nanodisc.

(A) Schematic of a series of SNAP-25 truncations without cysteine mutation. In the C-terminal SNARE motif of SNAP-25 (SNAP-25 C) sequence, layers are indicated by grey bars. The truncation sites are indicated by upward pointing arrows. (B) Schematic diagram for monitoring the structure of a ternary SNARE complex incorporated into a single nanodisc using total internal reflection smFRET imaging. In the ternary SNARE complex, syntaxin 1A 241C (red) was labeled with Cy5, VAMP2 72C (blue) were labeled with Cy3, and SNAP-25 truncation without cysteine mutation (green) was not labeled. The Cy3 and Cy5 dyes are in green and red, respectively. The nanodisc, doped with biotin-PEG-DSPE lipid (biotin, light yellow; PEG, grey), was immobilized on streptavidin (pink)-decorated quartz slide surfaces via the biotin-streptavidin interaction. (C) A representative fluorescence (donor, green; acceptor, red), and FRET (blue) time trace from the ternary-SNARE complex in high FRET state. Single step photo-bleaching event and typical counter switch between donor and acceptor during FRET were observed in the trace. (D)

Histograms of the FRET efficiency distribution for the ternary SNARE complexes with different SNAP-25 truncations (green). The distribution showed one single predominant high FRET population for SNAP-25 truncations. The peaks in the histograms were fitted with Gaussians (red). Total of 15, 124, 244, 546, 658, and 653 traces was included for the histograms, from top to bottom. (E) Relative co-localized Cy3-Cy5 spots for SNAP-25 truncations normalized to SNAP-25 WT. The data are shown as means ± SD.

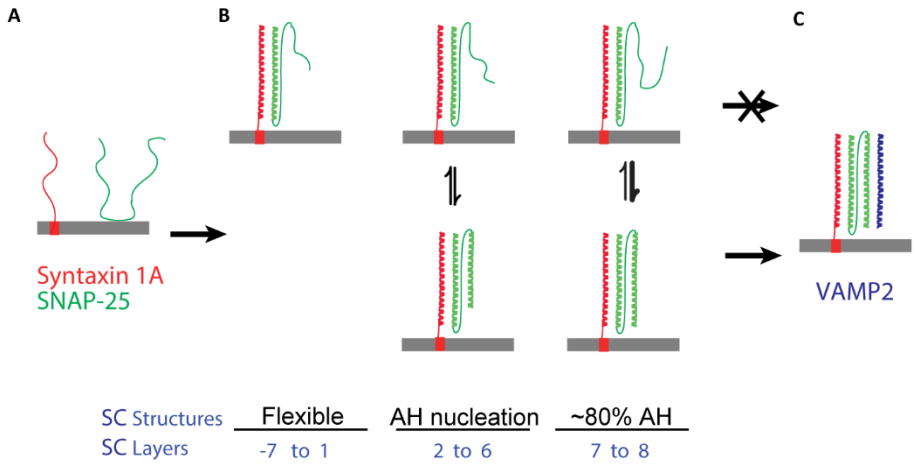

Figure 4 An Alpha-Helix Nucleation Process within the SC Layers Influences the Assembly and Structure of the Binary and Ternary SNARE Complexes.

(A) Monomeric syntaxin 1A and SNAP-25 proteins before the 1:1 t-SNARE complex formation. Syntaxin 1A and SNAP-25 are in red and green, respectively. The lipid bilayer is in grey. (B) The 1:1 t- SNARE complex formation between syntaxin 1A and SNAP-25 with SC layers truncations. The SC upstream layers themselves are not capable of nucleating an alpha-helical structure that binds to syntaxin 1A and SN (left). The SC downstream layers (from layer +2 to +6) help SC upstream layers with alpha helix nucleation gradually (middle). The last two downstream layers in SC (layer +7 and +8) are not involved in further increasing SC alpha-helix nucleation. For wild-type SNAP-25 or SNAP-25 without SC last two layers, around 80% 1:1 t-SNARE complexes have a tightly-zippered SC upstream layers while only 20% adopt a structure with flexible SC upstream layers (right). Fluctuating traces indicate the equilibrium between the unstructured and well-structured 1:1 t-SNARE complexes. The SC downstream layers (from +2 to +6) can gradually shift the equilibrium toward the well-structured binary complex population at the SC upstream layers. The lipid bilayer is in grey. (C) The ternary SNARE complex formation. VAMP2 is in blue. Only

the 1:1 t-SNARE complexes with tightly-zippered SC upstream layers are accessible to VAMP2 binding. The lipid bilayer is in grey.

Supplementary Information

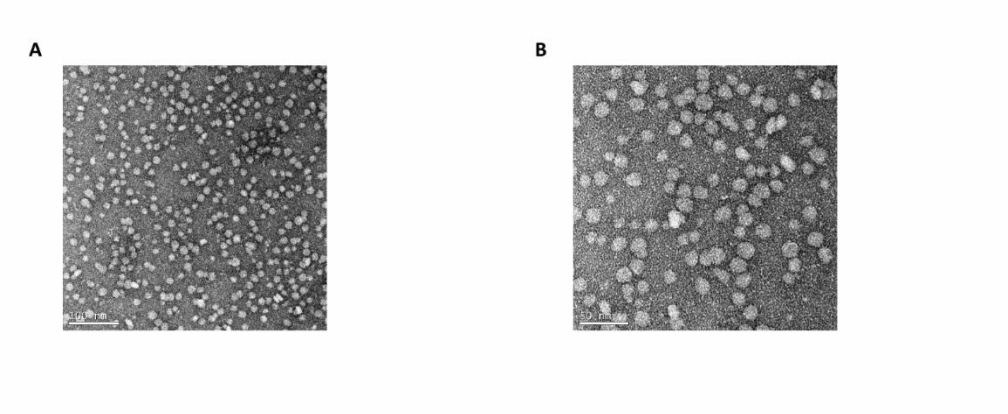

Figure S1 Negative stain transmission electron microscopy (TEM) of syntaxin containing nanodiscs.

(A) TEM image of syntaxin containing nanodiscs with 100 nm scale bar. (B) TEM image of syntaxin containing nanodiscs with 50 nm scale bar.

CHAPTER 5: GENERAL SUMMARY

General Conclusion

Soluble N-ethylmaleimide-sensitive factor attachment protein receptor (SNARE) proteins mediate synaptic vesicle membrane fusion by forming a ternary SNARE complex (Wickner & Schekman, 2008). Assembly of the SNAREs into the *trans*-complexes bridges the opposing synaptic vesicle membrane and plasma membrane, initiating their fusion by bringing them into close proximity. Calcium influx triggers the completion of the SNARE assembly reaction accompanied by the *cis*-SNARE complex formation (Y. A. Chen, Scales, Patel, Doung, & Scheller, 1999; Rizo & Xu, 2015; Tang et al., 2006; Yang et al., 2010). Precise and accurate neurotransmitter release depends on a cascade of exquisitely orchestrated protein-protein and protein-lipid interactions, thus emphasizing the importance of the investigation of the SNARE-mediated synaptic exocytosis regulation.

Previous *in vitro* studies utilizing nuclear magnetic resonance (NMR), X-ray crystallography, hydrogen-deuterium exchange (HDX) and isothermal titration calorimetry (ITC) have yielded critical insights into the effects of SNARE regulators on SNARE structure and function (X. Chen et al., 2002; Kümmel et al., 2011). However, questions have been raised regarding the absence of two opposing membranes during *in vitro* SNARE function regulation studies (Su, Ishitsuka, Ha, & Shin, 2008; Weninger, Bowen, Choi, Chu, & Brunger, 2008; Zhang et al., 2016). The soluble domain of SNAREs without two opposing membranes used in these studies might only represent the post-fusion *cis*-SNARE complex. In our research, we utilized both *trans*-SNAREpin and *cis*-SNAREpin to mimic the *trans*-SNARE and the *cis*-SNARE by using nanodiscs. Our single-molecule FRET system with nanodiscs enabled us to investigate the

conformational changes of different SNARE complexes in the presence of more native lipid environment at the single-molecule level.

We first investigated the role of a major SNARE accessory protein complexin by using *trans*-SNAREpin and *cis*-SNAREpin system in nanodiscs. Our study shows that, for *trans*-SNARE complex, complexin rearranges the C-terminal domain (CTD) structure of the SNARE motif while maintains the N-terminal domain (NTD) structure of the SNARE motif. In the CTD, complexin splits the full-zippered *trans*-SNARE, which could be the structural explanation about why complexin inhibits SNARE-mediated spontaneous membrane fusion. For the *cis*-SNARE complex, complexin maintains the structure of the CTD of the SNARE motif, which is consistent with a previous study that found complexin stabilizes the interface between syntaxin and VAMP2 helices (X. Chen et al., 2002). Also, our results show that complexin N-terminal domain could keep v- and t-SNAREs CTD distance closer than that in the half-zippered intermediate state, which can serve as a structural basis about why the N-terminal domain of complexin increases the membrane fusogenicity (Xue et al., 2007, 2010; Yin, Kim, & Shin, 2016).

Botulinum neurotoxin (BoNT) A and E site-selectively cleave SNAP-25 at the C-terminus to inhibit SNARE-dependent membrane fusion. SNAP-25 A and E, the cleaved versions of SNAP-25 by BoNT A and E, respectively, only lose the last 9 and last 26 residues from SNAP-25 C-terminus (Schiavo et al., 1993). Our single-molecule FRET data show that for SNAP-25 A, an apparent (20%) fully-zippered *trans*-SNARE population was shifted towards the half-zippered *trans*-SNARE population. The binary t-SNARE complex pairing with VAMP2 is not influenced by SNAP-25 A while severely hindered by SNAP-25 E. The results suggest that BoNT A inhibits SNARE-dependent membrane fusion by reducing fully-zippered *trans*-SNARE population, while

BoNT E completely abolishes SNARE-dependent membrane fusion by severely eliminating well-structured SNARE complex formation (Khounlo, Kim, Yin, & Shin, 2017).

We also systematically examined the effect of the 16 layers at the SNAP-25 C-terminal motif (SC). We discovered an exquisite alpha-helix nucleation process happened at the SC downstream layers. Our results show that SC upstream layers are not capable of forming a well-structured complex with SNAP-25 N-terminal motif (SN) and syntaxin 1A. The alpha-helix nucleation begins from the SC downstream layer '+2' and increases gradually towards layer '+6'. Around 80% wild-type SNAP-25 can form a well-structured binary complex with syntaxin 1A, which is similar for SNAP-25 A. In contrast, the SNAP-25 E SC residues are almost totally incapable to form a well-structured complex with SN and syntaxin 1A. This might explain why BoNT E but not BoNT A induces neurodegeneration. Our results suggest that the well-structured binary complex serves as a critical platform for regulatory proteins and membrane recycling, which are indispensable for neuron survival.

References

Chen, X., Tomchick, D. R., Kovrigin, E., Arac, D., Machius, M., & Su, T. C. (2002). Three-dimensional structure of the complexin/SNARE complex. *Neuron*, *33*(3), 397–409.

Chen, Y. A., Scales, S. J., Patel, S. M., Doung, Y., & Scheller, R. H. (1999). SNARE complex formation is triggered by Ca2+ and drives membrane fusion. *Cell*, *97*(2), 165–174.

Khounlo, R., Kim, J., Yin, L., & Shin, Y. (2017). Botulinum toxins A and E inflict dynamic destabilization on t-SNARE to impair SNARE assembly and membrane fusion. *Structure*, *25*, 1–8. http://doi.org/10.1016/j.str.2017.09.004

Kümmel, D., Krishnakumar, S. S., Radoff, D. T., Li, F., Giraudo, C. G., Pincet, F., … Reinisch, K. M. (2011). Complexin cross-links prefusion SNAREs into a zigzag array. *Nature Structural & Molecular Biology*, *18*(8), 927–933. http://doi.org/10.1038/nsmb.2101

Rizo, J., & Xu, J. (2015). The Synaptic Vesicle Release Machinery. *Annual Review of Biophysics*, *44*, 339–367. http://doi.org/10.1146/annurev-biophys-060414-034057

Schiavo, G., Santuccib, A., Dasguptac, B. R., Mehtad, P. P., Jontesd, J., Benfenati, F., … Montecucco, C. (1993). Botulinurn neurotoxins serotypes A and E cleave SNAP-25 at distinct COOH-terminal peptide bonds. *FEBS Letters*, *335*(1), 99–103.

Su, Z., Ishitsuka, Y., Ha, T., & Shin, Y. (2008). The SNARE complex from yeast is partially unstructured on the membrane. *Structure*, *16*(7), 1138–1146. http://doi.org/10.1016/j.str.2008.03.018

Tang, J., Maximov, A., Shin, O. H., Dai, H., Rizo, J., & Sudhof, T. C. (2006). A complexin/synaptotagmin 1 switch controls fast synaptic vesicle exocytosis. *Cell*, *126*(6), 1175–1187. http://doi.org/10.1016/j.cell.2006.08.030

Weninger, K., Bowen, M. E., Choi, U. B., Chu, S., & Brunger, A. T. (2008). Accessory proteins stabilize the acceptor complex for synaptobrevin , the 1 : 1 syntaxin / SNAP-25 complex. *Structure*, *16*(2), 308–320. http://doi.org/10.1016/j.str.2007.12.010

Wickner, W., & Schekman, R. (2008). Membrane fusion. *Nature Structural and Molecular Biology*, *15*(7), 658–664. http://doi.org/10.1038/nsmb.1451

Xue, M., Craig, T. K., Xu, J., Chao, H.-T., Rizo, J., & Rosenmund, C. (2010). Binding of the complexin N terminus to the SNARE complex potentiates synaptic-vesicle fusogenicity. *Nature Structural & Molecular Biology*, *17*(5), 568–575. http://doi.org/10.1038/nsmb.1791

Xue, M., Reim, K., Chen, X., Chao, H.-T., Deng, H., Rizo, J., … Rosenmund, C. (2007). Distinct domains of complexin I differentially regulate neurotransmitter release. *Nature Structural & Molecular Biology*, *14*(10), 949–958. http://doi.org/10.1038/nsmb1292

Yang, Y., Shin, J., Oh, J., Jung, C. H., Hwang, Y., Kim, S., … Kweon, D.-H. (2010). Dissection of SNARE-driven membrane fusion and neuroexocytosis by wedging small hydrophobic molecules into the SNARE zipper. *Proceedings of the National Academy of Sciences*, *107*(51), 22145–22150. http://doi.org/10.1073/pnas.1006899108

Yin, L., Kim, J., & Shin, Y. (2016). Complexin splits the membrane-proximal region of a single SNAREpin. *Biochemical Journal*, *473*(14), 2219–2224. http://doi.org/10.1042/BCJ20160339

Zhang, X., Rebane, A. A., Ma, L., Li, F., Jiao, J., Qu, H., … Zhang, Y. (2016). Stability, folding dynamics, and long-range conformational transition of the synaptic t-SNARE complex. *Proceedings of the National Academy of Sciences*, *113*(50), E8031–E8040. http://doi.org/10.1073/pnas.1605748113

ACKNOWLEDGEMENT

First and foremost, I would like to express my sincere thanks and profound gratitude to my major professor, Dr. Yeon-Kyun Shin, for all your valuable support and guidance. You have been an excellent research mentor for me. Your guidance and advice really taught me work hard to grow as a productive and independent scientist. I am also ever thankful for the many great opportunities you provided for me to improve my scientific knowledge and research skills during my whole Ph.D. period.

I then would like to thank all my committee members: Professor Guru Rao, Professor Scott Nelson, Professor Mark Hargrove, Professor Dipali Sashital, and Professor Nigel Reuel. Thanks for all your support, your valuable perspectives and insights to improve my critical thinking ability and my research projects. Without your time and your dedication, my thesis would not have been able to be improved.

I also would like to extend my thanks to my lab mates. Thank previous lab members for teaching me how to do the experiments. Thank previous lab member Jaewook Kim and current lab members Brenden Hawk, Ryan Khounlo, and Andrew Wiese for your great collaborations. I would like to thank you all for your help and advice. Thanks for all the hours you have spent with me to help and support each other to do great research.

I am also so grateful for my collaborators I worked with at Iowa State. I really learned a lot from you. It has been really a great opportunity and experience to work with you.

Thank you to all the friends I met here during my graduate study. Even though getting good research accomplished is always not easy, your friendships allow me to recover from the

difficulties and the tiredness after experiments day and night. Thanks for sharing the joys and sorrows with each other.

I would express my special thanks to my family for your enduring love and support. I first would thank my parents. Even though you are geographically so far from me, you always care so much about each step of my life and my research here. Your discussion with me almost every week really supports me spiritually. I would also thank my grandma. Thank you grandma for babysitting me when I was a child. Even though you have experienced so many difficulties within the family, you always have unending optimism and wholeheartedly dedicate yourself to the ones you love. All your love, dedication, and encouragement for me from my childhood really supports me to pursue my childhood dream of doing science. I would never be able to accomplish this without all your love.